NEBRASKA TRANSPORTATION CENTER

NEBRASKA DEPARTMENT OF TRANSPORTATION

MID-AMERICA TRANSPORTATION CENTER

Report SPR-P1 M076

Final Report
26-1121-4042-001

CPT-Based Pile Design

Chung R. Song, Ph.D., A.E.
Associate Professor
Department of Civil Engineering
University of Nebraska-Lincoln

Seunghee Kim, Ph.D.
Assistant Professor

Binyam Bekele
Graduate Research Assistant

Jingtao Zhang
Graduate Research Assistant

Alex Silvey
Graduate Research Assistant

2019

Nebraska Transportation Center
262 Prem S. Paul Research Center at Whittier School
2200 Vine Street
Lincoln, NE 68583-0851
(402) 472-1993

"This report was funded in part through grant[s] from the Federal Highway Administration [and Federal Transit Administration], U.S. Department of Transportation. The views and opinions of the authors [or agency] expressed herein do not necessarily state or reflect those of the U.S. Department of Transportation."

CPT-BASED PILE DESIGN
Final Report

Chung R. Song, Ph.D., A.E.
Associate Professor
Department of Civil Engineering
University of Nebraska-Lincoln

Seunghee Kim, Ph.D.
Assistant Professor
Department of Civil Engineering
University of Nebraska-Omaha

Binyam Bekele, Jingtao Zhang, and Alex Silvey
Graduate Research Assistants

A Report on Research Sponsored by

Nebraska Department of Transportation
(NDOT)

December 2018

TECHNICAL REPORT DOCUMENTATION PAGE

1. Report No. NDOT: SPR-P1 M076 NTC: 26-1121-4042-001	**2. Government Accession No.**	**3. Recipient's Catalog No.**	
4. Title and Subtitle CPT Based Pile Design		**5. Report Date** January 1, 2019	
		6. Performing Organization Code:	
7. Author(s) Chung R. Song, Seunghee Kim, Binyam Bekele, Jingato Zhang and Alex Silvey		**8. Performing Organization Report No.** 26-1121-4042-001	
9. Performing Organization Name and Address University of Nebraska-Lincoln, Department of Civil Engineering 262 Prem Paul Research Center at Whittier School 2200 Vine St., Lincoln NE 68503		**10. Work Unit No.**	
		11. Contract or Grant No.	
12. Sponsoring Agency Name and Address Nebraska Department of Transportation (NDOT) 1500 Nebraska Highway 2 Lincoln NE 68503		**13. Type of Report and Period** Final Report, 7/1/2017 – 12/31/2018	
		14. Sponsoring Agency and Code	
15. Supplementary Notes			

Abstract

The geotechnical design of a pile foundation is concerned with the determination of the safe magnitude of an external load that the foundation can carry without jeopardizing the stability of the supported structure. In recent years, in-situ sounding tests are becoming a more attractive method to predict pile capacity due to the rapid development of testing instruments, improved understanding of their mechanics and interpretation, and cost efficiency. The cone penetration test (CPT) and its upgraded version, the piezocone penetration test (PCPT), are the most widely used in situ sounding tests to predict pile capacity. This research report compared eight CPT-based and three PCPT-based methods for potential application of the best performer(s) by the Nebraska Department of Transportation (NDOT) to predict pile capacity. Several statistical as well as non-statistical comparison criteria were adopted. According to the evaluation output, the modified (calibrated) Tumay and Fakhroo (1982) method was found to be the best performer for H-piles, and the modified De Ruiter and Beringen (1979) method was found to be the best performer for pipe and precast prestressed concrete piles. For a complete design of pile foundations, the settlement criterion has to be incorporated. The settlement of pile foundations must not exceed a certain tolerable magnitude of settlement to ensure the safety of the structure supported. In this regard, this research project adopted the t – z curve approach to predict pile settlements. Several existing t – z curve approaches based on analytical and numerical techniques were assessed and their relative accuracy was investigated. An easy to use software for the computation of settlement was also developed.

17. Key Words cone penetration test; pile capacity; pile dynamic analyzer; LRFD		**18. Distribution Statement**	
19. Security Classification (of this report) Unclassified	**20. Security Classification (of this page)** Unclassified	**21. No of Pages** 120	**22. Price**

Contents

List of Figures

List of Tables

ACKNOWLEDGMENT

The authors would like to thank Nebraska Department of Transportation (NDOT) for the financial support needed to complete this research. Also, NDOT Technical Advisory Committee (TAC) for their technical support, discussion and comments.

DISCLAIMER

The contents of this report reflect the views of the authors, who are responsible for the facts and the accuracy of the information provided herein. This document is disseminated under the sponsorship of the U.S. Department of transportation's University Transportation's Centers Program, in the interest of information exchange. The U.S. Government assumes no liability for the contents of thereof.

ABSTRACT

The geotechnical design of a pile foundation is concerned with the determination of the safe magnitude of an external load that the foundation can carry without jeopardizing the stability of the supported structure. In recent years, in-situ sounding tests are becoming a more attractive method to predict pile capacity due to the rapid development of testing instruments, improved understanding of their mechanics and interpretation, and cost efficiency. The cone penetration test (CPT) and its upgraded version, the piezocone penetration test (PCPT), are the most widely used in situ sounding tests to predict pile capacity. This research report compared eight CPT-based and three PCPT-based methods for potential application of the best performer(s) by the Nebraska Department of Transportation (NDOT) to predict pile capacity. Several statistical as well as non-statistical comparison criteria were adopted. According to the evaluation output, the modified (calibrated) Tumay and Fakhroo (1982) method was found to be the best performer for H-piles and the modified De Ruiter and Beringen (1979) method was found to be the best performer for pipe and precast prestressed concrete piles. LRFD reliability based approach was employed to reach at suitable resistance factors that accounts for the geotechnical uncertainties in the design of pile foundations. For a complete design of pile foundations, the settlement criterion has to be incorporated. The settlement of pile foundations must not exceed a certain tolerable magnitude of settlement to ensure the safety of the structure supported. In this regard, this research project adopted the $t - z$ curve approach to predict pile settlements. Several existing $t - z$ curve approaches based on analytical and numerical techniques were assessed and their relative accuracy was investigated. An easy-to-use software for the computation of settlement was also developed.

PART A
CPT BASED PILE DESIGN

Chapter 1 INTRODUCTION

1.1 Background

Pile foundations are the most common type of foundation systems used by the Nebraska Department of Transportation (NDOT) to support bridge structures. They are the preferred choice over the conventional shallow foundations as they tend to reduce the risk of scouring, which is shown to be the leading cause of bridge failure at water crossings in the United States (Wardhana and Hadipriono, 2003), and offer relatively higher bearing capacity for bridge foundations immediately resting on weak sub-surface conditions. Nebraska has a wide range of geologic conditions across the state, ranging from wind deposited silts and sands, which may be susceptible to scouring and offer reduced bearing capacity, to highly overconsolidated glacial deposits and shallow formations of rocks or rock-like intermediate geomaterials (IGMs) such as limestone, sandstone, and shale, which offer quality bearing strata for driven piles.

The geotechnical design of a pile foundation is concerned with the determination of the safe magnitude of an external load the foundation can carry without jeopardizing the stability of the supported structure. To achieve this, a factor of safety or a resistance factor is usually applied to the predicted ultimate or nominal bearing capacity (simply termed as pile capacity), which is the amount load required to initiate shear failure of the foundation. Most importantly, the geotechnical design must ensure that the anticipated super-structural loading is sufficiently lower than the nominal soil resistance.

Piles may derive their bearing capacity through shaft and/or toe resistances depending on the type of pile used. Displacement piles (e.g. closed end pipe piles, precast prestressed concrete piles) derive their capacity predominantly from shaft resistance, whereas in non-displacement piles (e.g. H-piles), toe resistance is a predominant source of the total pile capacity. NDOT typically uses driven steel H-piles, steel closed-end pipe piles (pipe pile), and precast prestressed concrete piles (PPC), specifies H-piles for toe resistance controlled designs, and pipe piles and PPC for shaft resistance controlled designs.

Pile capacity may be determined based on the following methods: Static analysis (analytical), full-scale field static, dynamic, or statnamic loading tests, pile driving formulas and analysis based on in-situ sounding tests. In recent years, in-situ sounding tests are becoming a more attractive method for determing pile capacity due to the rapid development of testing instruments, improved understanding of their mechanics and interpretation, and reduced cost as compared to full scale pile loading tests (Eslami and Gholami, 2006; Eslami et al., 2011). Among the available in situ tests, the standard penetration test (SPT) and the CPT are the commonly used tests for the design and analysis of piles (Bandini and Salgado, 1998). In contrast to the SPT, the CPT is superior in terms of application to pile analysis and design as the load bearing mechanism in CPT is similar to the load bearing mechanisms in actual driven piles. In fact, pile capacity prediction has been the earliest application of CPT (Abu-Farsakh and Titi, 2004). However, due to the difference in the size and penetration rate between CPT and the actual pile, intermediate factors that account for these effects are required to relate CPT results with pile capacity.

Prediction of pile capacity based on CPT generally follows two main approaches: (1) a direct approach, and (2) an indirect approach. In a direct approach, pile capacity is directly associated with the CPT cone tip resistance, (q_c), and/or the local sleeve friction, (f_s). Whereas in an indirect approach, q_c and f_s are first used to evaluate the soil strength parameters and these parameters are then used to evaluate pile capacity based on static analysis (Cai et al., 2009). Several direct CPT-based pile design and analysis methods have been proposed in the past such as Schmertmann (1978); De Ruiter and Beringen (1979); Bustamante and Gianeselli (1982), etc. With the improvement of the traditional CPT into the piezocone penetration test (PCPT) with the inclusion of pore pressure, (u), measurement capability, some PCPT-based methods were also proposed. For example, Almeida et al. (1996); Eslami and Fellenius (1997) and Takesue et al. (1998), used the pore pressure measurements in addition to q_c and f_s. The ever-increasing demand of driven piles as well as a reliable and cost efficient pile design method necessitated frequent evaluations of the CPT/PCPT-based methods with regard to the more reliable static loading tests (e.g. Briaud and Tucker, 1988; Abu-Farsakh and Titi, 2004; Cai et al., 2009) or dynamic loading tests (e.g. Eslami et al., 2011; Nguyen et al., 2016) for local calibrations.

The static loading test is considered the best method to obtain reliable pile capacity (e.g Nguyen et al., 2016). However, the testing procedure is time consuming and costly (Eslami et al., 2011). On the other hand, the dynamic loading test method is fast, requires little space, allows verification of structural integrity of piles while driving, and provides substantial cost savings (Likins and Rausche, 2008). Yet, this method may require an experienced personnel having adequate understanding of stress wave propagation in piles for the interpretation of the test results. NDOT uses a dynamic load testing method to verify the bearing capacity of driven piles. One of the most widely used dynamic load testing systems by NDOT is the Pile Driving Analyzer (PDA), which is manufactured and supported by *Pile Dynamics Inc*. NDOT first implemented the PDA in early 2000. The test utilizes force and acceleration signals received by strain gauges and accelerometers attached to the pile head to estimate pile capacity based on the concepts of stress wave propagation. Alongside PDA, the pile capacity may be obtained using a computer program called the Case Pile Wave Analysis Program (CAPWAP), which is a more complex but reliable and accurate method. CAPWAP utilizes the data collected via PDA for post pile capacity analyses. Basically, it relies on signal matching analysis between the measured (obtained from PDA) and computed signals (obtained by varying the static and dynamic behavior of the soil and distribution of resistance along the shaft and toe of the pile). The analysis iterates through different possible and reasonable soil resistance distribution along the shaft and toe and static and dynamic properties of the soil until a best match is obtained between the measured and computed signals. The signal matching could be performed interactively or automatically. Moreover, several researchers (e.g. Likins and Rausche, 2004) have validated a good correlation between pile capacities predicted from dynamic (CAPWAP) and static loading tests.

1.2 Problem Statement

The CPT/PCPT based methods use different approaches to determine toe resistance and shaft resistance of piles, and each of these methods presumably have strengths and limitations related to pile type and soil conditions. Thus, further evaluations and proper calibration of the methods is required to apply them for Nebraska soil conditions. The incorporation of

CPT/PCPT-based method into the current NDOT pile design practice may enhance bearing capacity predictions by relying on shear strength of soils predicted from in-situ tests rather than laboratory tests, which are performed on a non-representative boundary conditions as well as samples subjected to disturbances during sampling and transportation. This means that the CPT/PCPT based methods may substantially alleviate major limitation of laboratory testing. Furthermore, they will provide a higher resolution (pile capacity predicted at, for example, 0.02 m interval) leading to a more detained bearing capacity prediction at an appreciably reduced design cost.

1.3 Objectives of the Study

The objective of this research was to evaluate eight CPT-based and three PCPT-based pile capacity prediction methods for driven piles in Nebraska and propose a CPT/PCPT-based pile design method. The well-known CP- based methods evaluated in this study were: Aoki and de Alencar (1975); Clisby et al. (1978); Schmertmann (1978); De Ruiter and Beringen (1979); Philipponnat (1980); Tumay and Fakhroo (1982); Price and Wardle (1982) and Bustamante and Gianeselli (1982). The PCPT methods were: Almeida et al. (1996); Eslami and Fellenius (1997) and Takesue et al. (1998). Data that had the following records were collected from NDOT: (1) driven pile records, (2) dynamic load test data, (3) boring information, and (4) PCPT records. A PCPT record excluding the pore pressure measurement was used as a CPT record. The pile database mainly consisted of H-piles, pipe piles, and PPC piles. The dynamic load test data (CAPWAP) was used as a reference pile bearing capacity for the purpose of the evaluation. The evaluation and suggestion of a bearing capacity determination method was carried out in two stages; first, calibration factors were computed for H-piles, pipe piles, and PPC piles, separately which were applied to the toe and skin friction resistances obtained based on the CPT/PCPT methods. This was done by optimizing the CPT/PCPT predicted pile capacity (Q_p) and PDA measured pile capacity (Q_m) values using Excel Solver add-in. Then, in the second stage, evaluation of the best performing method out of all was performed based on combinations of the techniques used in Abu-Farsakh and Titi (2004); Eslami et al. (2011), that is by using rank index (RI).

RI is comprised of other sub-ranks obtained from the following criteria:

1. The slope of the best fit line between Q_p and Q_m and the square root of the residual sum of squares ($\sqrt{RSS}$) between perfect prediction ($Q_{p,best}$) and Q_p.
2. The coefficient of variation (COV) of Q_p/Q_m.
3. The 50% (P_{50}) and 90% (P_{90})cumulative probabilities.
4. The ±20% accuracy from histogram and lognormal distribution of Q_p/Q_m.

The *RI* for a given method was computed by summing up ranks computed from each criterion. The method with the lowest *RI* was considered the best performing method. After the determination of the best performing method(s), a comparison of the proposed CPT based methods with the currently adopted LRFD based EN (engineering news) driving formula by NDOT was conducted using a risk analysis (Briaud and Tucker, 1988) to assess the difference in terms of reliability. Finally, LRFD reliability based analysis was performed to reach suitable resistance factors. These factors allowed the determination of design pile capacity to account for the geotechnical uncertainties related to soil property variability and variability in pile capacity predictions by the proposed CPT-based methods.

Chapter 2 LITERATURE REVIEW

2.1 Introduction

Prediction of pile capacity is regarded as a difficult task due to the involvement of several factors affecting the capacity and their uncertainties. For example, in static analysis of pile capacity, since incorporation of all these factors is impractical, different assumptions and simplifications are taken into account. These assumptions and simplifications along with the uncertainties of input parameters makes static analysis prone to accumulated errors. In light of this, the best way to predict pile capacity is commonly considered to be the static pile loading test. However, the test procedure is time consuming and costly (Eslami et al., 2011).

A dynamic loading test is an alternative to the static pile loading test, which is cost efficient and relatively fast. The test requires little space and allows verification of pile integrity while driving. Studies have proven the reliability of the dynamic methods by comparing them with static loading test results (e.g. Likins and Rausche, 2004). In spite of this, the interpretation of the test results may require experienced field personnel having a thorough understanding of stress wave propagation in piles after an applied impact load on the pile head.

To circumvent the limitations of pile loading tests in general, studies have tried to correlate pile loading test results with the more versatile in-situ sounding tests, such as: SPT and CPT/PCPT. The primary advantage of these correlations based on in-situ sounding tests is that pile capacity could be obtained without the need to drive full scale piles in the field, which may alleviate the associated cost and time for mobilization of resources, installation, and testing of the pilot pile. Although the literature shows that both SPT and CPT/PCPT are used for prediction of pile capacity, CPT/PCPT is considered to be superior over SPT in this particular application area. This is mainly due the fact that the mechanics

of CPT/PCPT resembles piles more than SPT does. Furthermore, the CPT/PCPT can offer continuous sounding results as opposed to discrete results from SPT that makes it more ideal when pile capacity prediction at a higher resolution is needed. In this chapter, a detailed review of the well-known CPT/PCPT based pile capacity prediction methods is performed. In addition, the fundamentals of a high strain dynamic loading test (HSDPT), from which the reference pile capacities were obtained in this study, is reviewed.

2.2 Pile Capacity from CPT/PCPT Results

The cone penetration test (CPT) and its upgraded version, the piezocone penetration test (PCPT) has gained popularity for the characterization and evaluation of in-situ properties of soil layers. In this test, a series of cylindrical rods with a cone at the end is pushed into the ground at a constant rate and the cone tip resistance, q_c, sleeve friction, f_s resistance, and pore water pressure, u are measured. Although the test is primarily suited for soft soils, it can be conducted in stiff to very stiff soils and in some cases, soft rocks with the modern high capacity pushing equipment. CPT/PCPT is advantageous to other in-situ tests in that: (1) it provides continuous profile q_c, f_s, and (u), (2) it is repeatable and reliable, (3) its relatively low cost, (4) fast operation, and (5) strong theoretical basis for interpretation. The main limitations are: (1) it is not suitable in gravel/cemented layers, (2) there is no soil sample during penetration (testing), and (3) there is relatively higher capital investment (Robertson and Cabal, 2010). The most commonly used cross sections of a PCPT penetrometer are those with 10 cm^2 and 15 cm^2 projected area, as shown in Figure 2.1. The standard penetration rate is 2 cm/s. The interval of reading can be maintained as low as 20 mm but not more than 200 mm as most standards require the reading interval to be at least below 200 mm (Robertson and Cabal, 2010).

One of the oldest applications of the CPT is the prediction of the bearing capacity of piles (Abu-Farsakh and Titi, 2004). The close similarity of the mechanics between CPT and driven piles lead to the correlation between the two. The measurements taken during CPT/PCPT, which are the q_c and f_s, are analogous to the load bearing mechanism of piles through pile toe resistance and shaft resistance, respectively. However, due to the difference in the scale

Figure 2.1: Range of PCPT penetrometers (source: Robertson and Cabal 2010)

and penetration rate between CPT/PCPT and actual piles, correlation factors that account for these differences are required to match CPT/PCPT results with pile capacity.

The prediction of pile capacity from CPT/PCPT results follow either an indirect approach or a direct approach (Cai et al., 2009). In an indirect approach, the CPT/PCPT results are used to estimate the shear strength characteristics of the bearing soils, and then theoretically/semi-theoretically developed equations are used to estimate the pile bearing capacity. Mostly, empirical correlations are used to obtain shear strength properties of soils in this approach, which makes it prone to accumulated errors from errors in the empirical correlations as well as in the theoretical equations used to predict the bearing capacity. To the contrary, in a direct approach, the CPT/PCPT results are used directly, without an intermediate step, to estimate the pile bearing capacity. This approach is advantageous as the amount of errors induced in the estimation of the bearing capacity could be substantially reduced by skipping the intermediate step. Because of its relative merit, the direct approach is adopted in this study.

2.3 *Pile Capacity Based on Direct Approach*

The general equation applied for the prediction of pile capacity is given by Eq. 2.1. The pile capacity, (Q_u), is obtained by summing the toe resistance or base resistance, (Q_t) and shaft resistance (shaft resistance) (Q_s).

$$Q_u = Q_t + Q_s = r_t A_t + \sum_{i=1}^{n} r_{s(i)} A_{s(i)} \tag{2.1}$$

where r_t = unit toe resistance [F/L^2], $r_{s(i)}$ = unit shaft resistance for the i^{th} soil layer [F/L^2], A_t = pile toe area [L^2], and $A_{s(i)}$ = pile shaft area along the i^{th} soil layer [L^2]. The bearing mechanism of piles is shown in Figure 2.2.

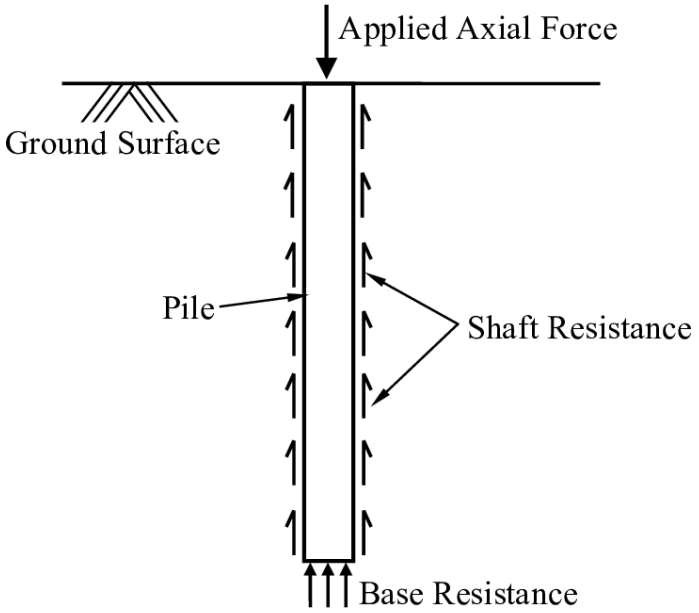

Figure 2.2: Load resistance mechanism of pile foundation (source: Basu et al. 2008)

Pile capacity mainly depends on the type of pile and the soil condition in which the piles are embedded. Because of this, the CPT/PCPT based methods based on the direct approach incorporate several different correlation factors, which depend on the type of piles and soils. In this study, Eight CPT based and three PCPT based methods were selected. A detailed summary of these methods is presented in Table 2.1.

Table 2.1: Summary of the CPT and PCPT methods used in this study

Method	r_t (unit toe resistance)	r_s (unit shaft resistance)	Remark
Aoki and de Alencar (1975)	$r_t = q_{ca}/F_b$; q_{ca} = average cone tip resistance around the pile tip, F_b = 1.75-3.5 depending on the pile type	$r_s = a_s q_{c(side)}/F_s$; q_{side} = average cone tip resistance along the soil layer, F_s = 3.5-7.0 depending on the type of pile, a_s = (1.4-6.0) % depending on the type of soil	CPT-based
Clisby et al. (1978) (Penpile Method)	In clay: $r_t = 0.25 q_{ca}$; In sand: $r_t = 0.125 q_{ca}$	$r_s = f_s/(1.5 + 0.0145 f_s)$; f_s = local sleeve friction in kPa	CPT-based
Schmertmann (1978)	$r_t = (q_{c1} + q_{c2})/2 \leq 15$ MPa; q_{c1} = minimum of the average q_c values from 0.7 to $4B$ below the pile tip, q_{c2} = minimum of q_c values $8B$ above the pile tip, where B = pile diameter	In clay: $r_s = k_s f_s \leq 120$ kPa; k_s = 0.2-1.25. In sand: $Q_s = k[\sum_{d=0}^{4B}(d/8B) f_s A_s + \sum_{d=8B}^{L} f_s A_s]$; d = depth, A_s = lateral surface area, k = depends on D/B ratio, where D = embedment depth.	CPT-based
De Ruiter and Beringen (1979) (European Method)	In clay: $r_t = N_c s_u \leq 15$ MPa, $s_u = q_c a/N_k$, $N_c = 9$, $N_k = 15$ to 20; In sand: The same as Schmertmann (1978)	In clay: $r_s = a s_u \leq 120$ kPa, $a = 1$ for NC clay and 0.5 for OC clay; In sand: $r_s = minimum(f_s, q_c/300, q_c/400, 120$ kPa)	CPT-based
Philipponnat (1980)	$r_t = k_b(q_{ca1} + q_{ca2})/2$; k_b = 0.35-0.50 depending on the soil type, q_{ca1} and q_{ca2} = average q_c within $3B$ above and below the pile tip respectively	$r_s = a_s q_c(side)/F_s \leq 120$ kPa; F_s = 50-200 depending on the soils type, a_s = depends on pile type; a_s = 1.25 for precast concrete pile	CPT-based
Tumay and Fakhroo (1982)	similar to schmertmann (1978)	$r_s = m f_{ca} \leq 72$ kPa; $m = 0.5 + 9.5e^{-0.09 f_{ca}}$; f_{ca} = average friction load [kPa]	CPT-based
Price and Wardle (1982)	$r_t = k_b q_{ca} \leq 15$ MPa; k_b = 0.35 and 0.30 for driving and jacked piles respectively	$r_s = k_s f_s \leq 120$ kPa; k_s = 0.53, 0.62, 0.49 for driven, jacked and bored piles respectively	CPT-based

Method	r_t (unit toe resistance)	r_s (unit shaft resistance)	remark
Bustamante and Gianeselli (1982)	$r_t = k_c q_{ca}$; q_{ca} = average q_c within a zone $1.5B$ above and below the pile tip, k_c = 0.20-0.55 depending on soils type and pile installation method	$r_s = q_c(side)/a_{LCPC}$; a_{LCPC} = 30-200 depending on the soil type, installation method and pile type	CPT-based
Almeida et al. (1996)	$r_t = (q_t - \sigma_{vo})/k_2$; $q_t = q_c + 0.8u_2$: u_2 = pore pressure at the cone shoulder, k_2 = 2.7,1.5,3.4 for driven piles, jacked piles in soft clay, jacked piles in stiff clay respectively	$r_s = (q_t - \sigma_{vo})/k_1$; $k_1 = 11.8+14 \log Q_t$; $Q_t = (q_t - \sigma_{vo})/\sigma'_{vo}$: σ_{vo} = in situ total overburden stress, and σ'_{vo} = in situ effective overburden stress	PCPT-based
Eslami and Fellenius (1997)	$r_t = q_{eq}$: q_{eq} = geometric mean of effective cone tip resistance, (q_e), for a zone $2B$ above and $4B$ below the pile tip for pile installed through a strong to a weak soil layer and $8B$ above and $4B$ below the pile tip for pile installed through a weak to a strong soil layer: $q_e = q_t - u_2$	$r_s = c_s q_e$; c_s = (0.4-8)% depending on the soil type	PCPT-based
Takesue et al. (1998)	In clays: $r_t = q_t - u_2$, In sands: $r_t = 0.1(q_t - u_2)$	For Δu < 300 kPa: $r_s = (\Delta u + 950)f_s/1250$, For 300 < Δu < 1250 kPa: $r_s = (\Delta u - 100)f_s/200$; $\Delta u = u_2 - u_0$, u_0 = initial hydrostatic pore pressure	PCPT-based

2.3.1 Aoki and de Alencar (1975)

Aoki and de Alencar (1975) proposed the following equation, shown in Eq. 2.2 for the prediction of unit toe resistance, r_t:

$$r_t = \frac{q_{ca}}{F_b} \tag{2.2}$$

where q_{ca} = average cone tip resistance around the pile tip [F/L^2], and F_b = empirical factor that depends on the type of pile. F_b is provided in Table 2.2.

Table 2.2: Empirical factors, F_b and F_s

Pile type	F_b	F_s
Bored	3.5	7.0
Franki	2.5	5.0
Steel	1.75	3.5
Precast concrete	1.75	3.5

The unit shaft resistance, r_s, is obtained from the following equation:

$$r_s = \frac{a_s}{F_s} q_{c(side)} \tag{2.3}$$

where $q_{c(side)}$ = average cone tip resistance along the pile shaft [F/L^2], F_s = empirical factor that depends on the type of pile shown in Table 2.2, and a_s = empirical factor that depends on the type of soil shown in Table 2.3.

Table 2.3: Empirical factor a_s in %

Soil type	a_s	Soil type	a_s	Soil type	a_s
Sand	1.4	Sandy silt	2.2	Sandy clay	2.4
Silty sand	2.0	Sandy silt with clay	2.8	Sandy clay with silt	2.8
Silty sand with clay	2.4	Silt	3.0	Silty clay with sand	3.0
Clayey sand with silt	2.8	Clayey silt with sand	3.0	Silty clay	4.0
Clayey sand	3.0	Clayey silt	3.4	Clay	6.0

2.3.2 Clisby et al. (1978)

This method, which is also known as the *Penpile Method*, was proposed by Clisby et al. (1978) for the Mississippi Department of Transportation. The unit toe resistance, r_t, is computed

from Eq. 2.4a and Eq. 2.4b for a pile tip embedded in clay and sand soils, respectively.

$$r_t = 0.25 q_c \tag{2.4a}$$

$$r_t = 0.125 q_c \tag{2.4b}$$

where q_c = cone tip resistance around the pile tip [F/L^2]. The unit shaft resistance, r_s, is computed using the following equation:

$$r_s = \frac{f_s}{1.5 + 0.0145 f_s} \tag{2.5}$$

where f_s = local sleeve friction [kPa].

2.3.3 Schmertmann (1978)

For the determination of toe resistance, the zone of pile tip support was assumed to be within $0.7B$ to $4B$ below the pile tip and $8B$ above the pile tip, where B is the diameter of the pile. Schmertmann (1978) proposed the following relationship to predict unit toe resistance, r_t:

$$r_t = \frac{q_{c1} + q_{c2}}{2} \leq 15 \text{ MPa} \tag{2.6}$$

where q_{c1} = average cone tip resistance of zones ranging from $0.7B$ to $4B$ below the pile tip [F/L^2], and q_{c2} = average cone tip resistances over a distance $8B$ above the pile tip [F/L^2].

Per the Schmertmann (1978), the shaft resistance in sands is estimated based on the following equation:

$$F_s = K \int_{d=0}^{8B} \frac{d}{8B} f_s A_s + \int_{d=8B}^{L} f_s A_s \tag{2.7}$$

where F_s = shaft resistance [F], K = ratio of unit pile friction to unit sleeve friction from Figure 2.3, f_s = local sleeve friction [F/L^2], d = depth to the f_s value being considered [L], B = pile width or diameter [L], A_s= pile-soil contact shaft area [L^2]. The unit shaft resistance in clay soils is obtained as follows:

$$r_s = a_c \bar{f}_s \tag{2.8}$$

where $\bar{f}_s$ = average local sleeve friction [F/L^2], a_c = ratio of pile to penetrometer sleeve friction from Figure 2.4.

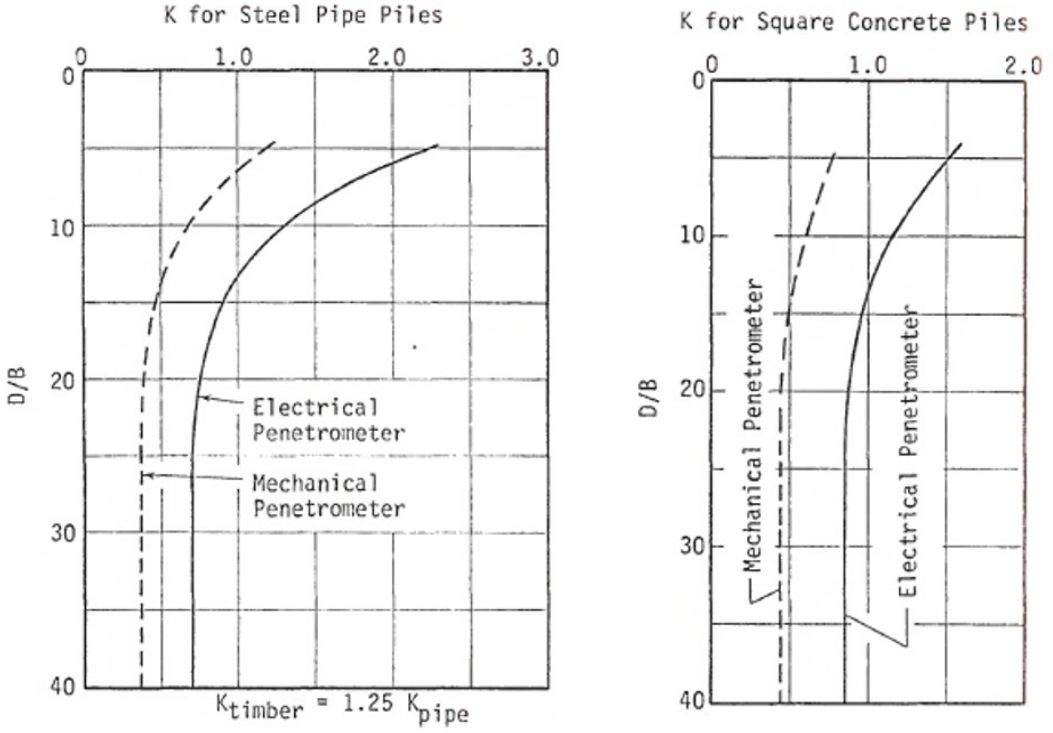

Figure 2.3: Ratio of pile unit shaft resistance to local sleeve friction: (a) steel pipe piles, (b) square concrete piles, after Schmertmann (1978)

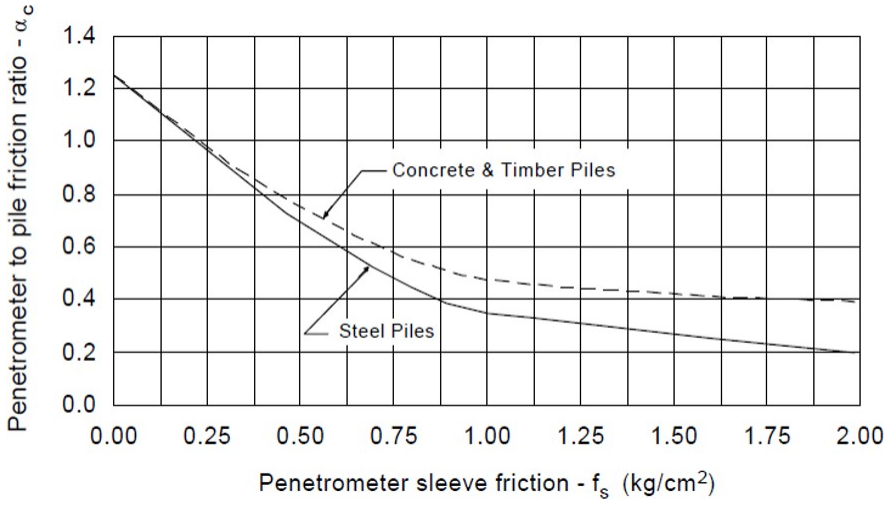

Figure 2.4: Penetrometer to pile friction ratio, a_c, after Schmertmann (1978)

2.3.4 De Ruiter and Beringen (1979)

This method was proposed from a study made in the North Sea and is also known as the *European method*. The unit toe resistance, r_t, of piles embedded in clay soils is given by:

$$r_t = N_c s_u \tag{2.9a}$$

$$s_u = \frac{q_{ca}}{N_k} \tag{2.9b}$$

where N_c = bearing capacity factor = 9, N_k = cone factor typically ranging from 15 to 20, q_{ca}= average cone tip resistance around the pile tip similar to the Schmertmann (1978) method [F/L^2], and s_u = undrained shear strength [F/L^2].

Unit shaft resistance, r_s, in clay soils is estimated using the following equation:

$$r_s = \alpha s_u \tag{2.10}$$

where α = adhesion factor; $\alpha = 1$ for normally consolidated soils and $\alpha = 0.5$ for overconsolidated soils.

In sands, the unit toe resistance, r_t, is computed in the same way as Schmertmann (1978) method while the unit shaft resistance, r_s is given per the following equation:

$$r_s = \min\ f_s,\ q_c/300, 120 \text{ kpa}] \tag{2.11}$$

where min [ ] = minimum of [ ], f_s = local sleeve friction [kPa], q_c = cone tip resistance [kPa].

2.3.5 Philipponnat (1980)

The unit toe resistance, r_t, per this method is given as a function of cone tip resistance as follows:

$$r_t = k_b q_{ca} \tag{2.12}$$

where k_b = bearing capacity factor which depends on the soil type and is given in Table 2.4 and q_{ca} = average cone tip resistance computed as shown in Eq. 2.13.

$$q_{ca} = \frac{q_{ca}(A) + q_{ca}(B)}{2} \tag{2.13}$$

where $q_{ca}(A)$, $q_{ca}(B)$ = average cone tip resistances $3B$ above and below the pile tip respectively [F/L^2].

Table 2.4: k_b values as a function of soil type

Soil type	k_b
Gravel	0.35
Sand	0.40
Silt	0.45
Clay	0.50

The unit shaft resistance, r_s, is calculated from cone tip resistance as follows:

$$r_s = \frac{a_s}{F_s} q_{cs} \leq 120 \text{ kPa} \tag{2.14}$$

where F_s = an empirical factor that depends on the soil type and is given in Table 2.5, and a_s = a factor that depends on pile type. For precast concrete driven piles, a_s = 1.25.

Table 2.5: F_s as a function of soil type

Soil type	F_s
Clay and calcareous clay	50
Silt, sandy clay, and clayey sand	60
Loose sand	100
Medium dense sand	150
Dense sand and gravel	200

2.3.6 Tumay and Fakhroo (1982)

Per (Tumay and Fakhroo, 1982) method, the unit toe resistance, r_t, is computed in a similar fashion with the Schmertmann (1978) method as follows:

$$r_t = \frac{q_{c1} + q_{c2}}{4} + \frac{q_a}{2} \leq 15 \text{ MPa} \tag{2.15}$$

where q_{c1} = average cone tip resistance below $4B$ below the pile tip [F/L^2], q_{c2} = average minimum cone tip resistance $4B$ below the pile tip [F/L^2], and q_a = average minimum cone tip resistance $8D$ above the pile tip [F/L^2], where B is the pile diameter [L].

The unit shaft resistance, r_s, is proposed as shown below:

$$r_s = mf_{ca} \leq 72 \text{ kPa} \tag{2.16}$$

where f_{ca} = average load friction [F/L^2] given in Eq. 2.17, and m = friction coefficient given in Eq. 2.18.

$$f_{ca} = \frac{\sum_{i=1}^{N} f_i \Delta z_i}{\sum_{i=1}^{N} \Delta z_i} \tag{2.17}$$

where f_i = local sleeve friction at the ith soil layer [F/L^2], Δz_i = depth of the ith soil layer, and N = total number of soil layers.

$$m = 0.50 + 9.5 \exp(-0.09 f_{ca}) \tag{2.18}$$

2.3.7 Prince and Wardle (1982)

According to this method, the unit toe resistance, r_t, of piles was estimated from the cone tip resistance, q_c, using the following equation:

$$r_t = k_b q_c \leq 15 \text{ MPa} \tag{2.19}$$

where k_b = an empirical factor that depends on the pile type. For driven piles, $k_b = 0.35$ and for jacked piles, $k_b = 0.3$.

The unit shaft resistance, r_s, is computed from the local sleeve friction, f_s, obtained from a CPT test using the following relationship:

$$r_s = k_s f_s \leq 120 \text{ kPa} \tag{2.20}$$

where k_s = an empirical factor that depends on the pile type. For driven piles, k_s =0.53, for

jacked piles, $k_s = 0.62$, and for bored piles $k_s = 0.49$.

2.3.8 Bustamante and Gianeselli (1982)

This method was proposed by Bustamante and Gianeselli (1982) based on analyses of 197 pile loading tests with various bearing strata conditions. It is also known as the *LCPC (Laboratoire Central des Ponts et Chausees) method*. The unit toe resistance, r_t, per this method is as follows:

$$r_t = k_c q_{ca} \tag{2.21}$$

where k_c = bearing capacity factor given in Table 2.6, and q_{ca} = average cone tip resistance [F/L^2] determined based on the procedure outline in Figure 2.5.

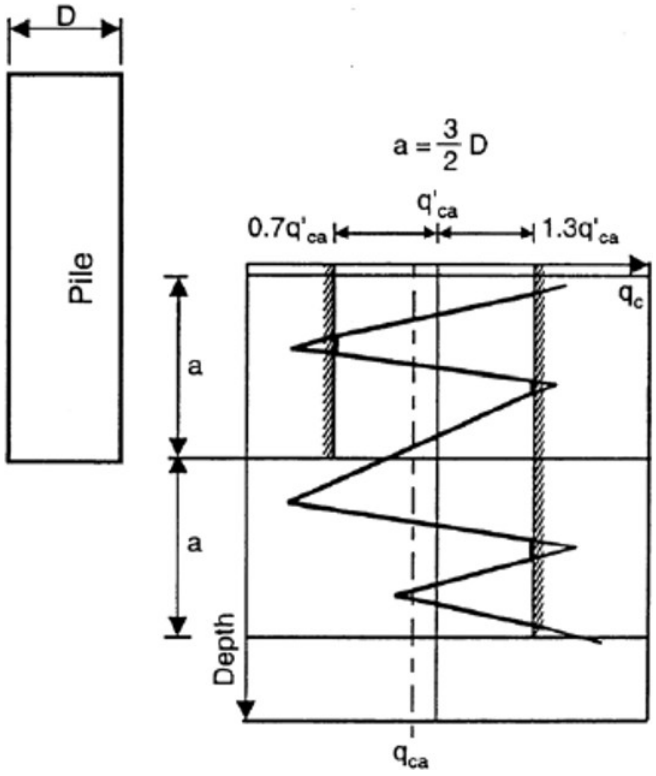

Figure 2.5: Procedure for calculation of q_{ca}, after Bustamante and Gianeselli (1982)

The unit shaft resistance, r_s, is estimated from the following equation:

$$r_s = \frac{q_c(side)}{a_{LCPC}} \tag{2.22}$$

Table 2.6: k_c as a function of soil and pile type

Nature of soil	q_c [MPa]	k_c	
		Group I [1]	Group II [2]
Soft clay and mud	1	0.40	0.50
Moderately compacted clay	1 to 5	0.35	0.45
Silt and loose sand	5	0.40	0.50
Compacted to stiff clay and compacted silt	5	0.45	0.55
Soft chalk	5	0.20	0.30
Moderately compacted sand and gravel	5 to 12	0.40	0.50
Weathered to fragmented chalk	5	0.20	0.40
Compacted to very compact sand and gravel	12	0.30	0.40

[1] plain bored piles; mud bored piles; micro piles (grouted under low pressure); cased bored piles; hollow auger bored piles; piers; barrettes.

[2] cast screwed piles; driven precast piles; prestressed tubular piles; driven cast piles; jacked metal piles; micro piles (small diameter piles grouted under high pressure with diameter < 250 mm); driven grouted piles (low pressure grouting); driven metal piles; driven rammed piles; jacket concrete piles; high pressure grouted piles of large diameter.

where $q_c(side)$ = cone tip resistance for side layers [F/L^2], and $\alpha_{LCP\ C}$ = friction coefficient given in Table 2.7.

2.3.9 Almeida et al. (1996)

According to this method, the unit toe resistance, r_t, is obtained from:

$$r_t = \frac{q_t - \sigma_{v0}}{k_2} \tag{2.23}$$

where q_t = cone tip resistance corrected for pore pressure effect [F/L^2], σ_{v0} = in situ overburden stress [F/L^2], and k_2 = a factor that depends on the pile and soil types; k_2 = 2.7 for driven piles, k_2 = 1.5 for jacked piles in soft clay, and k_2 = 3.4 jacked piles in stiff clay.

The unit shaft resistance, r_s, is given by:

$$r_s = \frac{q_t - \sigma_{v0}}{k_1} \tag{2.24}$$

Table 2.7: $a_{LCP\ C}$ as a function of soil and pile type

Nature of soil	q_c [MPa]	Category									
		Coefficients, a_{LCPC}				Maximum limit of r_s					
		I		II		I		II		III	
		A [1]	B [2]	A [3]	B [4]	A	B	A	B	A [5]	B [5]
Soft clay and mud	5	30	90	90	30	0.015	0.015	0.015	0.015	0.035	
Moderately compact clay	1 to 5	40	80	40	80	0.035 (0.08) *	0.035 (0.08)	0.035 (0.08)	0.035	0.08	≤ 0.12
Silt and loose sand	≤ 5	60	150	60	120	0.035	0.035	0.035	0.035	0.08	-
Compact to stiff clay and compact silt	> 5	60	120	60	120	0.035 (0.08)	0.035 (0.08)	0.035 (0.08)	0.035	0.08	≥ 0.2
Soft chalk	5	100	120	100	12	0.035	0.035	0.035	0.035	0.08	-
Moderately compact sand and gravel	5 to 12	100	200	100	200	0.08 (0.12)	0.035 (0.08)	0.08 (0.12)	0.08	0.12	≥ 0.2
Weathered to fragmented chalk	> 5	60	80	60	80	0.12 (0.15)	0.08 (0.12)	0.12 (0.15)	0.12	0.15	≥ 0.2
Compact to very compact sand and gravel	> 12	150	300	150	200	0.12 (0.15)	0.08 (0.12)	0.12 (0.15)	0.12	0.15	≥ 0.2

[1] plain bored piles; mud bored piles; hollow auger bored piles; micropiles (grouted under low pressure); cast screwed piles; piers; barrettes.
[2] cased bored piles; driven cast piles.
[3] driven precast piles; prestressed tubular piles; jacket concrete piles.
[4] driven metal piles; jacked metal piles.
[5] driven grouted piles; driven rammed piles.
[6] high pressure grouted piles of large diameter ¿250 mm; micropiles (grouted under high pressure).
* Note: maximum limit unit skin friction f: bracket values apply to careful execution and minimum disturbance of soil due to construction

where k_1 is presented in Eq. 2.25.

$$k_1 = 11.8 + 14 \log Q_t \tag{2.25a}$$

$$Q_t = \frac{q_t - \sigma_{v0}}{\sigma'_{v0}} \tag{2.25b}$$

where Q_t = normalized cone tip resistance, σ'_{v0} = in situ effective overburden stress [F/L^2].

2.3.10 Eslami and Fellenius (1997)

This method was proposed by (Eslami and Fellenius, 1997) based on 102 cases around the world. The unit toe resistance, r_t, is given as follows:

$$r_t = q_{eq} \tag{2.26}$$

where q_{eq} = the geometric mean of the effective cone resistance [F/L^2], q_e, for a zone $2B$ above and $4B$ below the pile tip for a pile installed through a strong to a weak soil layer and $8B$ above and $4B$ below the pile tip for a pile installed through a weak to a strong soil layer [F/L^2]. q_e is given by:

$$q_e = q_t - u_2 \tag{2.27}$$

where q_t = corrected cone tip resistance for pore pressure effect [F/L^2], and u_2 = pore pressure at the cone shoulder [F/L^2].

Per (Eslami and Fellenius, 1997), the unit shaft resistance, r_s, is given by:

$$r_s = c_s q_e \tag{2.28}$$

where c_s = an empirical coefficient, which is a function of soil type and is given in Table 2.8.

Table 2.8: c_s as a function of soil types

Soil type	c_s(%)
Soft sensitive soils	8.0
Clay	5.0
Stiff clay and mixture of clay and silt	2.5
Mixture of sand and silt	1.0
Sand	0.4

2.3.11 Takesue et al. (1998)

In this method, the unit toe resistance, r_t, in clay soils is similar to the Eslami and Fellenius (1997) method. However, the unit toe resistance, r_t, in sand soils is given by:

$$r_t = 0.1 q_t \tag{2.29}$$

where q_t = corrected cone tip resistance for pore pressure effect [F/L^2].

The unit shaft resistance, r_s, is given as function of the measure pore pressure and local sleeve friction during PCPT and is given according to the following equations:

$$r_s = \frac{\Delta u + 950}{1250} f_s \tag{2.30a}$$

$$r_s = \frac{\Delta u - 100}{200} f_s \tag{2.30b}$$

where $\Delta u = u_2 - u_0$, u_0 = hydrostatic pore pressure [kPa], and f_s = local sleeve friction [kPa]. Eq. 2.30a is for Δu < 300 kPa, and Eq. 2.30b is applied for 300 kPa < Δu < 1250 kPa.

2.4 *High Strain Dynamic Pile Testing (HSDPT)*

The high strain dynamic pile testing (HSDPT, ASTM-D4945 2008) has become a popular tool to assess the installation process and bearing capacity of piles (Likins and Rausche, 2008). The key concept behind this test is that measurements retrieved during pile installation could be used to analyze the bearing capacity of piles since the driving process will

induce complete failure of the soils. Several studies have demonstrated the capability of the HSDPT method to predict ultimate bearing capacity of pile accurately by comparing it with the static pile loading test results (e.g. Likins and Rausche, 2004). The HSDPT may offer reliable bearing capacity with relative advantages of overall cost minimization, less required space, and less testing time as compared to static pile loading test. However, the HSDPT needs thorough understanding of wave propagation mechanisms for accurate interpretation of the test results.

The HSDPT is commonly used to verify the load bearing capacity of driven piles by NDOT engineers. One of the commonly used systems is the Pile Driving Analyzer (PDA). The PDA was first used by NDOT in the early 2000s, and is still used today. The system utilizes field instrumentation such as strain gauges and accelerometers attached to the pile head in order to measure the induced force and acceleration in the pile during driving, respectively. Then, soil resistance distribution is obtained by analyzing the data collected based on the concepts of one dimensional wave propagation. The PDA is conducted most of the time towards the end of the installation depth.Typical attachment of the accelerometer and strain gauge to the pile head is shown in Figure 2.6.

Figure 2.6: Accelerometer and strain gauge attached to the pile head

Using PDA, pile capacity may be analyzed in two ways: (1) it can be analyzed and displayed by the PDA system itself (using Case Method), or (2) the PDA data can be processed in a more complex post-PDA analysis computer program called Case Pile Wave

Analysis Program (CAPWAP) for more accurate and reliable prediction. Both cases are discussed in the next subsections.

2.4.1 Pile Capacity by PDA: Case Method

The total soil resistance is evaluated based on the measured force and velocity signals as well as using information such as the pile geometry, pile material density and elastic modulus. Typical force and velocity signals during the dynamic test is shown in Figure 2.7.

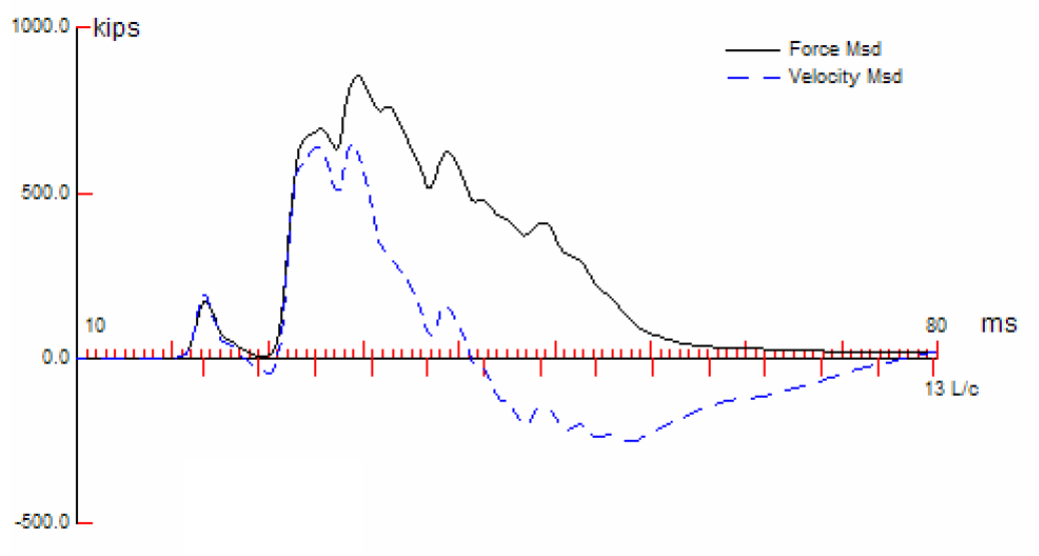

Figure 2.7: Typical force and velocity signals during dynamic test (source: Alvarez et al. 2006)

In the PDA, the Case Method (Rausche et al., 1985) is employed to compute the total soil resistance from the measured velocity and force traces as shown in Eq. 2.31.

$$R(t^*) = \frac{1}{2}\left[F_m(t^*) + F_m\left(t^* + \frac{2L}{c}\right)\right] + \frac{Z}{2}\left[v_m(t^*) - v_m\left(t^* + \frac{2L}{c}\right)\right] \tag{2.31}$$

where R = total soil resistance [F], F_m = measured force [F], v_m = measured velocity [L/T], Z = impedance [M/T] , L = pile length [L], c = stress wave propagation speed (wave speed)

[L/T], and t^* = sampling time [T]. c and Z are given by the following equations:

$$c = \sqrt{\frac{E}{\rho}} \tag{2.32a}$$

$$Z = \frac{EA}{c} \tag{2.32b}$$

where ρ = density of the pile material [M/L^3] and A = pile cross-sectional area [L^2]. Soil resistance calculation using Eq. 2.31 consists of calculation of average internal forces at time interval $2L/c$ apart and average acceleration for the same time interval. It could also viewed be as an equation of motion with an average acceleration resulting from a resultant force between the total soil resistance (external) and average internal forces within the pile. The sampling time, t^*, is usually taken as the time at which the first major velocity peak occurs to ensure enough pile set and mobilization of the soil resistance. Moreover, due to rapid penetration of the pile during impact driving, the total resistance depicted in Eq. 2.31 has a dynamic part (velocity dependent) in addition to the static part (displacement dependent). The total resistance (known quantity) is written as a summation of the static and dynamic resistances as follows:

$$R = R_s + R_d \tag{2.33}$$

where R_s = static resistance [F], and R_d = dynamic resistance [F]. Since the total resistance is known, the static resistance can be obtained if the dynamic resistance is determined. The dynamic resistance is assumed to be proportional to the toe velocity as follows:

$$R_d = Jv_b \tag{2.34}$$

where v_b = velocity of the pile toe [L/T], and J = viscous damping constant [FT/L]. In this case, the damping is assumed to concentrate around the pile (Rausche et al., 1985). By superimposing pile toe velocity in a free pile and pile velocity induced because of soil resistance, and using Eq. 2.31 , the following equation, which represents the static resistance

is obtained.

$$R_s(t^*) = \frac{1}{2}(1 - j_c)\, F_m(t^*) + Z v_m(t^*) \; + \frac{1}{2}(1 + j_c)\, F_m\left(t^* + \frac{2L}{c}\right) - Z v_m\left(t^* + \frac{2L}{L}\right) \qquad (2.35)$$

where $J_c = (1/Z)J$. Rausche et al. (1985) listed typical values of J_c by comparing a static pile loading test and PDA results as shown in Table 2.9.

Table 2.9: Suggested values of J_c (after Rausche et al. 1985)

Soil type in bearing strata	Suggested range, J_c
Sand	0.05-0.20
Silty sand or sandy silt	0.15-0.30
Silt	0.20-0.45
Silty clay and clayey silt	0.40-0.70
Clay	0.60-1.10

The computed static resistance of soils based on the closed form solution shown in Eq. 2.35 assumes a rigid-plastic soil behavior and damping is concentrated around the pile tip. The calculated soil resistance from Eq. 2.35 depends on the selection of J_c, and sampling time, $t*$. Moreover, to be consistent with the assumption of rigid-plastic soil behavior, this method requires sufficient impact energy to be applied on the pile so that the induced pile set is enough to mobilize all the available soil resistance. Thus, in a condition where the hammer energy is small relative to the soil capacity, PDA may underpredict the pile capacity. Because of all the aforementioned reasons, the Case Method is usually considered less reliable and rather taken as a good first indicator of pile capacity (Likins and Rausche, 2008; Rausche et al., 2017).

2.4.2 Pile Capacity by CAPWAP

A more realistic and reliable pile bearing capacity is computed by using CAPWAP (Case Pile Wave Analysis Program) (Likins and Rausche, 2008). Unlike PDA, CAPWAP has additional capabilities to model soil resistance distribution along the pile shaft and at the toe, pile damping, splices, non-uniformity, and multiple shaft materials. It relies on signal matching analysis (SMA) between the measured wave-up signal (obtained from the measured

velocity and force signals) with an artificially generated signal by varying the distribution of soil resistance and other soil parameters along the pile shaft and at the pile toe.

The force, $F(t)$, signal measured at the pile head (sensor location) can be split to downward (wave-down) an upward (wave-up) moving components Rausche et al. (2010):

$$W_d(t) = \frac{1}{2}\left[F_m(t) + Zv_m(t)\right] \tag{2.36a}$$

$$W_u(t) = \frac{1}{2}\left[F_m(t) - Zv_m(t)\right] \tag{2.36b}$$

where W_d = wave-down $[F]$, and W_u = wave-up $[F]$. The wave-down curve primarily represents the input from the hammer system, and the wave-up curve represent reflections from soil resistance and pile non-uniformity. Assuming a uniform pile, the wave-up component measured at the pile head is assumed to represent the soil resistance (Rausche et al., 1985):

$$F_m(t) - Zv_m(t) = \sum_{i=1}^{n} R_i(t) \tag{2.37}$$

where R_i = soil resistance at i^{th} location out of n number of soil resistance concentrations along the pile shaft [F]. This concept is illustrated in Figure 2.8, where the offset between the Zv and F signals is the result of soil resistance. As previously noted, the soil resistance is comprised of the static and dynamic components.

The wave-up SMA proceeds by first assuming the resistance distribution along with soil parameters that define the static (quake) and dynamic (damping) resistances, and then by taking the Zv_m signal as a boundary condition, a complementary artificial force signal is sought until a quality match is obtained with the measured complementary force, F_m, signal. This SMA process may be performed interactively or automatically but, in general, this process could be time consuming as the analysis evolves several unknown parameters (including soil resistance, quake and damping) that need to be varied for the best match (GRL engineers, 2018).

A numerical modeling technique that is either based on the lumped mass finite difference approach (Smith, 1962) or the method of characteristics (de Jong, 1956) is commonly adopted to simulate the soil-structure interaction and perform the SMA. The CAPWAP

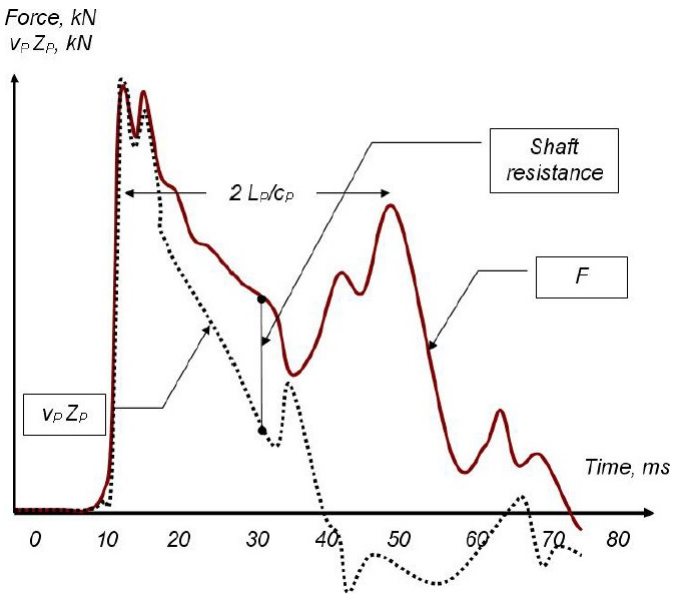

Figure 2.8: A miss-match between F and $\upsilon_m Z$ signals due to soil resistance (Source: Massarsch 2005)

signal mathcing analysis is typically based on the method of characteristics, where the pile is divided into segments of 1 m length with elastic properties and optional pile damping (GRL engineers, 2018). The static and dynamic behavior of the soil is modeled based on the greatly expanded rheological model of Smith (1962), which incorporates elastoplastic soil behavior (represented by spring and slider for the static component), and viscous and radiation damping (represented by dashpot for the dynamic component). These soil resistances are lumped at a certain interval along the pile shaft. A simplified traditional Smith (1962) soil model is shown in Figure 2.9, which constitutes the spring and slider (static) and dashpot (dynamic) systems.

The total soil resistance, which is lumped at a certain pile node, may be expressed as a summation of the static and dynamic resistances, similar to the definition presented in Eq. 2.33 as follows:

$$R(t) = f_{gl} R_s(t) + R_d(t) \tag{2.38}$$

where f_{gl} = gain/loss factor. The gain/loss factor is associated with soil set-up and relaxation after pile driving. This factor is determined by performing a restrike test and by comparing the static resistances during driving and after the restrike test (Rausche et al.,

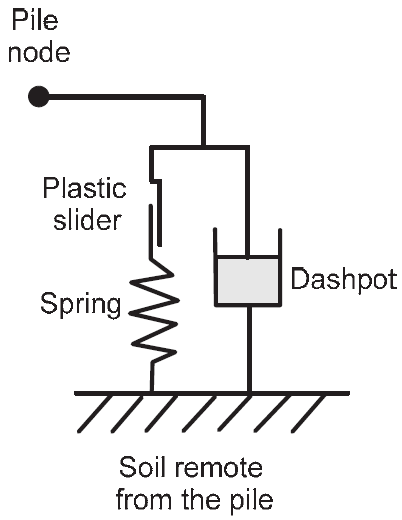

Figure 2.9: Traditional soil resistance model (after Smith 1962)

2010). Generally, f_{gl} is less than unity for the toe resistance while it is greater than unity for the shaft resistance (Rausche et al., 2010).

The static resistance, R_s, versus pile displacement, u, relationship is modeled by a piece-wise linear line, which is defined by soil parameters like *gap* and *quake*. The gap defines the displacement upto which no static resistance develops, and quake defines the displacement in excess of a gap in which the elastic response occurs or the relationship between R_s and u is linear. Any pile displacement in excess of the gap plus quake is regarded as permanent displacement and will mobilize the ultimate soil resistance. Separate values of quake are assigned for the toe and shaft resistances, whereas gap is only assigned to the toe resistance and taken as *zero* for the shaft resistance.

The dynamic resistance, R_d, is defined based on the basic (Smith, 1962) approach as follows:

$$R_d(t) = j_s R_s(t) v_p(t) \tag{2.39}$$

where j_s = smith damping factor [T/L], and $v_p(t)$ = pile velocity [L/T]. Separate values of smith damping, j_s, are assigned to the toe and shaft resistances. Then, the total resistance, R_t could be rewritten as follows (assuming f_{gl} = 1):

$$R(t) = R_s(t) \left(1 + j_s v_p(t)\right] \tag{2.40}$$

Therefore, in CAPWAP SMA, the following main variables are used: (1) assumed static resistance distribution (toe and shaft resistances), (2) toe and shaft quake, and (3) toe and shaft smith damping factors. Typical recommendations for the limits of CAPWAP soil resistance parameters are provided in Table 2.10.

Table 2.10: Recommended values for limits of soil resistance parameters for CAPWAP SMA(after Rausche et al. 2010)

Parameter	Shaft,min	Shaft,max	Toe,min	Toe,max
$quake$	$1\ mm$	$7.5\ mm$	$1\ mm$	$u_{max} - gap$
j_s	$0.04\ s/m$	$1.4\ s/m$	$0.04\ s/m$	$1.4\ s/m$

Match Quality in CAPWAP

The quality of signal matching between the measured and computed wave-up curves is a very important aspect of CAPWAP that determines the accuracy of estimated pile bearing capacity. In this regard, the strength of matching between the two curves is indicated by the quantity, MQ, which stands for $Match\ Quality$ in the CAPWAP user interface window. This value is obtained by summing the absolute values of the difference between the measured and computed wave-up curves. Since this difference has a unit of force, the result is further divided by the maximum measured force to normalize it and make MQ a dimensionless number (Rausche et al., 2010). There is no definite upper or lower bounds of MQ for an acceptable CAPWAP result. In general, by generating the lowest possible MQ value, a good correlation between dynamic and static test results could be achieved (e.g. Likins and Rausche, 2004). Typical range of MQ is from 2 to 4, with values less than 0.5 being nearly impossible and values greater than 6 producing unreliable capacity prediction (Rausche et al., 2010).

Uniqueness of CAPWAP

Due to the large number of variables that need to be specified during the stress wave matching process, the uniqueness of the solution obtained from CAPWAP has been regraded as doubtful (e.g. Danziger et al., 1996; Buckley et al., 2017). Several studies outlined that the particular soil resistance distribution obtained from CAPWAP is highly subjective and

can vary from one user to another. The question of uniqueness mainly emanates from the discrepancy between the number of unknown variables and the number of available equations in the problem. The total number of primary unknowns that could significantly affect the magnitude of mobilized soil resistance are $3N + 3$, where N is the number of nodes on the shaft. Shaft resistance, shaft quake, and shaft damping are unknowns per each node on the shaft. The remaining three unknowns came from toe resistance, toe quake, and toe damping. Although there are other unknowns in the problem, their affect on the predicted soil resistance is negligible and they are only used for cosmetic improvement of the signal matching (Buckley et al., 2017). In contrast, the available equations are equal to the number of shaft and toe resistances (i.e. $N + 1$), as noted in Eq. 2.37. Since the number of unknowns surpass the number of equations, it implies that parameter values in the problem have to be iteratively changed until a good match is obtained. Different users may end up with different sets of best fit soil parameter values leading to non-unique soil resistance distributions.

To investigate the uniqueness of CAPWAP results, Buckley et al. (2017) did signal matching analysis using three independent users/operators on the same PDA result. Based on the study conducted by Buckley et al. (2017), it was found that the CAPWAP soil resistance distribution varied from user to user although the match quality fell within 1.7 to 1.9 for all users. Particularly, a significant difference in the split between shaft and toe resistances were obtained. However, the total resistance was found to vary within a $\pm 10\%$ from the mean among different users.

2.4.3 Pile Setup and Relaxation

Based on extensive field investigations, it is recognized that pile capacity may increase with time. This time dependent increase in pile capacity is known as *pile setup or freeze*. This phenomenon is almost common in all types of driven piles (although more significant in displacement piles) embedded in saturated clay, loose to medium silt, sandy silt, silty sand, and fine sand (Komurka et al., 2003). The opposite of pile setup may occur in piles embedded in dense silts, weathered shale (Rausche et al., 2010), and heavily overconsolidated clays (Jardine and Bond, 1989), where the pile capacity decreases with time. This phenomenon is termed as *pile relaxation or negative pile setup*.

The complete mechanism of pile setup is not fully understood. However, the majority of the pile setup is attributed to the dissipation of pore pressure at the end of driving (EOD) and subsequent increase in effective stress, which in turn causes an increase in soil resistance. Based on this mechanism, a long-term setup is expected in cohesive (e.g. clay) and mixed soils (e.g. clayey fine sand, clayey silt) and, whereas a short-term pile setup is expected in sand soils and gravels. It is reported, however, that a long-term pile setup may occur in fine grained sand soils and silts owing partly due to the breakdown of a driving-induced arching effect on the pile shaft and partly due to aging (effect of creep) (Axelsson, 2002). Moreover, several research findings have indicated that pile setup primarily influences the shaft resistance due to the substantial lateral displacement and eventual stiffening of the adjacent soils during pile installation (Fellenius et al., 2000).

On the other hand, negative pile setup (pile relaxation) could be possible in dilatant soils (e.g. dense to very dense silts and fine sands and heavily overconsolidated soils) where effective stress temporarily increases during pile installation due to the development of a negative excess pore pressure and thereafter, decreases as the negative excess pore pressure is dissipated (Jardine and Bond, 1989; Komurka et al., 2003). In addition to this, weathered shale and weak laminated rocks (Hannigan et al., 1997; Rausche et al., 2010) may experience pile relaxation. As opposed to pile setup, pile relaxation is thought to have more influence on toe resistance than shaft resistance (Komurka et al., 2003; Rausche et al., 2010).

Incorporating the effect of pile setup/relaxation in the design of piles can provide an economical design by either reducing the length or the number of piles required in the design. However, the availability of reliable and feasible methods to obtain the magnitude of pile setup/relaxation is seldom (Ng et al., 2012). In current practice, measurement of pile setup/relaxation may be possible based on static or dynamic tests (restrike test) conducted at different times after EOD. However, when using these tests, the cost saving by accounting pile setup/relaxation into the pile design often needs to be justified with the cost of performing the tests for an extended period. Apart from direct measurement using instrumented field tests, empirical correlations has been proposed in the literature (e.g. Skov and Denver, 1988) to predict pile setup in particular. These equations are site specific and may need calibration using restrike tests to determine some of the constants in the equations; plus, they are not

extensively validated for practical application (Ng et al., 2012).

2.5 *Conclusions*

The general form of the CPT/PCPT-based methods reviewed is similar. However, each method proposed different values for the empirical coefficients depending on the type of pile and soil conditions they were derived in. Since the methods are site specific, their application to a different site condition should be preceded by proper evaluations and calibrations of the methods using reliable pile capacities determined from either static or dynamic loading tests (HSDPT).

Several studies have shown the validity of the HSDPT to be a reliable approach to predict pile capacity through comparative studies with static load test results. Besides its reliability, the HSDPT is advantageous because it provides cost savings, and requires less space as well as less testing time. One of the widely-used HSDPT system is the PDA. The PDA may provide pile capacity in two ways: one is within the PDA system itself and the other is using a post analysis tool called CAPWAP. Due to a more detailed modeling of the soil-structure interaction in CAPWAP, it is regarded as a more reliable and accurate tool to obtain pile capacity as compared to the results obtained from the built-in logic within the PDA. Due to the involvement of several unknown parameters in CAPWAP analysis, the uniqueness of the soil resistance distribution obtained by this method has been questionable. Furthermore, the CAPWAP provides pile capacity available at the time of testing. But, multiple studies have shown that pile capacity may vary with time due the effect of pile setup/relaxation. The pile setup/relaxation phenomenon is primarily a function of soil type and pile geometry. Moreover, pile setup is usually more pronounced on the shaft resistance, and pile relaxation is prominent on the toe resistance. To account for these effects, usually a restrike test is conducted after a certain period of elapsed time from EOD.

Chapter 3 METHODOLOGY

3.1 Introduction

The primary objective of this research was to evaluate different CPT/PCPT-based pile prediction models and propose a modified method that is applicable for Nebraska soil conditions. To achieve this goal, data were collected from NDOT for bridge site locations that had the following records: (1) driven pile records, (2) dynamic load test data, (3) boring information, and (4) PCPT records. These data were used to evaluate the in-place capacity of the piles (considered as measured pile capacity) installed at the bridge sites. On the other hand, the CPT/PCPT-based methods discussed in the previous chapter were used to predict pile capacities. The measured and predicted pile capacities were compared and evaluated to distinguish the best performing method(s) using the rank index (*RI*). Furthermore, the same PCPT data excluding the pore pressure measurements was used in the CPT-based methods.

3.2 Test Sites

The test sites were selected in order to obtain representative soil conditions for the majority of the existing bridge site locations as well as potential future bridge foundation work. Two factors primary influenced the selection of the test sites. First, not all soil conditions in Nebraska are favorable for PCPT investigations; second, the availability of the load test data (PDA).

Sites with significant layers of dense sand and gravel that offer high bearing resistance at relatively shallower depths are difficult to be penetrated by the pushed CPT equipment. This is certainly one of the limitations of the CPT (Robertson and Cabal, 2010). Thus, most of the sites selected are composed of softer, and fine-grained materials. In fact, as pile

foundations are normally required in such soil conditions, it is logical to restrict the site selection tending towards these types of materials. Although sites with relatively thin layers of granular (coarse grained) soil conditions were included in the bearing capacity evaluations, those sites with thick layers (more than 15 m) of dense sand and gravel (highly angular), which are typically abundant in the western Nebraska, were disregarded.

In NDOT practice, the PDA is mainly used as a verification to ensure whether the design capacity is met and to monitor pile drivability to help construction engineers decide project-specific pile driving adjustments. Considering this, PDA is usually conducted on piles that support structures of high importance and with high load capacity. In other scenarios, the PDA is implemented on structures selected based on cost/benefit analysis, and the variability of the soil condition. Thus, bridge structures that had complete PCPT logs as well as PDA results were compiled and used for further analyses. Figure 3.1 shows the location of sites selected in this study.

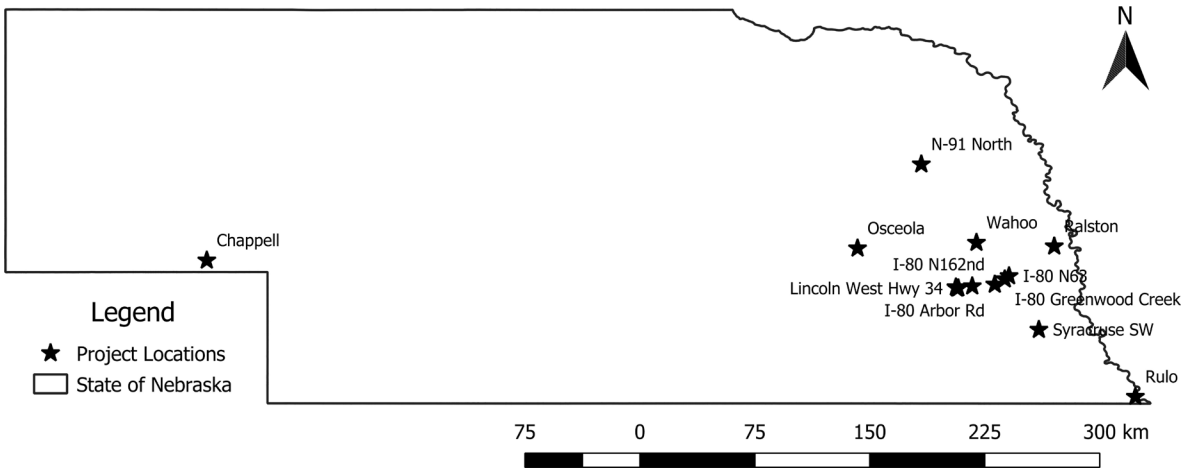

Figure 3.1: Locations of sites selected in this study

The site selection process resulted in a total of 14 projects which are comprised of 16 bridges structures. Each bridge structure was further comprised of substructures (i.e. Abutments and Piers). For each substructure, their corresponding PCPT and PDA results were organized. In some cases, common PCPT data was shared for two substructures which are adjacent to each other. In other cases where quality PDA results exist but PCPT data is absent, NDOT staff conducted new PCPT to have a complete data set of PDAs as well as

PCPT.

3.3 Piles

The pile data base consisted of steel H-piles, closed end pipe piles and precast prestressed concrete (PPC) piles. H-piles most commonly used by NDOT are HP10x42, HP12x53, and HP14x89 sizes. Steel pipe piles are almost all 12.75" O. D. with 3/8 in. wall thickness and welded plate bottoms. A prestressed concrete pile used by the state can be square, circular, or hexagonal with 28-day strength ranging from 4000-5000 psi. In this study H-piles, pipe piles, and square precast prestressed concrete piles (PPC) were evaluated. 45 H-piles, 41 pipe piles, and 6 PPC cases were analyzed.

3.4 PCPT Data

PCPT data was acquired from the logging software in [*.csv] format. The log information consisted of depth, tip resistance (q_c), local sleeve friction (f_s), and pore pressure at the cone shoulder (u_2) data that was measured as the cone penetrated through the ground. The PCPT data also provided soil classification based on the Robertson et al. (1986) soil behavior type (SBT) chart.

3.5 Soil classification

Soil classification was necessary in order to determine the appropriate values of empirical coefficients, which are dependent on the type of soils in the CPT/PCPT-based methods. To alleviate the need for soil sampling and subsequent laboratory testing to classify the soils, the PCPT data itself was used to identify the type of soils based on previously established CPT-based soil classification methods. Several CPT-based soil classification charts had been proposed in the past (Douglas and Olson, 1981; Robertson et al., 1986; Robertson, 1990). Among these methods, the Robertson et al. (1986) soil classification results at 2 cm interval were directly available along with q_c, f_s, and u_2 data.

The Douglas and Olson (1981) soil classification method was regarded as the most comprehensive. However, it is too complicated for practical application (Bloomquist et al., 2007). After that, Robertson et al. (1986) came up with a soil behavior type (SBT) classification chart that was easier to apply. Despite its simplicity, it had one major shortcoming in that the effect of the depth of penetration on the cone tip resistance values was not incorporated in the soil classification scheme (Bloomquist et al., 2007). For this reason, it is believed that some error could be introduced eventually when this chart is used to classify soils below 30 m (100 ft). However, since most on-shore pile foundations are within this range, this shortcoming may not pose a significant problem. Later on, by properly accounting for the effect of depth, Robertson (1990) proposed an updated normalized soil behavior type chart (SBT_n) where, the cone tip resistance was normalized with the overburden stress to address the influence of depth.

To this end, the CPT-based soil classification chart proposed by Robertson et al. (1986) was used in this study considering that: (1) the pile foundations in NDOT's bridge construction practice may not extend beyond 30 m, (2) the Robertson et al. (1986) soil classification output was readily available within the PCPT data acquired from NDOT, and (3) the method was easier to apply and implement in program coding. The Robertson et al. (1986)classification chart is shown in Figure 3.2 below.

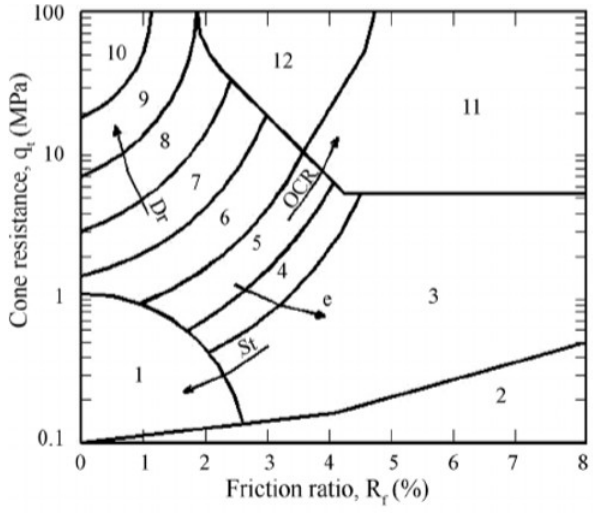

Zone	Soil behavior type
1	sensitive fine grained
2	organic material
3	clay
4	silty clay to clay
5	clayey silt to silty clay
6	sandy silt to clayey silt
7	silty sand to sandy silt
8	sand to silty sand
9	Sand
10	Very stiff fine grained (overconsolidated or cemented)
11	Very stiff fine grained
12	Sand to clayey sand

Figure 3.2: Soil Behavior Type (SBT) chart, after Robertson et al. (1986)

3.6 Dynamic Load Test Data

The CAPWAP processed PDA signals are used to yield the reference pile capacities. For the purpose of this study, PDA results over the entire installation length of the pile were used because this could maximize the utilization of a single PCPT data for several CPT-PDA correlations at different depths. The match quality, MQ, was kept as low as possible to ensure accurate pile capacity predictions.

Owing to the uncertainty about the uniqueness of CAPWAP soil resistance distribution, which may result in an unreliable split between shaft and toe resistances, this study used the gross soil resistance as a reference pile capacity. Thus, the gross pile capacity predicted via CAPWAP is evaluated against the summation of toe and shaft resistances predicted via CPT/PCPT-based methods.

Moreover, the effect of pile setup/relaxation effects needs to be addressed. From the general soil condition of Nebraska, it is possible that driven piles, especially in eastern Nebraska, may pass through cohesive soils, fine grained granular soils, and overconsolidated glacial tills. Therefore, it is expected that both short-term as well as long-term pile setup may be possible. On top of this, the presence of overconsolidated soils and shale also present the possibility of pile relaxation. Thus, appropriate evaluation needs to account for both pile setup and relaxation in the pile capacity evaluation. The current dynamic test results (PDA) available in this study corresponds to EOD condition and unfortunately, due to the lack of restrike pile capacity data set along with the EOD data set, the quantification of pile setup/relaxation for a reasonably accurate pile capacity evaluation was not performed in this study. The use of empirical equations was not favored as they are mainly proposed to predict pile capacity increment (setup), and they may result in unnecessarily overestimating the pile capacity because the effect of relaxation may prevail as well. Based on engineering judgment, the effect of pile setup/relaxation was disregarded in this study. The increase in shaft resistance (setup) may be counterbalanced by the decrease in the toe resistance (relaxation) and disregarding the effect of pile setup/relaxation may be justified in this regard. However, the authors suggest collecting and analyzing future EOD and restrike dynamic test results for the assimilation of Nebraska-specific pile setup/relaxation factors in the future.

3.7 In Place Pile Capacity from Pile Driving Records

Driving records were also used to predict the pile capacity using the current NDOT LRFD (load resistance factor design) approach based on the EN (Engineering News) formula as shown in Eq. 3.1. This equation represents an official and well-verified bearing capacity estimation method for driving piles in Nebraska.

$$\varphi Q_u = \frac{4E}{s + 0.5} \tag{3.1}$$

where Q_u = ultimate (nominal) pile capacity [F], E = hammer energy defined by $E = WH$, where W = ram weight of the hammer [kips], H = fall height of the ram [ft.], and s = pile set [in/blow], and φ = resistance factor = 0.7. The proposed CPT/PCPT-based method was compared with pile capacities estimated based on Eq. 3.1.

3.8 Evaluation Methodology

Performance evaluation of the CPT/PCPT-based methods was performed using statistical analyses as well as non-statistical analyses. Several researchers adopted the same technique to assess the prediction capability of CPT/PCPT based methods in the past (e.g. Briaud and Tucker, 1988; Long and Wysockey, 1999; Abu-Farsakh and Titi, 2004; Cai et al., 2009; Nguyen et al., 2016). Relying entirely on statistical analyses may lead to misleading conclusions regarding the performance of the methods (Briaud and Tucker, 1988). Thus, it is usually recommended to inspect the predicted versus measured pile capacity plots before passing judgment on the prediction capability of a method.

Henceforth in this report, the measured pile capacity, which was obtained from CAPWAP, is designed by Q_m and sometimes also referred to as $Q_{P\ DA}$ in this report; the predicted pile capacity, which was obtained based on the CPT/PCPT methods, is designated by Q_p and sometimes will be designated as $Q_{CP\ T}$. The ratio Q_p/Q_m has an optimum value of 1 for a perfect prediction ,and away from this optimum scenario, it may be less than unity or

greater than unity for underprediction and overprediciton, respectively. The least possible Q_p/Q_m is 0 and the highest is positive infinity ($+\infty$).

Before carrying out the evaluation of the CPT/PCPT-based methods, piles were categorized as displacement and non-displacement piles as the mechanism of load support is different in these types of piles. In this regard, H-piles were categorized under non-displacement piles, where toe resistance is assumed to be the predominant source of total pile capacity. On the other hand, pipe piles and PPC were categorized as displacement piles in which major load resistance comes from shaft resistance.

Thereafter, different statistical and plot-based evaluation schemes were applied to the ratio Q_p/Q_m in order to assess the relative accuracy and precision of the CPT/PCPT-based methods. The accuracy and precision of prediction is mainly depicted by the central tendency or the mean and the standard deviation of Q_p/Q_m, respectively(Briaud and Tucker, 1988). The particular method is accurate if the mean is closer to 1 ,and precise when the standard deviation is closer to zero. Based on previous works, statistical criteria incorporating the above measures as well as other non-statistical measures that showed the quality of Q_p vs Q_m plots were used in the evaluation process (Briaud and Tucker, 1988; Long and Wysockey, 1999; Abu-Farsakh and Titi, 2004; Eslami et al., 2011). The evaluation scheme adopted the following four criteria:

1. The slope of the best fit line between Q_p and Q_m and the square root of residual sum of squares ($\sqrt{RSS}$) between perfect prediction ($Q_{p,best}$) and Q_p.
2. The coefficient of variation (COV) of Q_p/Q_m.
3. The 50% (P_{50}) and 90% (P_{90})cumulative probabilities.
4. The $\pm$20% accuracy from histogram and lognormal distribution of Q_p/Q_m.

A rank (R_i) was used to indicate the performance of a given CPT/PCPT-based method for the i^{th} criterion. Finally, a rank index (RI) was used to determine the overall performance by simply summing each R_i from each criterion, as shown in Eq. 3.2. The method with the lowest RI was considered as the best performing method.

$$RI = \sum_{i=1}^{4} R_i \tag{3.2}$$

Details of the each criterion is described in the following subsection.

3.8.1 Criterion 1

The first criterion is comprised of two sub-criterion. The first sub-criterion compares the magnitude of the slope of the best-fit line passing through the origin for the Q_p vs Q_m plot. It reveals the tendency of a given CPT/PCPT method to either overestimate or underestimate the measured pile capacity, Q_p. The best method is considered to be the one with a slope closer to 1.

The second sub-criterion was the square root of the residual sum of squares ($\sqrt{RSS}$) between an ideal (perfect) prediction ($Q_{p,ideal}$) and actual prediction (Q_p). This sub-criterion shows the accumulated deviation of a given CPT/PCPT method from the ideal scenario. The higher the $\sqrt{RSS}$ is, the lower the performance of the method, and vice versa. The two criteria are shown in Figure 3.3. For instance, the slope of the best-fit line in Figure 3.3 shows underprediction. Based on Figure 3.3, the square root of the residual sum of squares was computed as:

$$\sqrt{RSS} = \sqrt{\sum_{i=1}^{N} (Q_{p,i} - Q_{m,i})^2} \tag{3.3}$$

where $Q_{p,i}$ = predicted pile capacity by the CPT/PCPT method [F], and $Q_{m,i}$ = measured pile capacity using CAPWAP [F]. The rank for criterion 1 was obtained by summing the sub-ranks obtained from corresponding sub-criteria.

3.8.2 Criterion 2

The second criterion was the coefficient of variation (COV). COV is obtained by normalizing the standard deviation by the mean for the Q_p/Q_m data set as shown in Eq. 3.4. This statistical measure shows the extent of data scattering relative to the mean and it is considered to be indicative of the precision of the CPT/PCPT-based methods. Generally, the lower the COV, the better the performance of the method.

$$COV = \frac{\sigma}{\mu} \tag{3.4}$$

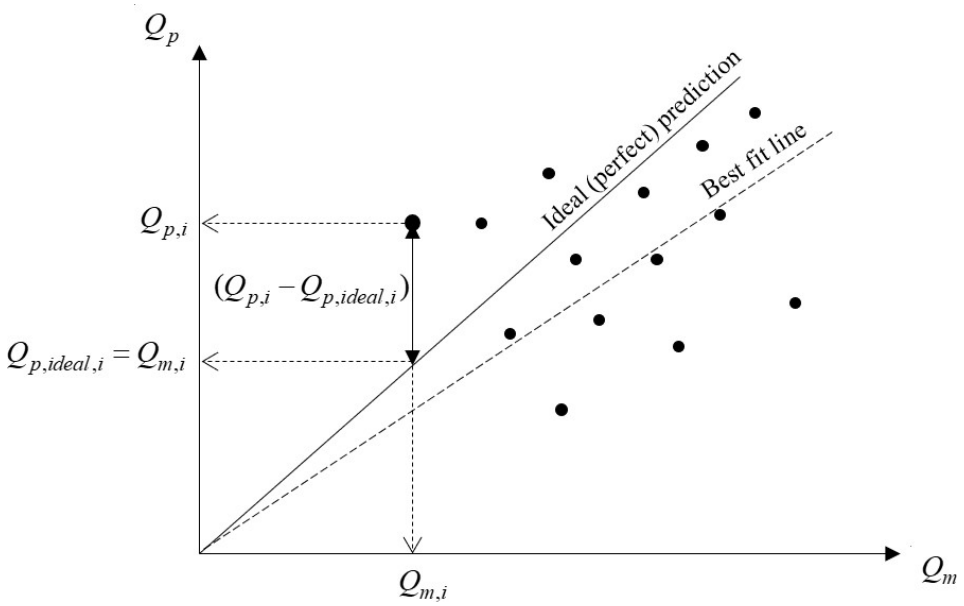

Figure 3.3: Slope of the best-fit line and residuals

where σ = standard deviation of Q_p/Q_m, and μ = mean of Q_p/Q_m.

3.8.3 Criterion 3

The third criterion was based on the 50% (P_{50}) and 90% (P_{90}) cumulative probabilities. These statistical measures were computed by arranging the Q_p/Q_m ratio in ascending order and then using the following equation (Long and Wysockey, 1999):

$$P = \frac{i}{n+1} \tag{3.5}$$

where i = order number, and n = total number of Q_p/Q_m ratios.

This criteria was comprised of two sub-criteria. The first sub-criterion was the magnitude of P_{50}. P_{50} shows the particular Q_p/Q_m value halfway through the data and depicts the tendency of the method to either underestimate or overestimate pile capacity. This measure is more advantageous than simply computing the mean because the mean could be biased by the largest and smallest Q_p/Q_m values. The closer P_{50} is to 1, the better the performance of the method. The second sub-criterion was the difference between P_{90} and P_{50}. The smaller this difference is, the better the performance of the method because it shows reduced scatter

of Q_p/Q_m values above the P_{50} value. The rank for criteria three was obtained by summing the sub-ranks corresponding to each sub-criterion.

3.8.4 Criterion 4

The fourth criterion evaluated the ±20% accuracy level based on the histogram and log-normal distribution. As the name implies, these measures depict what probability of the predicted pile capacity will be within $0.8Q_m \leq Q_p \leq 1.2Q_m$ range. Rather than using a single mean value as a measure of accuracy, the ±20% accuracy level is advantageous given that little room for variation of Q_p/Q_m is allowed.

Due to the possible variation of Q_p/Q_m from 0 to $+\infty$ with an optimum value of 1, the distribution of Q_p/Q_m is unsymmetrical about the mean (Briaud and Tucker, 1988) and thus the log-normal distribution is recommended to mimic the probability distribution of Q_p/Q_m. There were two sub-criteria in this category. In the first sub-criterion, the ±20% accuracy level was obtained based on the histogram plot. In the second sub-criterion, it was obtained based on log-normal distribution assumption. Although both sub-criteria reveal the same measure, one is based on measured values, and the other is based on assumed probability distribution using the mean and standard deviation of the measured values (forecast the general trend). The histogram was drawn by considering the frequency Q_p/Q_m in a certain bin size, while the log-normal distribution was obtained by using a probability density function, $f(x)$, shown in Eq. 3.6 following (Abu-Farsakh and Titi, 2004).

$$f(x) = \frac{1}{\sqrt{2\pi}\sigma_{\ln} x} \exp\left[-\frac{1}{2}\left(\frac{\ln(x) - \mu_{\ln}}{\sigma_{\ln}}\right)^2\right] \tag{3.6}$$

where $x = Q_p/Q_m$, $\mu_{\ln}$ = mean of $\ln(Q_p/Q_m)$, and $\sigma_{\ln}$ = standard deviation of $\ln(Q_p/Q_m)$. The rank for criterion 4 was obtained by summing the sub-ranks corresponding to each sub-criterion.

3.9 *Calibration Methodology*

After carrying out the evaluation of all the CPT/PCPT-based methods, it was found that some methods show better performance in terms of precision and weak performance in terms of accuracy. As discussed in the previous chapter, the methods are empirical and site specific. To improve the prediction accuracy of those methods, a calibration was performed. The calibration process mainly followed a procedure of minimizing the squared residual between the measured and predicted pile capacities aiming to enhance the accuracy of the methods. Separate calibration factors were assigned to the predicted toe and shaft resistances from the CPT/PCPT methods for displacement (HP piles) and non-displacement (PP and PPC piles). The following basic logic was employed to calibrate the CPT/PCPT-based methods:

$$Minimize \Rightarrow RSS = \sum_{i=1}^{N} \left(Q_{m,i} - \left(\eta Q_{t,i} + \theta Q_{s,i} \right) \right)^2 \tag{3.7}$$

where Q_t = predicted toe capacity [F], Q_s = predicted shaft capacity [F], and η, θ = calibration factors corresponding to toe and shaft resistance, respectively. η and θ are different for H-piles, pipe piles, and PPC piles. The MS-Excel application was used to perform the above calibration process. After the calibration of each method, re-evaluation was performed using the criteria discussed in Section 3.8.

Chapter 4 RESULTS AND DISCUSSIONS

4.1 Introduction

The performance of the CPT/PCPT-based pile design methods was evaluated based on the criteria discussed in the previous chapter, and results are presented in this chapter. The CAPWAP database was subdivided to a category of H-piles, pipe piles, and PPC piles and results of the evaluation are presented for each category separately. The chapter is organized in a way that first, an evaluation on the original CPT/PCPT-based methods is presented, and then an evaluation of the calibrated methods is presented. A comparison of the improvements on the performance of the methods was performed and discussed. Finally, the best performing methods were identified and compared with the NDOT LRFD- based pile driving formula results. The risk of Q_p being greater than Q_m was also compared between the best performing methods and the NDOT LRFD-based pile driving formula following a simple probabilistic analysis (Briaud and Tucker, 1988).

4.2 Initial Evaluation

4.2.1 H-Piles

Criterion 1

The first sub-criterion in this category was the slope of the best-fit line between Q_p and Q_m. Table 4.1 shows the summary of the sub-ranks for this sub-criterion, and Figure 4.1 shows the best-fit line for Q_p vs Q_m plots of the first top four best performers. In Table 4.1, R_1^* and R_2^* denote the sub-ranks for the slope of the best-fit line and $\sqrt{RSS}$ criteria. R_1 denotes the

overall rank for criterion 1. The Bustamante and Gianeselli (1982) method underestimated pile capacity and the other methods generally overestimated it.

The second sub-criterion, which was the square root of the residual sum of squares, showed that Price and Wardle (1982); Bustamante and Gianeselli (1982); Aoki and de Alencar (1975) performed well and obtained rank from 1^{st} to 3^{rd}, respectively.

Table 4.1: The slope of the best-fit line between Q_p and Q_m and $\sqrt{RSS}$ for H-piles

CPT/PCPT-based method	Q_p vs Q_m slope	$\sqrt{RSS}$	R^*_1	R^*_2	$R^*_1 + R^*_2$	R_1
Aoki and de Alencar (1975)	1.019	2672.36	1	3	4	2
Clisby et al. (1978)	0.574	3375.01	8	5	13	6
Schmertmann (1978)	1.309	4038.94	5	6	11	5
De Ruiter and Beringen (1979)	1.574	5200.99	9	9	18	9
Philipponnat (1980)	1.392	4400.78	7	7	14	7
Tumay and Fakhroo (1982)	1.268	3254.91	4	4	8	4
Price and Wardle (1982)	1.050	2358.93	2	1	3	1
Bustamante and Gianeselli (1982)	0.882	2494.17	3	2	5	3
Almeida et al. (1996)	1.381	4442.87	6	8	14	7
Eslami and Fellenius (1997)	1.977	8535.83	10	10	20	10
Takesue et al. (1998)	2.728	20414.43	11	11	22	11

Criterion 2

Based on this criterion, the precision of the CPT/PCPT-based methods was evaluated. Table 4.2 summarizes the results for this criterion. The De Ruiter and Beringen (1979) method showed the best precision. The Price and Wardle (1982) and Philipponnat (1980) followed second and third, respectively. The De Ruiter and Beringen (1979) method was found to perform relatively the worst in the previous criterion with a rank of 9. This clearly shows that the accuracy of the De Ruiter and Beringen (1979) method is poor whereas its precision is relatively excellent. As a justification for its poor accuracy, Table 4.6 shows the mean value of Q_p/Q_m is substantially high, which means it overestimated pile capacity substantially.

Criterion 3

The 50% (P_{50}) and 90% (P_{90}) cumulative probabilities were compared and ranks were obtained form this criterion. Table 4.3 summarizes the results of this criterion. The Aoki and

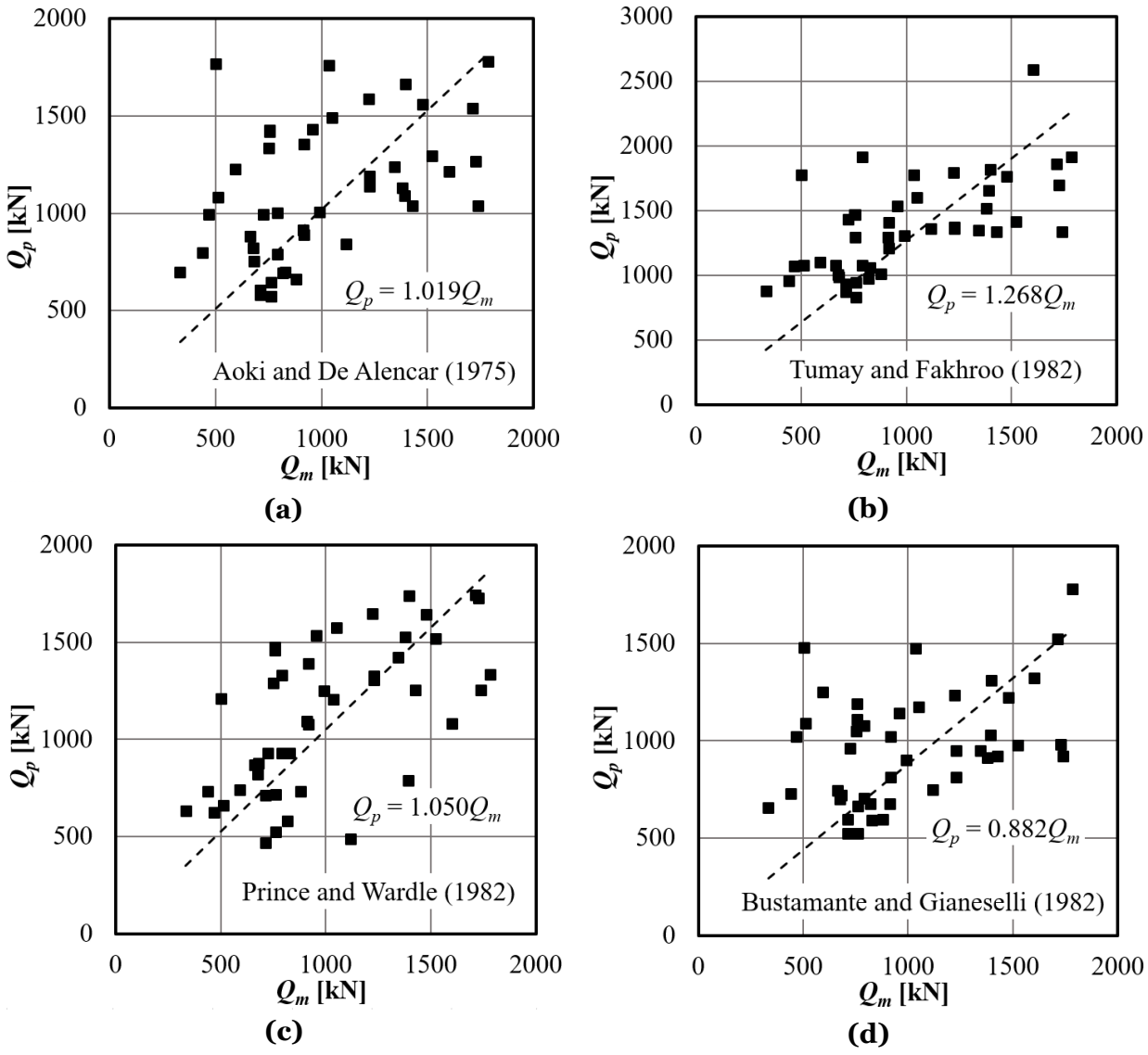

Figure 4.1: Best fit line plots of the top four best performers for H-piles

de Alencar (1975) method was the best performer in terms of the first sub-criterion, which indicated that the median is 1.00 and half of its predictions are overpredictions while half is underpredictions, as shown in Figure 4.2. However, the same method showed a higher scatter of overprediction as depicted in Figure 4.2 and scored a sub-rank of 9 in the $P_{90} - P_{50}$ sub-criterion. In terms of the second sub-criterion, Clisby et al. (1978) showed the best performance with a minimum scatter of Q_p/Q_m after the P_{50} value. However, the median for this method was 0.63 (P_{50}) and it highly underestimated pile capacity. The Price and Wardle (1982) method showed the best overall performance in this criterion, as shown in

Table 4.2: COV in the ratio Q_p/Q_m for H-piles

CPT/PCPT-based method	σ	μ	COV	R_2
Aoki and de Alencar (1975)	0.56	1.24	0.455	9
Clisby et al. (1978)	0.23	0.66	0.351	5
Schmertmann (1978)	0.70	1.55	0.450	8
De Ruiter and Beringen (1979)	0.61	1.86	0.326	1
Philipponnat (1980)	0.57	1.65	0.347	3
Tumay and Fakhroo (1982)	0.53	1.50	0.350	4
Price and Wardle (1982)	0.40	1.20	0.339	2
Bustamante and Gianeselli (1982)	0.52	1.09	0.473	10
Almeida et al. (1996)	0.58	1.65	0.353	6
Eslami and Fellenius (1997)	0.88	2.37	0.370	7
Takesue et al. (1998)	2.62	3.12	0.841	11

Table 4.3.

Table 4.3: 50% and 90% cumulative probabilities in the ratio Q_p/Q_m for H-piles

CPT/PCPT-based method	P_{50}	$P_{90}-P_{50}$	R_1^*	R_2^*	$R_1^*+R_2^*$	R_3
Aoki and de Alencar (1975)	1.00	1.08	1	9	10	5
Clisby et al. (1978)	0.63	0.37	6	1	7	2
Schmertmann (1978)	1.35	0.85	5	4	9	3
De Ruiter and Beringen (1979)	1.77	0.75	9	3	12	7
Philipponnat (1980)	1.55	0.96	8	6	14	8
Tumay and Fakhroo (1982)	1.32	0.85	4	5	9	3
Price and Wardle (1982)	1.18	0.54	3	2	5	1
Bustamante and Gianeselli (1982)	0.89	1.07	2	8	10	5
Almeida et al. (1996)	1.46	1.11	7	10	17	9
Eslami and Fellenius (1997)	2.23	1.06	11	7	18	10
Takesue et al. (1998)	2.23	4.26	10	11	21	11

Criterion 4

The relative accuracy of the CPT/PCPT-based methods over a range of ±20% overprediction/underprediction was evaluated with this criterion. Table 4.4 and Figure 4.3 show the results from this evaluation. The sub-criteria in this category were similar except one was based on histogram and the other was based on log-normal distribution obtained from the mean and standard deviation of $\ln(Q_p/Q_m)$. The Price and Wardle (1982) showed the best performance with an accuracy of ~ 58%. Then, the method of Aoki and de Alencar (1975)

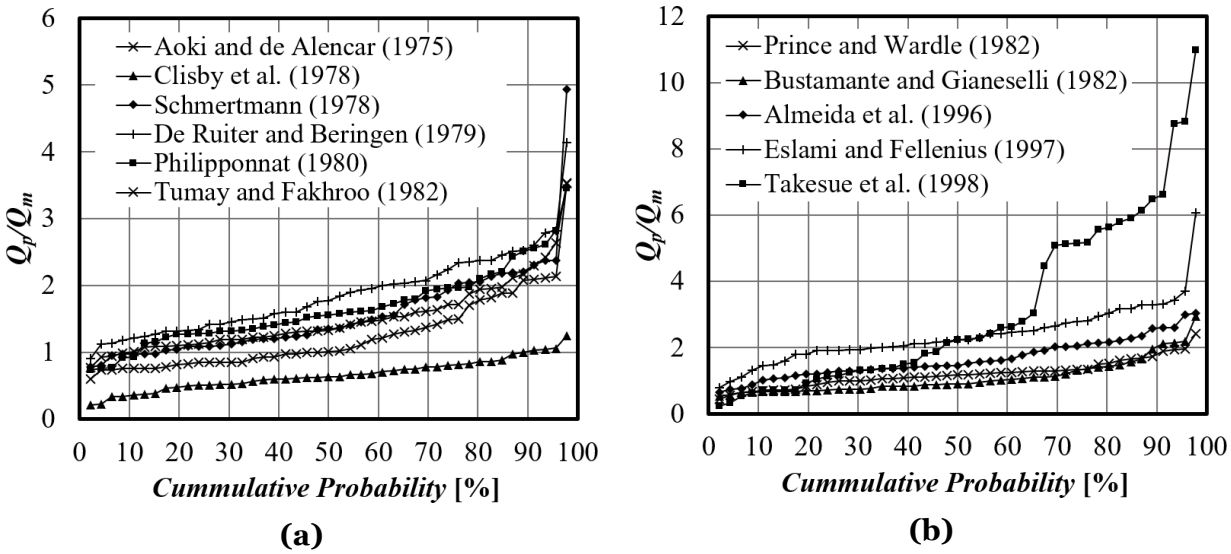

Figure 4.2: Cumulative probabilities of the ratio Q_p/Q_m values for H-piles

and Bustamante and Gianeselli (1982) showed the best second and third performances, respectively.

Table 4.4: ±20% accuracy level based on histogram and log-normal distribution for H-piles

CPT/PCPT-based method	Histogram	Log-normal	R_1^*	R_2^*	$R_1^* + R_2^*$	R_4
Aoki and de Alencar (1975)	61.36 %	53.14 %	1	3	4	2
Clisby et al. (1978)	40.91 %	33.51 %	5	6	11	6
Schmertmann (1978)	45.45 %	36.65 %	4	5	9	4
De Ruiter and Beringen (1979)	13.64 %	15.60 %	10	10	20	10
Philipponnat (1980)	27.27 %	29.01 %	7	8	15	7
Tumay and Fakhroo (1982)	40.91 %	37.17 %	5	4	9	4
Price and Wardle (1982)	59.09 %	57.68 %	2	1	3	1
Bustamante and Gianeselli (1982)	54.55 %	55.93 %	3	2	5	3
Almeida et al. (1996)	22.73 %	30.10 %	8	7	15	7
Eslami and Fellenius (1997)	6.82 %	6.76 %	11	11	22	11
Takesue et al. (1998)	20.45 %	18.17 %	9	9	18	9

Rank Index, *RI*

The overall rank of all CPT/PCPT based methods was computed by comparing the *RI*, which is simply the sum of all the ranks from each criterion (1 ~ 4). Table 4.5 shows the summary of the *RI* and the overall ranks for H-piles. Based on this table, the Price and

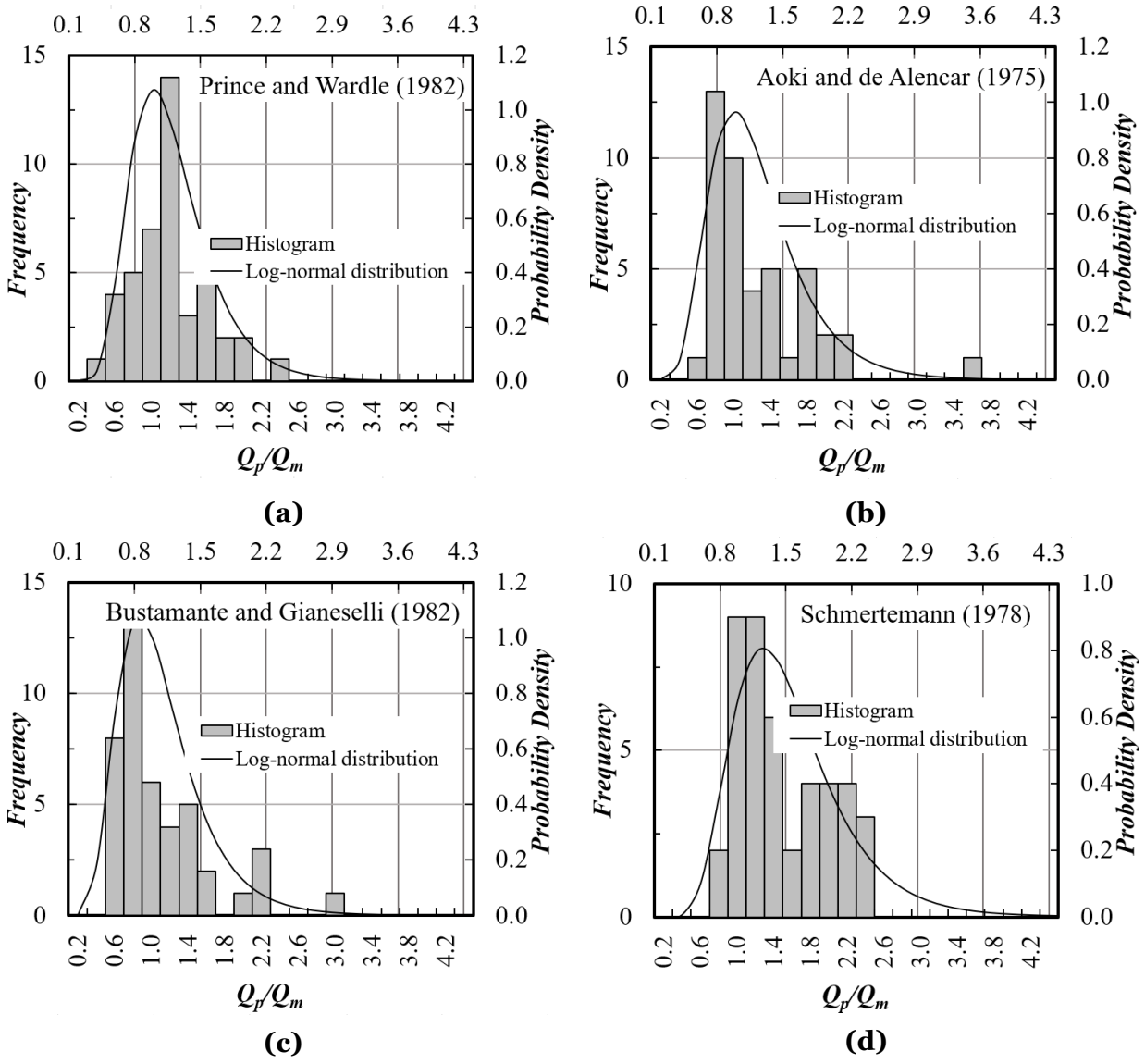

Figure 4.3: Histogram and log-normal distribution plots of the top four best performers for H-piles

Wardle (1982) method stood first and thus considered the best performing method. The Tumay and Fakhroo (1982) and Aoki and de Alencar (1975) methods were the second and third best performers with a *RI* of 15 and 18, respectively. However, as per the *RI* value, it is clear that these methods were significantly outperformed by the Price and Wardle (1982) method.

Table 4.5: Rank index (*RI*) and overall ranks of each CPT/PCPT-based methods for H-piles

CPT/PCPT-based method	Cr. 1	Cr. 2	Cr. 3	Cr. 4	*RI*	Rank
Aoki and de Alencar (1975)	2	9	5	2	18	3
Clisby et al. (1978)	6	5	2	6	19	4
Schmertmann (1978)	5	8	3	4	20	5
De Ruiter and Beringen (1979)	9	1	7	10	27	8
Philipponnat (1980)	7	3	8	7	25	7
Tumay and Fakhroo (1982)	4	4	3	4	15	2
Price and Wardle (1982)	1	2	1	1	5	1
Bustamante and Gianeselli (1982)	3	10	5	3	21	6
Almeida et al. (1996)	7	6	9	7	29	9
Eslami and Fellenius (1997)	10	7	10	11	38	10
Takesue et al. (1998)	11	11	11	9	42	11

4.2.2 Pipe and PPC Piles

Criterion 1

For pipe and PPC piles, the Price and Wardle (1982) and Bustamante and Gianeselli (1982) were equally the best performance, as shown in Table 4.6 and Figure 4.4. Both methods seem to very slightly overpredict pile capacity (by ~ 1%). Aoki and de Alencar (1975) was the third best performing method in this criterion. In terms of the $\sqrt{RSS}$ sub-criterion, both the Price and Wardle (1982) and the Bustamante and Gianeselli (1982) methods nearly had the same square root of residual sum of squares and clearly outperformed the other methods.

Criterion 2

In this category, the Tumay and Fakhroo (1982) method performed excellent as shown in Table 4.2. The Eslami and Fellenius (1997)and De Ruiter and Beringen (1979) methods followed second and third, respectively. Similar to the previous case, the Tumay and Fakhroo (1982) method had the best precision for pipe and PPC piles. However, its accuracy was poor and therefore its performance in criterion 1 was ultimately poor. In support of this, the mean value of this method showed that it overpredicted pile capacity on average by about 60%.

Table 4.6: The slope of the best-fit line between Q_p and Q_m and $\sqrt{RSS}$ for pipe and PPC piles

CPT/PCPT-based method	Q_p vs Q_m	$\sqrt{RSS}$	R^*_1	R^*_2	$R^*_1 + R^*_2$	R_1
Aoki and de Alencar (1975)	1.034	3069.78	3	3	6	3
Clisby et al. (1978)	0.555	3635.93	8	5	13	6
Schmertmann (1978)	1.235	4078.80	5	6	11	5
De Ruiter and Beringen (1979)	1.477	4841.62	9	7	16	8
Philipponnat (1980)	1.385	4969.71	6	8	14	7
Tumay and Fakhroo (1982)	1.224	3469.95	4	4	8	4
Price and Wardle (1982)	1.010	2915.20	1	2	3	1
Bustamante and Gianeselli (1982)	1.011	2896.55	2	1	3	1
Almeida et al. (1996)	1.414	4980.01	7	9	16	8
Eslami and Fellenius (1997)	1.833	7911.30	11	11	22	11
Takesue et al. (1998)	1.503	6806.36	10	10	20	10

Table 4.7: COV in the ratio Q_p/Q_m for pipe and PPC piles

CPT/PCPT based method	σ	μ	COV	R_2
Aoki and de Alencar (1975)	0.56	1.23	0.466	7
Clisby et al. (1978)	0.35	0.75	0.463	8
Schmertmann (1978)	0.73	1.55	0.475	10
De Ruiter and Beringen (1979)	0.74	1.84	0.403	3
Philipponnat (1980)	0.75	1.76	0.424	5
Tumay and Fakhroo (1982)	0.62	1.60	0.385	1
Price and Wardle (1982)	0.58	1.23	0.472	9
Bustamante and Gianeselli (1982)	0.50	1.16	0.435	6
Almeida et al. (1996)	0.72	1.74	0.411	4
Eslami and Fellenius (1997)	0.98	2.42	0.403	2
Takesue et al. (1998)	0.94	1.75	0.536	11

Criterion 3

For pipe and PPC piles, the Bustamante and Gianeselli (1982) method showed an excellent overall performance in this criterion, as shown in Table 4.8. Although the Price and Wardle (1982) showed better performance in terms of the 50% cumulative probability, its scatter after the median value is higher than the Bustamante and Gianeselli (1982) method. The P_{50} value of the Bustamante and Gianeselli (1982) method showed that more than 50% of the Q_p/Q_m ratios are greater than 1, which means that it generally overpredicted pile capacity. The methods of Clisby et al. (1978) and Aoki and de Alencar (1975) were the second and

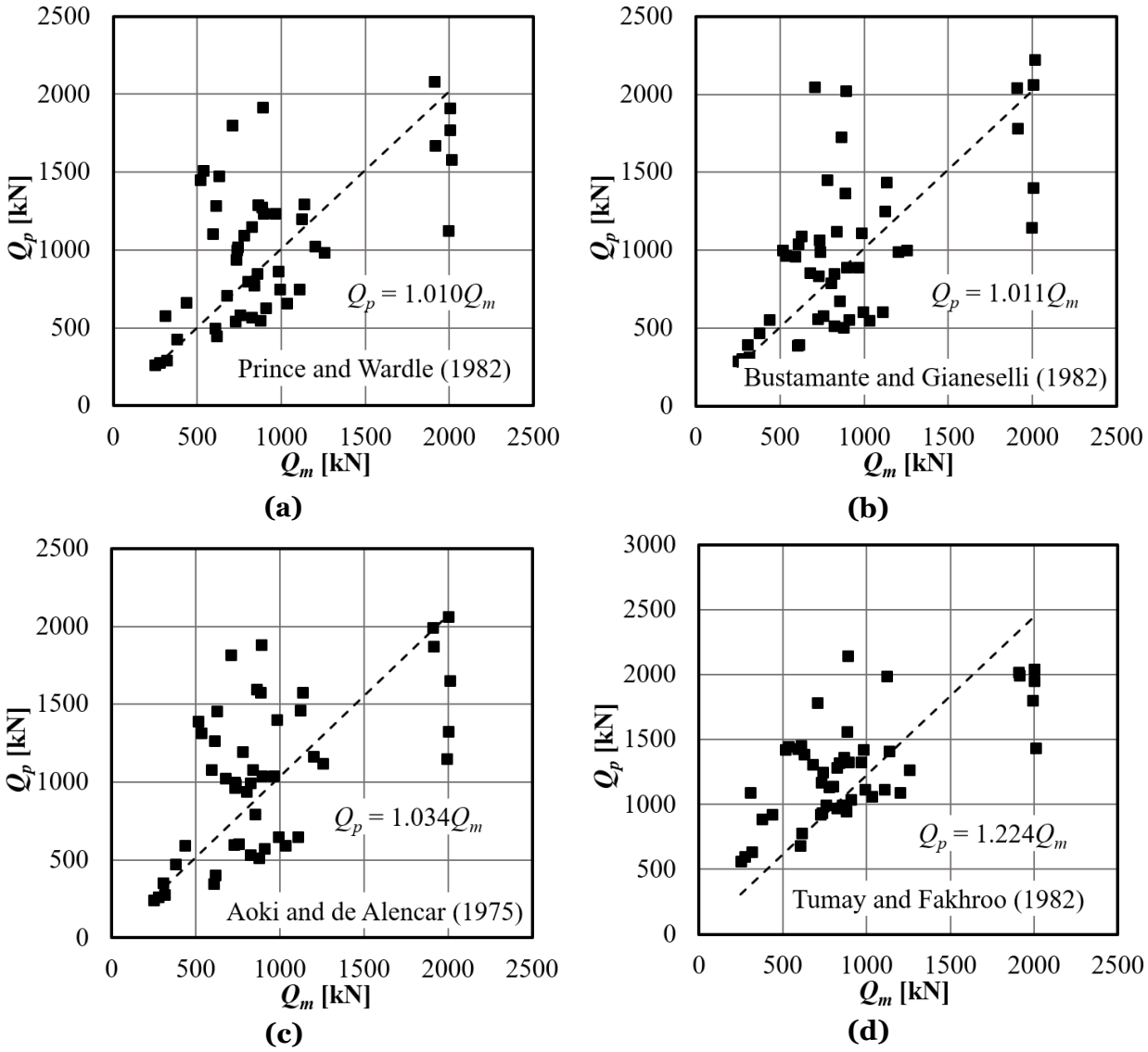

Figure 4.4: Best fit line plots of the top four best performers for pipe and PPC piles

third best performers, respectively. The cummulative probability trends shown in Figure 4.5 depicted the better performance of the Bustamante and Gianeselli (1982) and the Price and Wardle (1982) methods as compared to other methods, although the Bustamante and Gianeselli (1982) slightly outperformed the Price and Wardle (1982) method.

Criterion 4

In this pile type category, the Bustamante and Gianeselli (1982) performed excellent in terms of its ±20% accuracy, as shown Table 4.9 and Figure 4.6. Both the histogram and

Table 4.8: 50% and 90% cumulative probabilities in the ratio Q_p/Q_m for pipe and PPC piles

CPT/PCPT-based method	P_{50}	$P_{90}-P_{50}$	R_1^*	R_2^*	$R_1^*+R_2^*$	R_3
Aoki and de Alencar (1975)	1.14	0.97	3	4	7	3
Clisby et al. (1978)	0.73	0.44	4	1	5	2
Schmertmann (1978)	1.36	1.55	5	10	15	7
De Ruiter and Beringen (1979)	1.71	1.28	10	8	18	10
Philipponnat (1980)	1.63	1.18	9	7	16	8
Tumay and Fakhroo (1982)	1.45	0.96	7	3	10	5
Price and Wardle (1982)	1.05	1.11	1	6	7	3
Bustamante and Gianeselli (1982)	1.10	0.77	2	2	4	1
Almeida et al. (1996)	1.54	1.52	8	9	17	9
Eslami and Fellenius (1997)	2.00	1.97	11	11	22	11
Takesue et al. (1998)	1.42	1.02	6	5	11	6

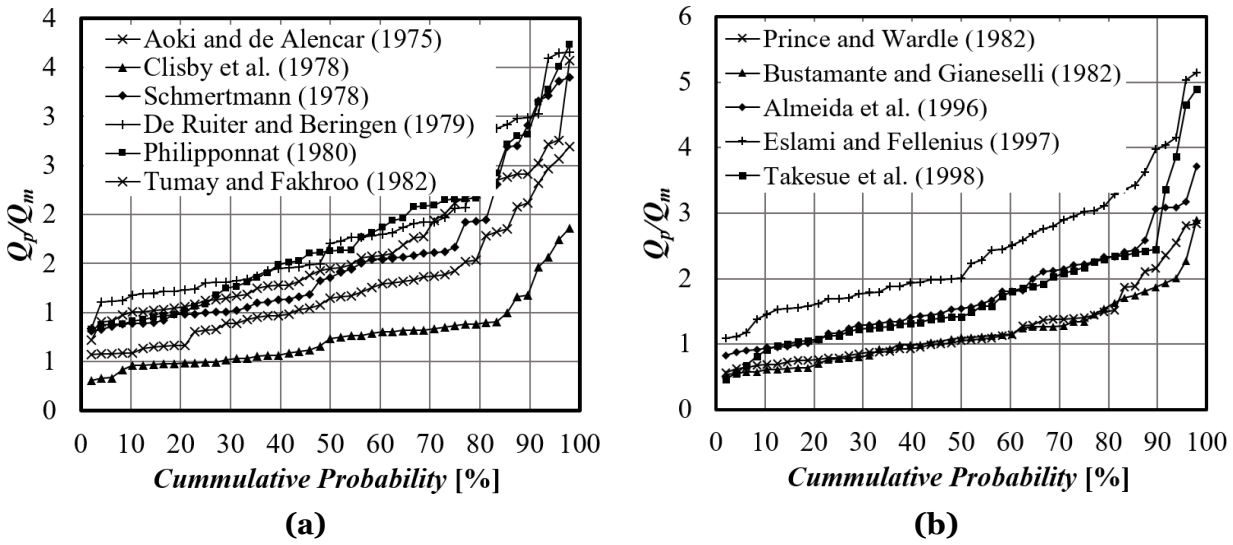

Figure 4.5: Cumulative probabilities of the ratio Q_p/Q_m values for pipe and PPC piles

log-normal distribution accuracy levels depicted that the Bustamante and Gianeselli (1982) was the best performer out of all other methods; the accuracy level was about 54%. The Price and Wardle (1982) and Clisby et al. (1978) methods were the second and third best performers, respectively.

Rank Index *RI*

Table 4.10 presents the overall ranks of all methods for pipe and PPC piles. Per this table, the Bustamante and Gianeselli (1982), Price and Wardle (1982), and Aoki and de Alencar

Table 4.9: ±20% accuracy level based on histogram and log-normal distribution for pipe and PPC piles

CPT/PCPT-based method	Histogram	Log-normal	R_1^*	R_2^*	$R_1^* + R_2^*$	R_4
Aoki and de Alencar (1975)	40.43 %	49.70 %	6	3	9	5
Clisby et al. (1978)	42.55 %	41.85 %	4	4	8	3
Schmertmann (1978)	46.81 %	37.91 %	3	5	8	3
De Ruiter and Beringen (1979)	23.40 %	21.74 %	10	10	20	10
Philipponnat (1980)	31.91 %	27.98 %	7	8	15	7
Tumay and Fakhroo (1982)	42.55 %	33.03 %	4	6	10	6
Price and Wardle (1982)	53.19 %	51.41 %	1	2	3	2
Bustamante and Gianeselli (1982)	53.19 %	53.45 %	1	1	2	1
Almeida et al. (1996)	29.79 %	27.88 %	8	9	17	9
Eslami and Fellenius (1997)	6.38 %	7.40 %	11	11	22	11
Takesue et al. (1998)	29.79 %	30.97 %	8	7	15	7

(1975) stood first, second, and third with a *RI* of 9, 15, and 16, respectively. The Bustamante and Gianeselli (1982) method, however, had outperformed the other two competitors substantially and was considered the best method for pipe and PPC piles. Moreover, it is worth noting that from Table 4.10, the Tumay and Fakhroo (1982) method showed the best precision in criterion 2. However, its accuracy was poor due to its substantial tendency to overestimate pile capacity.

Table 4.10: Rank index (*RI*) and overall ranks of each CPT/PCPT-based methods for pipe and PPC piles

CPT/PCPT-based method	Cr. 1	Cr. 2	Cr. 3	Cr. 4	*RI*	Rank
Aoki and de Alencar (1975)	3	7	3	5	18	4
Clisby et al. (1978)	6	8	2	3	19	5
Schmertmann (1978)	5	10	7	3	25	6
De Ruiter and Beringen (1979)	8	3	10	10	31	9
Philipponnat (1980)	7	5	8	7	27	7
Tumay and Fakhroo (1982)	4	1	5	6	16	3
Price and Wardle (1982)	1	9	3	2	15	2
Bustamante and Gianeselli (1982)	1	6	1	1	9	1
Almeida et al. (1996)	8	4	9	9	30	8
Eslami and Fellenius (1997)	11	2	11	11	35	11
Takesue et al. (1998)	10	11	6	7	34	10

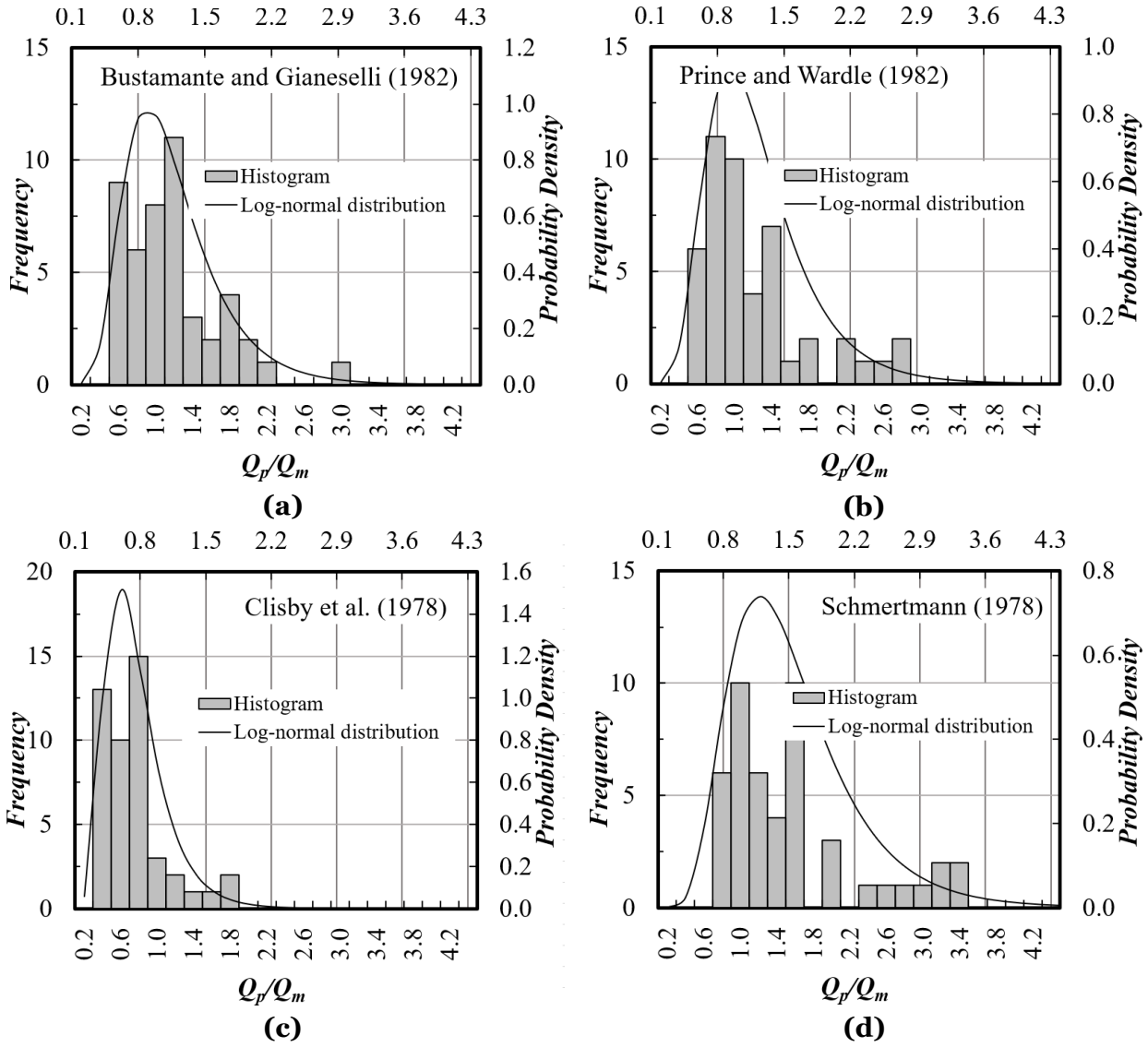

Figure 4.6: Histogram and log-normal distribution plots of the top four best performers for pipe and PPC piles

4.2.3 Concluding Remarks

From the initial evaluation result, it was noted that, for example, the De Ruiter and Beringen (1979) and Tumay and Fakhroo (1982) methods showed the best performance in terms of their precision (under criterion 2), but their accuracy was generally poor. The major source of their overall poor performance was attributed to the significant overprediction of pile capacity as indicated by the median as well as mean value of Q_p/Q_m.

Intuitively, one may reasonably propose that overprediction of pile capacity could be

retrofitted with the application of a calibration factor (reduction factor) that reduces the magnitude of all the predicted pile capacities at the same time. This concept, however, may not result in a significant change in the precision or scatter of the data points since the calibration factor is a constant and will be applied on all predicted pile capacities equally. However, as mentioned above, it may have a substantial impact on the accuracy of the methods. With the promising precision levels seen in the aforementioned methods as well as to examine any potential improvements in all methods, calibration of the methods and subsequent re-assessment based on the criteria set was performed.

Furthermore, all the PCPT-based methods generally showed poor performance except for the method of Eslami and Fellenius (1997) showed a good performance in terms of its precision in pipe and PPC piles. The poor performance of the PCPT based methods may be attributed to the substantially low or negative pore pressure measurements in overconsolidated soils leading to higher cone tip resistances and overprediction of pile capacity. Hence, it is believed that proper correction of pore pressure measurements is required before adopting the PCPT-based methods.

4.3 Calibration

Based on the calibration method described in section 3.9, all CPT/PCPT-based methods were calibrated mainly to improve their accuracy levels. An Excel application was employed for this optimization problem. Two separate factors corresponding to toe and shaft capacity were computed. Table 4.11 presents the calibration factors obtained from the calibration procedure. Using the calibration factors, re-assessment of all design methods was performed, and results and discussions are presented in the next section.

Table 4.11: Calibration factors, η and θ

CPT/PCPT-based methods	HP pile		PP pile	
	η	θ	η	θ
Aoki and de Alencar (1975)	0.76	0.95	1.18	0.53
Clisby et al. (1978)	3.25	1.16	3.43	0.88
Schmertmann (1978)	0.69	0.67	1.26	0.31
De Ruiter and Beringen (1979)	0.61	0.58	0.90	0.47
Philipponnat (1980)	1.01	0.54	1.37	0.35
Tumay and Fakhroo (1982)	0.50	0.89	1.15	0.40
Price and Wardle (1982)	1.05	0.81	1.28	0.63
Bustamante and Gianeselli (1982)	0.68	1.29	1.01	0.71
Almeida et al. (1996)	0.97	0.56	1.10	0.45
Eslami and Fellenius (1997)	0.42	0.47	0.55	0.43
Takesue et al. (1998)	1.64	0.15	0.96	0.44

4.4 Final Evaluation

4.4.1 H-Piles

Criterion 1

Table 4.12 presents the performance of all methods in regard to criterion 1. After calibration, the De Ruiter and Beringen (1979) showed the best performance among all methods with a best fit line slope of 0.928 and $\sqrt{\overline{RSS}}$ = 1932.21. Before the calibration, the Price and Wardle (1982) method was regarded as the best performer with a best fit line slope of 1.050 and $\sqrt{\overline{RSS}}$ = 2358. The Clisby et al. (1978) and De Ruiter and Beringen (1979); Price and Wardle (1982) methods were the second and third best performers, respectively, after calibration. Figure 4.7 shows the best fit lines for the top four best performers.

Criterion 2

The method of Tumay and Fakhroo (1982) showed the best performance in this criterion for HP piles. This method attained a *COV* of 0.303, as shown in Table 4.13. Previously, this method had a *COV* of 0.350 before the calibration was performed. The De Ruiter and Beringen (1979) and Price and Wardle (1982) methods were the second and third best performers, respectively, after calibration. During the initial evaluation, the De Ruiter and

Table 4.12: Best fit line slope and $\sqrt{RSS}$ between Q_p and Q_m for H-piles

CPT/PCPT-based method	Q_p vs Q_m slope	$\sqrt{RSS}$	R^*_1	R^*_2	$R^*_1 + R^*_2$	R_1
Aoki and de Alencar (1975)	0.885	2442.75	10	10	20	10
Clisby et al. (1978)	0.919	2047.99	2	3	5	2
Schmertmann (1978)	0.886	2427.10	9	9	18	9
De Ruiter and Beringen (1979)	0.928	1932.21	1	2	3	1
Philipponnat (1980)	0.909	2172.10	4	5	9	5
Tumay and Fakhroo (1982)	0.896	1924.10	6	1	7	3
Price and Wardle (1982)	0.916	2082.89	3	4	7	3
Bustamante and Gianeselli (1982)	0.896	2319.22	8	8	16	8
Almeida et al. (1996)	0.901	2264.61	5	6	11	6
Eslami and Fellenius (1997)	0.896	2315.90	6	7	13	7
Takesue et al. (1998)	0.756	3552.27	11	11	22	11

Beringen (1979) showed the best performance in this regard with a *COV* of 0.326. After calibration, this method attained a *COV* of 0.331, which increased very slightly. However, the accuracy of the same method had improved significantly by the calibration as depicted in the previous criterion.

Table 4.13: COV in the ratio Q_p/Q_m for H-piles

CPT/PCPT-based method	σ	μ	*COV*	R_2
Aoki and de Alencar (1975)	0.47	1.07	0.436	9
Clisby et al. (1978)	0.39	1.08	0.360	5
Schmertmann (1978)	0.48	1.05	0.452	10
De Ruiter and Beringen (1979)	0.36	1.10	0.331	2
Philipponnat (1980)	0.41	1.09	0.372	6
Tumay and Fakhroo (1982)	0.32	1.05	0.303	1
Price and Wardle (1982)	0.37	1.05	0.348	3
Bustamante and Gianeselli (1982)	0.44	1.10	0.401	8
Almeida et al. (1996)	0.40	1.08	0.372	7
Eslami and Fellenius (1997)	0.39	1.07	0.360	4
Takesue et al. (1998)	0.64	0.92	0.697	11

Criterion 3

In this criterion, the Clisby et al. (1978) method was found to be the best performer, as shown in Table 4.14. The Tumay and Fakhroo (1982) and Eslami and Fellenius (1997) were the second and third best performers, respectively. However, the Clisby et al. (1978) method just

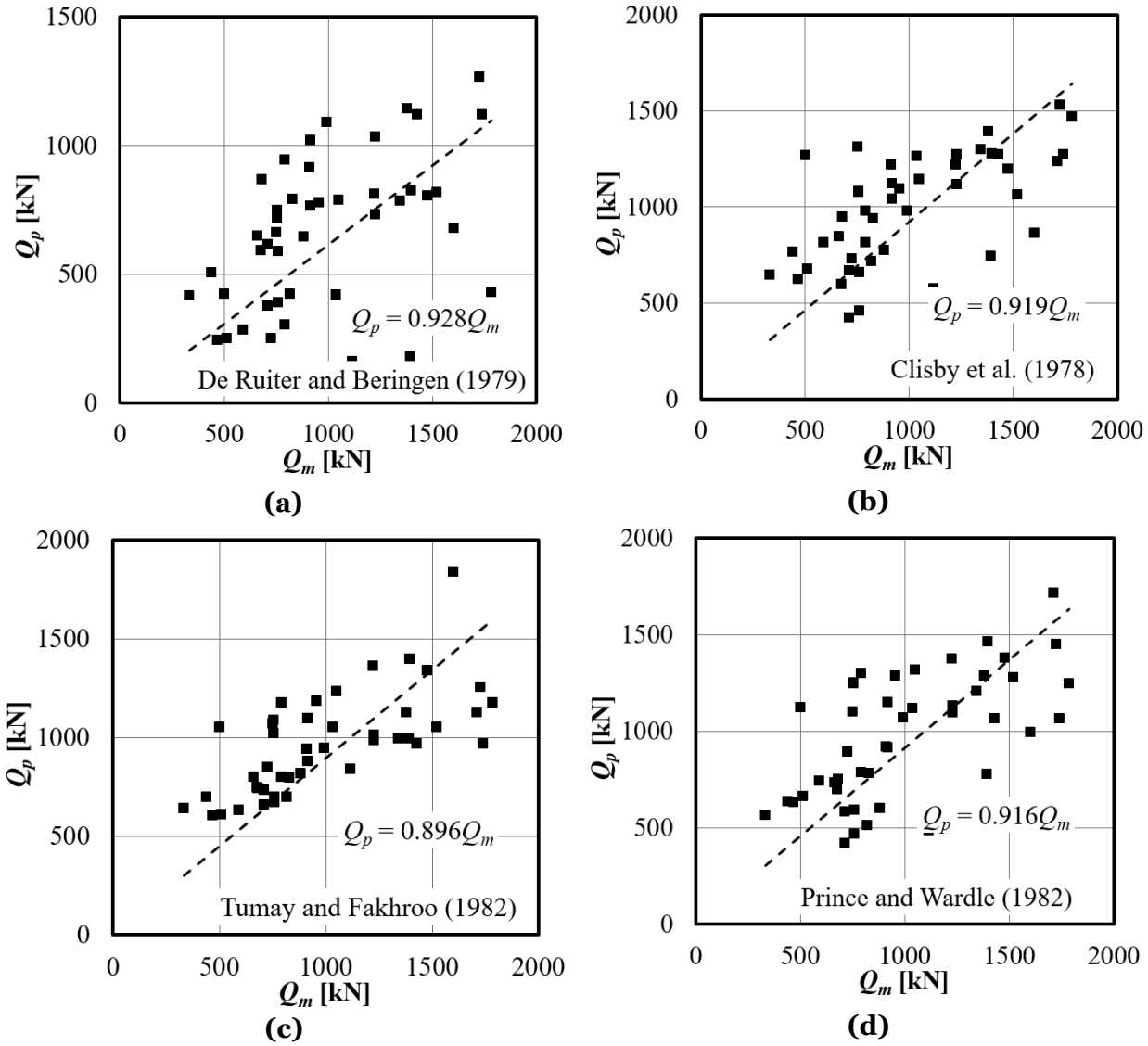

Figure 4.7: Best-fit line plots of the top four best performers for H-piles

slightly outperformed the Tumay and Fakhroo (1982) method as their P_{50} values were the same but slightly differing by their $P_{90} - P_{50}$ values. Before the calibration, the Clisby et al. (1978) method was underpredicting pile capacity substantially. After calibration though, its accuracy improved substantially and its P_{50} value became 1.01. Figure 4.8 shows that the cummulative probability trends for all methods are closer to each other than they were before calibration, and tend to pass through Q_p/Q_m =1 at 50% cumulative probability.

In the initial evaluation, the Price and Wardle (1982) method showed the best performance in this criterion. After calibration, although its accuracy is improved significantly (i.e

its P_{50} was reduced), its precision was decreased slightly. Due to the reduced precision, its $P_{90} - P_{50}$ value was increased and was outperformed by other improved methods.

Table 4.14: 50% and 90% cumulative probabilities in the ratio Q_p/Q_m for H-piles

CPT/PCPT-based method	P_{50}	$P_{90}-P_{50}$	R_1^*	R_2^*	$R_1^* + R_2^*$	R_3
Aoki and de Alencar (1975)	0.89	0.80	10	10	20	11
Clisby et al. (1978)	1.01	0.42	2	1	3	1
Schmertmann (1978)	0.91	0.60	8	5	13	7
De Ruiter and Beringen (1979)	1.04	0.43	7	3	10	5
Philipponnat (1980)	0.97	0.62	5	6	11	6
Tumay and Fakhroo (1982)	1.01	0.43	3	2	5	2
Price and Wardle (1982)	1.00	0.64	1	8	9	4
Bustamante and Gianeselli (1982)	0.97	0.83	6	11	17	8
Almeida et al. (1996)	0.91	0.74	9	9	18	9
Eslami and Fellenius (1997)	1.03	0.46	4	4	8	3
Takesue et al. (1998)	0.85	0.64	11	7	18	9

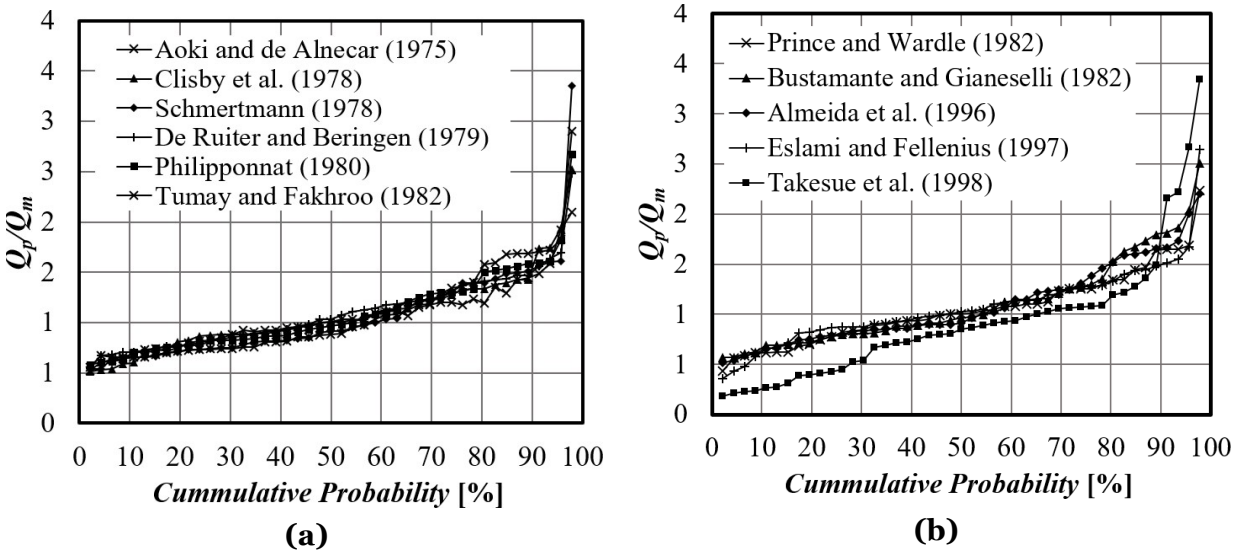

Figure 4.8: Cumulative probabilities of the ratio Q_p/Q_m values for H-piles

Criterion 4

Table 4.15 presents the ±20% accuracy levels after calibration. The Tumay and Fakhroo (1982) method showed an accuracy level of approximately 76%. The same method had an accuracy level of about 39% before the calibration was performed. This clearly showed that the accuracy of this method was substantially improved as a result of the calibration. The

second and third best performers were the De Ruiter and Beringen (1979) and Philipponnat (1980) methods, respectively. Figure 4.9 shows the histogram and log-normal distributions for the top four best performers. In the initial evaluation, the Price and Wardle (1982) was the best performer showing an accuracy level of 58%. After the calibration, although its accuracy level was slightly improved to about 61%, it was significantly outperformed by the Tumay and Fakhroo (1982) method, as depicted in Table 4.15.

Table 4.15: ±20% accuracy level based on histogram and log-normal distribution for HP piles

CPT/PCPT-based method	Histogram	Log-normal	R_1^*	R_2^*	$R_1^* + R_2^*$	R_4
Aoki and de Alencar (1975)	57.78 %	58.52 %	9	10	19	10
Clisby et al. (1978)	64.44 %	63.40 %	4	4	8	3
Schmertmann (1978)	57.78 %	60.60 %	9	7	16	9
De Ruiter and Beringen (1979)	66.67 %	67.23 %	2	2	4	2
Philipponnat (1980)	62.22 %	63.83 %	5	3	8	3
Tumay and Fakhroo (1982)	80.00 %	72.52 %	1	1	2	1
Price and Wardle (1982)	60.00 %	63.83 %	7	5	12	6
Bustamante and Gianeselli (1982)	62.22 %	59.68 %	5	9	14	8
Almeida et al. (1996)	60.00 %	61.14 %	7	6	13	7
Eslami and Fellenius (1997)	66.67 %	60.55 %	2	8	10	5
Takesue et al. (1998)	51.11 %	33.08 %	11	11	22	11

Rank Index, *RI*

The best performer among all methods was selected based on the *RI* value. Table 4.16 summarizes the *RI* and the corresponding overall ranks based on all the criteria set. Per this table, the Tumay and Fakhroo (1982) method was the best performer for H-piles with a *RI* of 7. Previously, this method was among the worst performers due to its poor accuracy. However, in this case, the accuracy level was significantly improved by the calibration and became the best performer.

4.4.2 Pipe and PPC Piles

Criterion 1

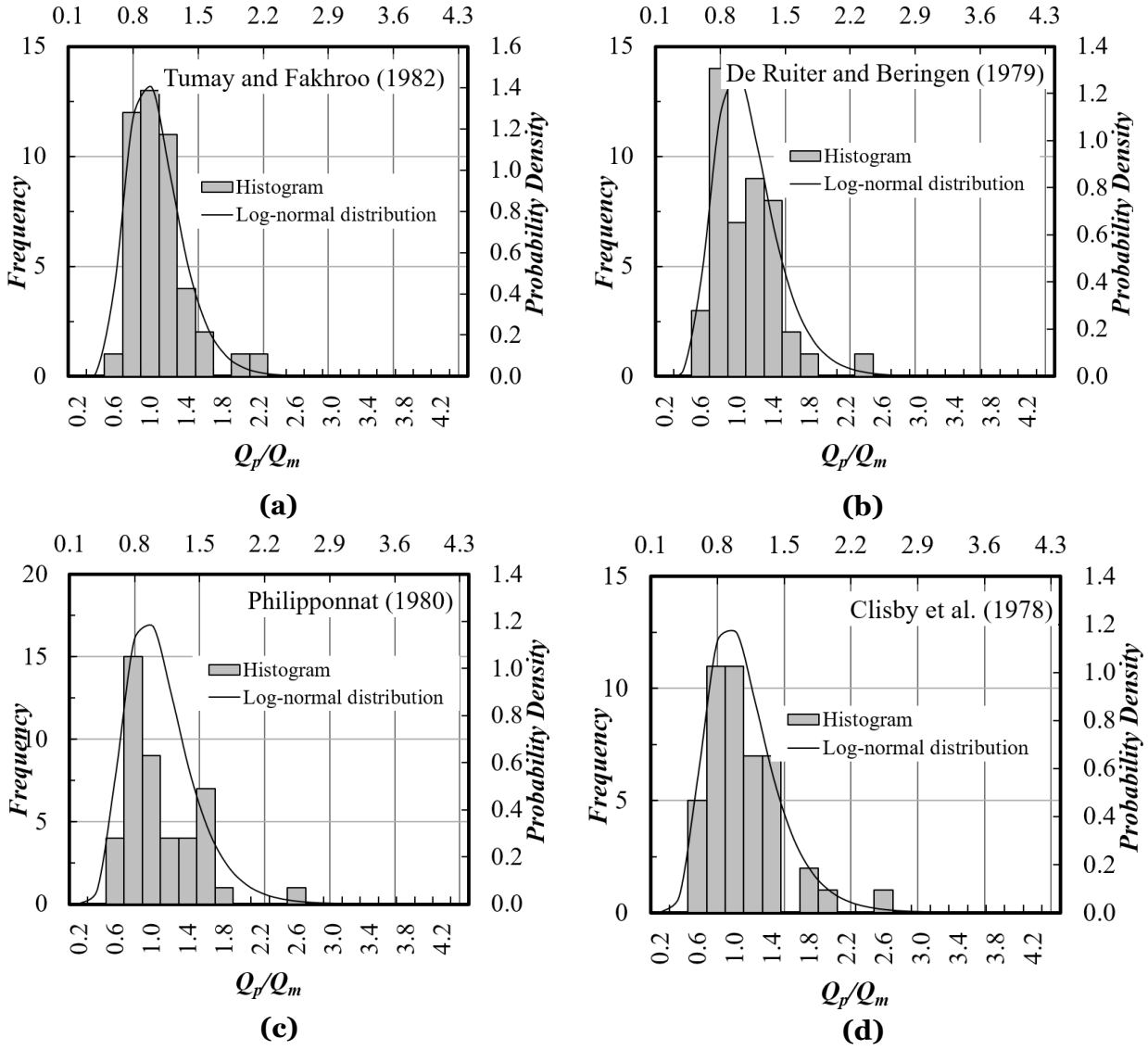

Figure 4.9: Histogram and log-normal distribution plots of the top four best performers for H-piles

Table 4.17 shows the results of criterion 1 for pipe and PPC piles. Per this table, the De Ruiter and Beringen (1979) and Tumay and Fakhroo (1982) methods showed the best performance. The former method had a rank of 8 and the later method had a rank of 4 during the initial evaluation, which means that the calibration had improved their accuracy. Moreover, the best performers in the initial evaluation showed little improvement and hence was outperformed by the above two methods. The Philipponnat (1980) method was the third best performer. Figure 4.10 shows the best-fit line for the top four best performers.

Table 4.16: Rank index (*RI*) and overall ranks of each CPT/PCPT-based methods for H-piles after calibration

CPT/PCPT-based method	Cr. 1	Cr. 2	Cr. 3	Cr. 4	*RI*	Rank
Aoki and de Alencar (1975)	10	9	11	10	40	10
Clisby et al. (1978)	2	5	1	3	11	3
Schmertmann (1978)	9	10	7	9	35	9
De Ruiter and Beringen (1979)	1	2	5	2	10	2
Philipponnat (1980)	5	6	6	3	20	6
Tumay and Fakhroo (1982)	3	1	2	1	7	1
Price and Wardle (1982)	3	3	4	6	16	4
Bustamante and Gianeselli (1982)	8	8	8	8	32	8
Almeida et al. (1996)	6	7	9	7	29	7
Eslami and Fellenius (1997)	7	4	3	5	19	5
Takesue et al. (1998)	11	11	9	11	42	11

Table 4.17: Best fit line and $\sqrt{RSS}$ between Q_p and Q_m for pipe and PPC piles

CPT/PCPT-based method	Q_p vs Q_m slope	$\sqrt{RSS}$	R^*_1	R^*_2	$R^*_1 + R^*_2$	R_1
Aoki and de Alencar (1975)	0.859	2639.85	8	8	16	8
Clisby et al. (1978)	0.845	2773.09	10	10	20	10
Schmertmann (1978)	0.878	2456.33	5	5	10	5
De Ruiter and Beringen (1979)	0.898	2106.66	2	1	3	1
Philipponnat (1980)	0.883	2404.61	3	3	6	3
Tumay and Fakhroo (1982)	0.909	2126.46	1	2	3	1
Price and Wardle (1982)	0.873	2508.28	6	6	12	6
Bustamante and Gianeselli (1982)	0.862	2616.08	7	7	14	7
Almeida et al. (1996)	0.883	2409.40	4	4	8	4
Eslami and Fellenius (1997)	0.857	2663.81	9	9	18	9
Takesue et al. (1998)	0.775	3337.54	11	11	22	11

Criterion 2

The Eslami and Fellenius (1997) method was found to be the best performer in this criterion, as shown in Table 4.18. Intially, this method had a *COV* of 0.403 before calibration. After calibration, its *COV* became 0.399, indicating slightly improved precision. However, the accuracy of this method is still little improved from the calibration as it can be seen from the mean (μ) value (overpredicts pile capacity). The Tumay and Fakhroo (1982) and De Ruiter and Beringen (1979) methods were second and third best performers, respectively. The best performer from the initial evaluation, which was the method Tumay and Fakhroo (1982)

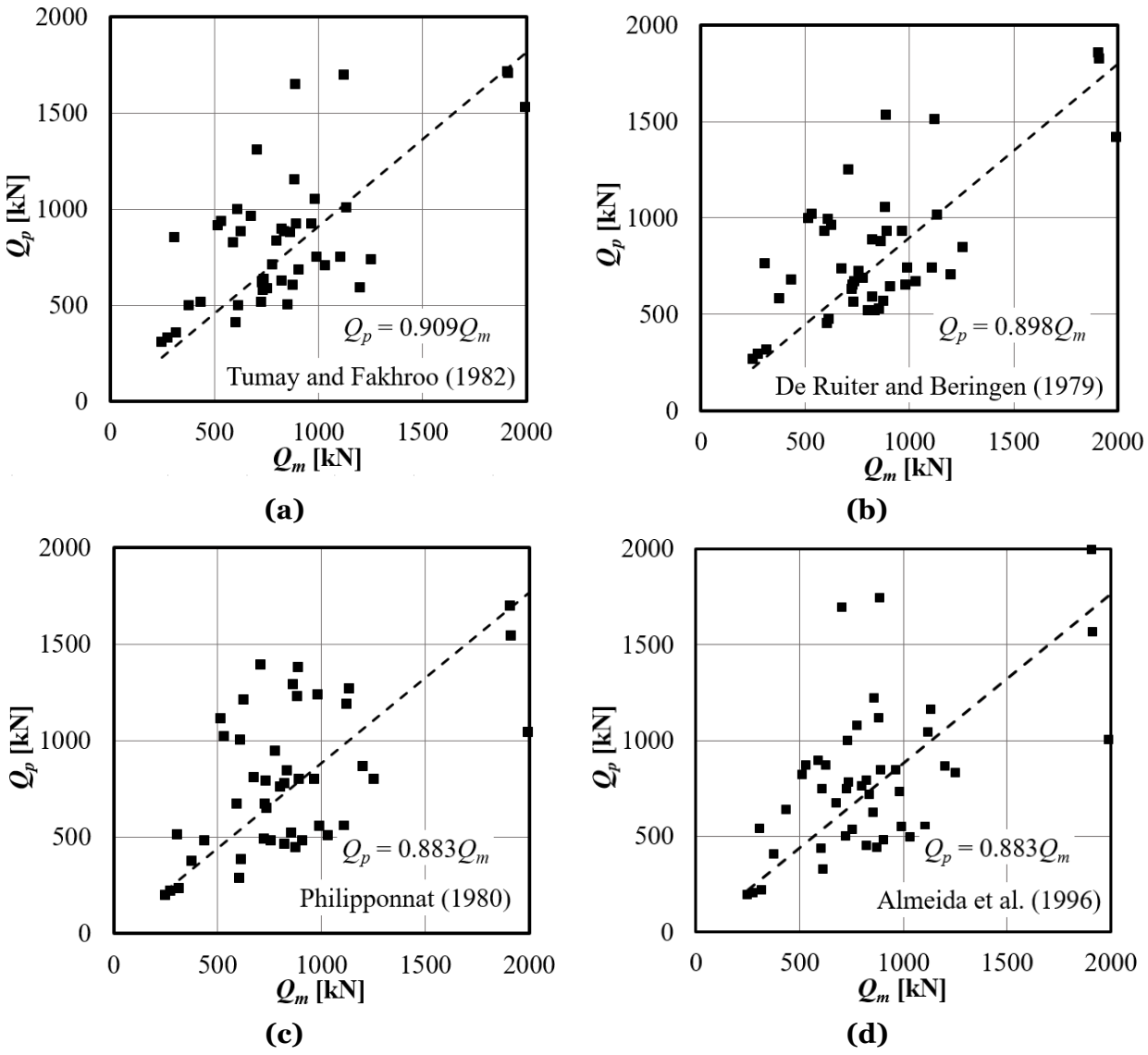

Figure 4.10: Best fit line plots of the top four best performers for H-piles

showed an increment of *COV* from 0.385 to 0.408 indicating slight reduction in precision while its accuracy is improved as revealed in criterion 1.

Criterion 3

Similar to H-piles, the Clisby et al. (1978) was found to be the best performer in this criterion, as shown in Table 4.19. As a result of the calibration, the P_{50} value raised from 0.73 to 0.98, which indicated an improved accuracy was achieved. However, its $P_{90} - P_{50}$ value increased from 0.44 to 0.69 indicating a reduced precision. Moreover, the Bustamante and Gianeselli

Table 4.18: COV in the ratio Q_p/Q_m for pipe and PPC piles

CPT/PCPT-based method	σ	μ	COV	R_2
Aoki and de Alencar (1975)	0.45	0.96	0.464	7
Clisby et al. (1978)	0.50	1.05	0.479	9
Schmertmann (1978)	0.48	0.97	0.494	10
De Ruiter and Beringen (1979)	0.43	1.05	0.411	3
Philipponnat (1980)	0.44	1.00	0.435	5
Tumay and Fakhroo (1982)	0.44	1.07	0.408	2
Price and Wardle (1982)	0.46	0.98	0.470	8
Bustamante and Gianeselli (1982)	0.42	0.95	0.441	6
Almeida et al. (1996)	0.42	1.00	0.424	4
Eslami and Fellenius (1997)	0.44	1.11	0.399	1
Takesue et al. (1998)	0.51	0.93	0.553	11

(1982) method was the second best performer while the De Ruiter and Beringen (1979) and Philipponnat (1980) methods were equally the third best performers. The cumulative probability trend in Figure 4.11 showed that all methods tend to pass the P_{50} = 1 point suggesting improvement in the accuracy of pile capacity prediction.

In the initial evaluation, the Bustamante and Gianeselli (1982) showed the best performance in this criterion with P_{50} and $P_{90} - P_{50}$ values of 1.10 and 0.77 respectively. After calibration however, the P_{50} and $P_{90} - P_{50}$ values became 0.89 and 0.65, respectively, indicating reduced accuracy and improved precision. Therefore, the calibration process did not achieve the intended target in this method, and it was eventually outperformed by other methods.

Criterion 4

The Tumay and Fakhroo (1982) method was found to be the best performer in terms of the ±20% accuracy level as shown in Table 4.20, with an accuracy level of about 60%. Before calibration, this method had an accuracy level of about 37%. Thus, the calibration of the method has increased its accuracy level significantly. It was also noted that the De Ruiter and Beringen (1979) and Clisby et al. (1978) methods performed equally as second best, close to the Tumay and Fakhroo (1982) method with an accuracy level of about 58% and 59%, respectively. Figure 4.12 shows the histogram and log-normal distributions for the top four best performers. During the initial evaluation, Bustamante and Gianeselli (1982) method

Table 4.19: 50% and 90% cumulative probabilities in the ratio Q_p/Q_m for pipe and PPC piles

CPT/PCP-based method	P_{50}	$P_{90}-P_{50}$	R_1^*	R_2^*	$R_1^*+R_2^*$	R_3
Aoki and de Alencar (1975)	0.89	0.79	7	6	13	7
Clisby et al. (1978)	0.98	0.69	1	3	4	1
Schmertmann (1978)	0.87	1.00	10	11	21	11
De Ruiter and Beringen (1979)	0.94	0.78	2	7	9	3
Philipponnat (1980)	0.92	0.75	4	5	9	3
Tumay and Fakhroo (1982)	0.91	0.84	5	8	13	7
Price and Wardle (1982)	0.88	0.98	8	10	18	10
Bustamante and Gianeselli (1982)	0.89	0.65	6	2	8	2
Almeida et al. (1996)	0.88	0.71	9	4	13	7
Eslami and Fellenius (1997)	0.93	0.91	3	9	12	5
Takesue et al. (1998)	0.77	0.57	11	1	12	5

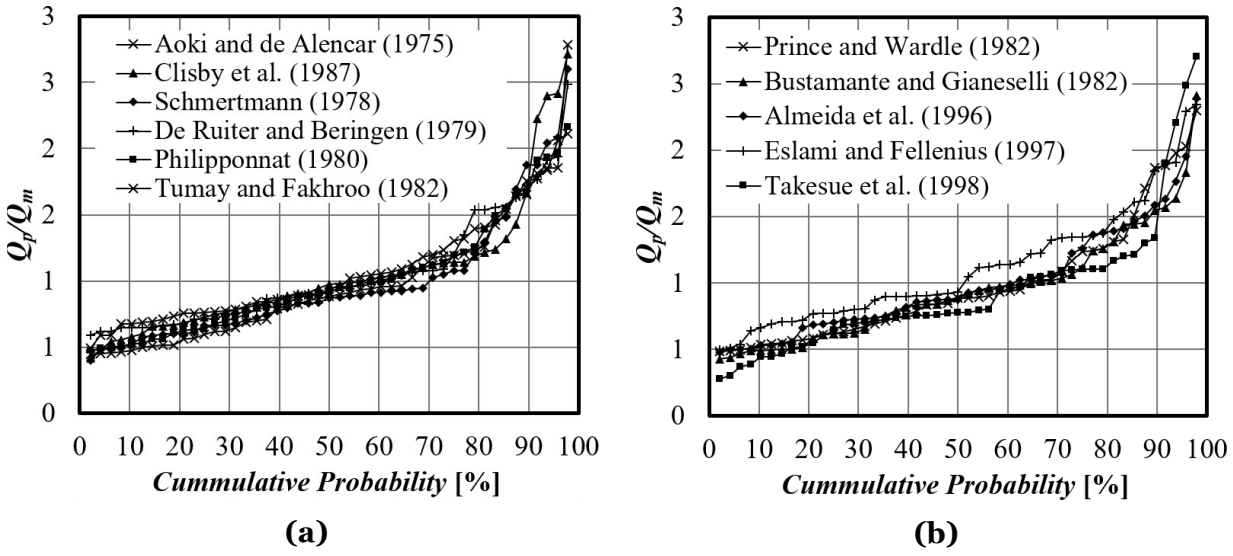

Figure 4.11: Cumulative probabilities of the ratio Q_p/Q_m values for pipe and PPC piles

showed the best performance with an accuracy level of 53%. There was no improvement of this accuracy level after calibration.

Rank Index *RI*

After the calibration was performed, the method originally proposed by De Ruiter and Beringen (1979) was found to be the top performer with an overall *RI* of 9. Table 4.21 summarizes the *RI* and the overall ranks of each method. The De Ruiter and Beringen (1979) method was among the worst performers in the initial evaluation. However, the

Table 4.20: ±20% accuracy level based on histogram and log-normal distribution for pipe and PPC piles

CPT/PCPT-based method	Histogram	Log-normal	R_1^*	R_2^*	$R_1^* + R_2^*$	R_4
Aoki and de Alencar (1975)	48.94 %	50.84 %	9	10	19	11
Clisby et al. (1978)	63.83 %	55.77 %	1	5	6	2
Schmertmann (1978)	51.06 %	52.66 %	8	9	17	8
De Ruiter and Beringen (1979)	55.32%	60.76 %	4	2	6	2
Philipponnat (1980)	53.19 %	54.95 %	6	6	12	6
Tumay and Fakhroo (1982)	59.57 %	61.17 %	2	1	3	1
Price and Wardle (1982)	46.81 %	53.07 %	11	7	18	10
Bustamante and Gianeselli (1982)	48.94 %	53.01 %	9	8	17	8
Almeida et al. (1996)	53.19 %	56.51 %	6	4	10	5
Eslami and Fellenius (1997)	55.32 %	57.86%	4	3	7	4
Takesue et al. (1998)	57.45 %	45.07 %	3	11	14	7

calibration of the method improved it accuracy, which was its weaker side.

Table 4.21: Rank index (*RI*) and overall ranks of each CPT/PCPT-based methods for pipe and PPC piles after calibration

CPT/PCPT-based method	Cr. 1	Cr. 2	Cr. 3	Cr. 4	*RI*	Rank
Aoki and de Alencar (1975)	8	7	7	11	33	8
Clisby et al. (1978)	10	9	1	2	22	6
Schmertmann (1978)	5	10	11	8	34	9
De Ruiter and Beringen (1979)	1	3	3	2	9	1
Philipponnat (1980)	3	5	3	6	17	3
Tumay and Fakhroo (1982)	1	2	7	1	11	2
Price and Wardle (1982)	6	8	10	10	34	9
Bustamante and Gianeselli (1982)	7	6	2	8	23	7
Almeida et al. (1996)	4	4	7	5	20	5
Eslami and Fellenius (1997)	9	1	7	4	19	4
Takesue et al. (1998)	11	11	5	7	34	9

4.5 *Proposed CPT-Based Design Methods*

In most of the design methods, the calibration process has improved their overall performance. Typically, those methods which performed worst in the initial evaluation due to their tendency of overpredicting pile capacity, became the best performers after the calibration. The best performer for H-piles was the modified (calibrated) Tumay and Fakhroo

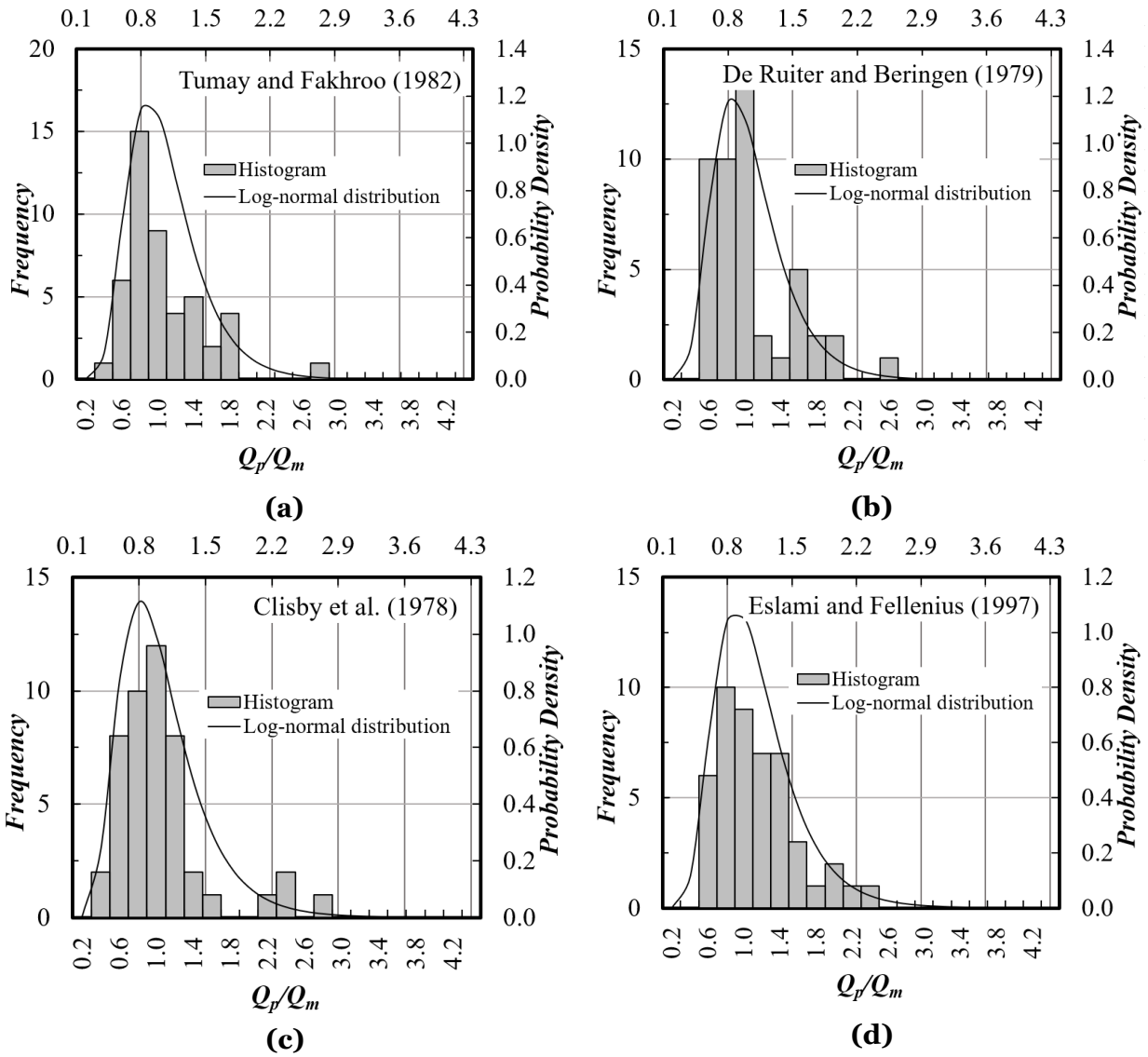

Figure 4.12: Histogram and log-normal distribution plots of the top four best performers for pipe and PPC piles

(1982) method. Whereas for pipe and PPC piles, the modified De Ruiter and Beringen (1979) method, which is also known as the *European Method*, was the best performer. The proposed CPT-based design methods are summarized in the following sections.

4.5.1 H-Piles

Employing the η and θ values obtained by the calibration method utilized in this study, a modified CPT-based method was proposed for HP piles. The η and θ values for the modified

Tumay and Fakhroo (1982) method were computed as 0.5 and 0.89 (here taken as ~ 0.90), respectively. For H-piles, the proposed unit toe resistance, r_t, equation is given by:

$$r_t = 0.5 \left(\frac{q_{c1} + q_{c2}}{4} + \frac{q_a}{2} \right) \leq 15\,\text{MPa}, \tag{4.1}$$

where q_{c1} = average cone tip resistance below $4B$ below the pile tip [F/L^2], q_{c2} = average minimum cone tip resistance $4B$ below the pile tip [F/L^2], and q_a = average minimum cone tip resistance $8D$ above the pile tip [F/L^2]. B is the pile diameter [L].

And the unit shaft resistance, r_s, was proposed as shown below:

$$r_s = m^* f_{ca} \leq 72\,\text{kPa} \tag{4.2}$$

where f_{sa} = average load friction [F/L^2] given in Eq. 4.3, and m^* = modified friction coefficient given in Eq. 4.4.

$$f_{ca} = \frac{\sum_{i=1}^{N} f_i \Delta z_i}{\sum_{i=1}^{N} \Delta z_i} \tag{4.3}$$

where f_i = local sleeve friction at the ith soil layer [F/L^2], Δz_i = depth of the ith soil layer, and N = total number of soil layers.

$$m^* = 0.45 + 8.55 \exp(-0.09 f_{ca}) \tag{4.4}$$

4.5.2 Pipe and PPC Piles

The modified De Ruiter and Beringen (1979) method was regarded as the best performer for pipe and PPC piles. The calibration factors η and θ were found to be 0.90 and 0.47 (taken as ~ 0.50), respectively. The unit toe and shaft resistances in clay and sand soils are given separately. The unit toe resistance, r_t, in clay soils is given as:

$$r_t = 0.90 N_c \frac{q_{ca}}{N_k} \tag{4.5}$$

where N_c = bearing capacity factor = 9, N_k = cone factor = 15 in this study, q_{ca} = average cone tip resistance around the pile tip given as follows:

$$q_{ca} = \frac{q_{c1} + q_{c2}}{2} \tag{4.6}$$

where q_{c1} = average cone tip resistance $0.7D$ to $4D$ below the pile tip [F/L^2], and q_{c2} = average cone tip resistance $8D$ above the pile tip [F/L^2]. The unit resistance in sandy soils is obtained from:

$$r_t = 0.90 q_{ca} \tag{4.7}$$

where q_{ca} = average cone tip resistance around the pile tip [F/L^2] given by Eq. 4.6.

The unit shaft resistance, r_s, in clay soils is given by the following equation:

$$r_s = 0.5 \alpha \frac{q_{ca}}{N_k} \tag{4.8}$$

where α = adhesion factor = 0.5, q_{ca} = average cone tip resistance around the pile tip [F/L^2] given by Eq. 4.6, and N_k = cone factor = 15. The unit shaft resistance, r_s, in sand soils is proposed as:

$$r_s = 0.5 \min\left[f_s,\ q_c/300,\ 120 \text{ kpa} \right] \tag{4.9}$$

where min[ ] = minimum of [ ], f_s = local sleeve friction [kPa], q_c = cone tip resistance [kPa].

4.6 *Proposed Methods Versus Driving Formula*

Using driving records collected from the NDOT database, the LRFD based locally calibrated EN driving formula, which is currently adopted by NDOT and shown in Eq. 3.1, was implemented and compared with the proposed CPT-based design methods. The required data such as hammer type, rammer weight, drop height, and pile set were all included within the collected data. The aim of the comparison was mainly to assess the feasibility of the CPT-based methods to replace the exiting LRFD based driving equation for the prediction of pile capacity. The comparison was performed in two ways: (1) based on plots of the measured pile capacity (Q_m), which is based on PDA (CAPWAP) versus the predicted pile

capacity (Q_p) by CPT-based method and LRFD's driving formula, and (2) based on risk analysis (Briaud and Tucker, 1988). The risk from the LRFD driving formula was used as a reference, and the risks of the CPT-based methods were compared with the reference value.

4.6.1 Measured vs Predicted Pile Capacity

Figure 4.13a shows the measured pile capacity via PDA versus predicted pile capacity based on the proposed CPT-based method and the LRFD driving formula for H-piles. Both the CPT-based method and the driving equation seem to underpredict the actual pile capacity. In general, the driving formula slightly underpredicts pile capacity based on the slope of the best-fit line. In fact, the LRFD approach already imposes some resistance factor on the ultimate pile capacity predicted by the driving formula; the slight underprediction of pile capacity may be attributed to this.

On the other hand, Figure 4.13b shows the measured pile capacity versus the predicted pile capacity by the proposed CPT based method and the LRFD driving formula for pipe and PPC piles. The CPT based approach showed more scatter compared to the LRFD driving formula predictions. In terms of the slope of the best fit line, the CPT-based method showed slight undeprediction than the driving formula even though resistance factors were not applied to the CPT-based-predicted ultimate pile capacity.

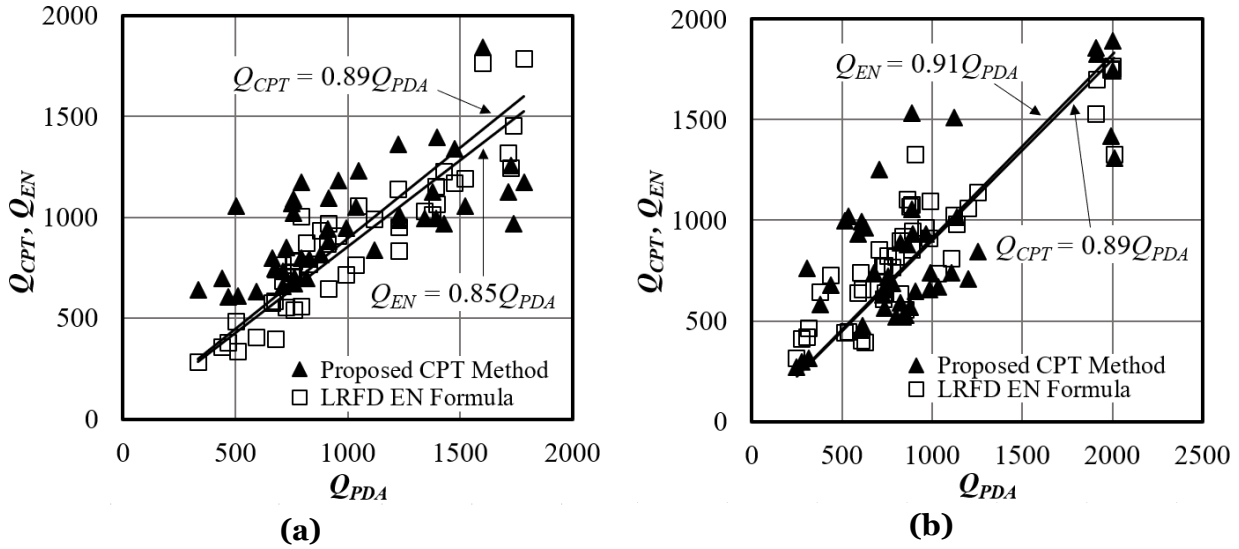

Figure 4.13: Measured vs predicted pile capacity: (a) H-piles, (b) pipe and PPC piles

4.6.2 Risk Analysis

Another important comparison was performed by considering the Q_p/Q_m ratios and employing a risk analysis following the method proposed by Briaud and Tucker (1988). Based on this approach, the risk of the predicted pile capacity being greater than the measured pile capacity was studied for both the CPT-based methods and the LRFD driving formula. This approach is defined by Eq. 4.10 as follows:

$$R = P\left(\frac{Q_p}{FS} > Q_m\right) \tag{4.10}$$

where R = risk [%], Q_p = predicted pile capacity either by the proposed CPT based method or the Nebraska-specific LRFD driving formula [F], Q_m = measured pile capacity by a dynamic load test (CAPWAP) [F], and FS = factor of safety. For a FS of 1, the risk of Q_p being greater than Q_m is compared for both methods. Details of how the plot relating the risk versus FS is described in Briaud and Tucker (1988).

Figure 4.14a shows the risk(%) versus FS for H-piles. Q_p was obtained by the proposed CPT-based method and currently adopted LRFD driving formula by NDOT. Per this figure, the risk of predicted capacity being greater than the measured pile capacity associated with the proposed CPT-based method is 54% and that of the LRFD driving equation is 23%. Making the risk level of the LRFD driving equation as a reference case, it showed that the proposed CPT-based method is risky by about 31%. Moreover, a FS of about 1.20 is required on the proposed CPT-based method to make the risk equivalent with the LRFD driving formula.

Figure 4.14b shows the risk(%) versus FS for pipe and PPC piles. In this case, the predicted pile capacity is based on the proposed CPT-based method for pipe and PPC piles and currently used the LRFD driving formula by NDOT. From this figure, the risk level associated with the proposed CPT-based method is found to be 41%. On the other hand, the LRFD driving formula has a risk of about 47%. If one takes the risk level of the LRFD driving formula to be the reference risk, then the proposed CPT-based method indicated to be less risky than the LRFD driving formula. This result seems to be surprising considering that the proposed CPT-based method was not factored yet. Strict conclusion about the

proposed CPT-based method being less risky may not be appropriate when taking into account that the analysis was done on a limited number of data sets.

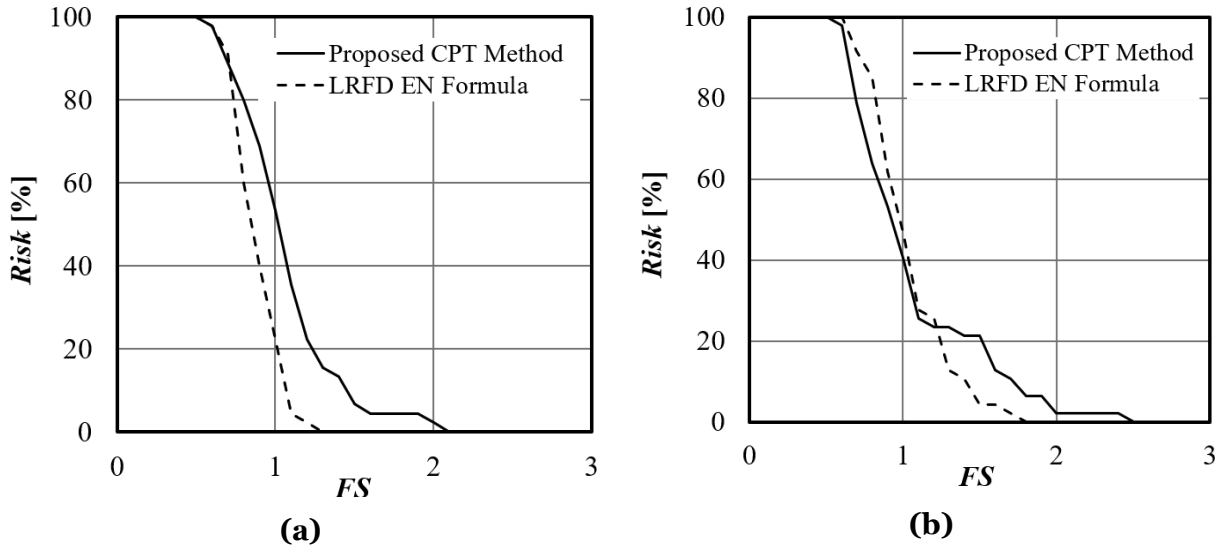

Figure 4.14: Risk vs factor of safety: (a) H-piles, (b) pipe and PPC piles

4.6.3 Concluding Remarks

Based on the comparison performed above, it was noted that the CPT-based performance was in line with expected results except for pipe and PPC piles category, in which especially, the risk associated with the proposed CPT-based method was less than the LRFD driving formula. Moreover, the risk analysis between proposed CPT-based methods and the LRFD driving formula results clearly showed the necessity of computing resistance factors corresponding to the proposed CPT-based methods. In fact, according to the results for pipe and PPC piles, resistance factors are not required as the risk of the unfactored CPT-based method was less than the LRFD driving formula. However, since the data set used for the comparison was limited, conclusions about the non-requirement of resistance factors cannot be forwarded. Overall, from the comparison of the two pile capacity prediction approaches, it can be concluded that the proposed CPT-based methods are in good agreement with the EN driving formula.

4.7 *LRFD Resistance Factors*

The design of pile foundation for bridge structures is a function of the loads and the soil resistances. The loads and soil resistances have various levels of uncertainty. In the traditional allowable (working) stress design (ASD) method, these uncertainties are incorporated in a single factor of safety (FS) whereas in the load-resistance factor design (LRFD) approach these uncertainties are quantified using probability-based methods (using probability density functions defined by their mean and standard deviation) (Paikowsky, 2004), and separate partial safety factors (load and resistance factors) are applied to satisfy a certain level of consistent reliability. The load and resistance factors are tied together through a reliability index (β), which is the quantification of the probability of failure (P_f), or simply the probability of the load effect exceeding the soil resistance. For example, $\beta = 2.33$ corresponds to $P_f = 1\%$. (Paikowsky, 2004) recommended a β value of 2.33 for redundant piles (piles in a pile group) and 3.00 ($P_f = 0.1\%$) for non-redundant piles. Therefore, in the LRFD approach, the FS concept is replaced by load factors, resistance factors, and a reliability index.

4.7.1 LRFD Bridge Design Specification

The general LRFD specification explained in Eq. 4.11, requires that the summation of factored loads is kept equal to or less than the summation of factored geotechnical resistances for all applicable geotechnical limit states (Abu-Hejleh et al., 2011). In this case, the strength limit state is applied, and the geotechnical resistance is considered as the pile capacity obtained from shear strength criterion.

$$\sum \eta_i \gamma_i Q_i \leq \sum \varphi_i R_{ni} \tag{4.11}$$

where Q_i = load on the foundation (e.g dead load), γ_i = load factor (e.g. dead load factor), R_{ni} = nominal geotechnical resistance (shaft or toe resistance), φ_i = resistance factor, and η_i = load factor related to ductility, redundancy, and operational importance. The load factors are usually greater than 1.0 and mainly account for the variability of loads, the lack

of accuracy in analysis, and the probability of different loads occurring at the same time. The resistance factors are applied to the nominal resistances and are generally less than 1.0. The resistance factors account for the variability of soil properties, structural dimensions, and uncertainty in the prediction of nominal resistance.

The Federal Highway Administration (FHWA) mandated the use of LRFD approach for all bridges after 2007. Although the FHWA madated the adoption of LRFD-based bridge design, not all DOT's have started using this approach (AbdelSalam et al., 2010), which may be due to the inherent conservatism of the method and subsequent increase in the cost of foundation work. (Paikowsky, 2004) attributed the conservatism of the LRFD when there is a wide variability in the determination of pile capacity (geotechnical aspect). To reduce the conservatism associated with the LRFD approach, local calibration of LRFD resistance factors is usually advised.

4.7.2 Locally Calibrated LRFD Resistance Factors

Locally calibrated LRFD resistance factors corresponding to each of the proposed CPT-based methods were obtained following a reliability based analysis. In this analysis, three main steps are included: (1) compilation of all available load test data, (2) statistical analysis, and (3) reliability analysis. In step 1, measured nominal strength and predicted nominal strength from the geotechnical design method to be calibrated were obtained. Measured nominal strength was obtained from dynamic load test data (PDA) and the predicted nominal strength was obtained from the proposed CPT-based methods. For each CPT-based method, a resistance bias, λ, was computed by dividing the measured pile capacity to the predicted pile capacity. In the statistical analysis stage, the mean bias, λ_R and coefficient of variation, COV, were computed. λ_R and COV account for variability in the predicted resistance with respect to the dynamic load test data. In the final stage, a reliability analysis was employed to compute the calibrated resistance factors. Three reliability analyses are commonly used (Abu-Hejleh et al., 2011). They are: (1) First Order Second Moment (FOSM), (2) First Order Reliability Method (FORM), and (3) Monte Carlo method. The first method is the simplest one and is already incorporated in AASHTO (American Association of State Highway and Transportation Officials) specifications. The second and

third methods are relatively complex and may require several steps. In this research, due to its relative simplicity, the FOSM method was employed to obtain the calibrated resistance factors.

Considering just dead and live loads (strength limit category I), and assuming log-normal distribution for the resistance, the resistance factor, φ, is computed following (Barker et al., 1991; Paikowsky, 2004):

$$\varphi = \left(\frac{\lambda_R}{\lambda_{QD}\frac{Q_D}{Q} + \lambda_{QL}\left(1-\frac{Q_D}{Q}\right)}\right)\left(\frac{\gamma_D\frac{Q_D}{Q} + \gamma_L\left(1-\frac{Q_D}{Q}\right)}{\lambda_{QD}\frac{Q_D}{Q} + \lambda_{QL}\left(1-\frac{Q_D}{Q}\right)}\right)\exp\left[\beta_T\sqrt{\ln\left(\left(1+COV_R^2\right)\left(1+COV_{QD}^2\right)^{\frac{Q_D}{Q}}\left(1+COV_{QL}^2\right)^{1-\frac{Q_D}{Q}}\right)}\right] \quad (4.12)$$

where λ_R = resistance bias factor, COV_R = coefficient of variation of resistance, λ_{QD}, λ_{QL} = dead load and live load bias factors respectively, COV_{QD}, COV_{QL} = coefficient of variation of dead load and live load respectively, Q_D/Q_L = dead load to live load ratio, and β_T = target reliability index. The probabilistic characteristics of the dead and live loads were taken from AASHTO (Nowak, 1999) as follows:

$$\gamma_L = 1.75 \quad \lambda_{QL} = 1.15 \quad COV_{QL} = 0.2 \quad (4.13a)$$

$$\gamma_D = 1.25 \quad \lambda_{QD} = 1.05 \quad COV_{QD} = 0.1 \quad (4.13b)$$

The dead load to live load ratio, Q_D/Q_L may vary from 2 to 3 (Abu-Hejleh et al., 2011). Q_D/Q_L was taken as 3 since the calibration would be insensitive above 3 (Abu-Farsakh et al., 2013).

For the soil resistance, the probabilistic characteristics were defined by using the resistance bias and variation coefficient of $Q_{P\ DA}/Q_{CP\ T}$ results from the proposed method for H-pile, pipe, and PPC piles. λ_R and COV_R for H-piles were obtained as 1.03 and 0.276, respectively. For pipe and PPC piles, λ_R and COV_R were obtained as 1.09 and 0.324, respectively. Assuming piles will be installed as a group, the target reliability index, β_T , was considered as 2.33 (corresponding to 1% probability of failure). After substituting the respective values of all the input parameters in Eq. 4.12, calibrated resistance factor for H-pile was computed as 0.60, and for pipe and PPC piles, it was computed as 0.55.

Chapter 5 COMPUTER PROGRAM: CPILE

5.1 Introduction

CPT-based pile design involves a long computational process. To facilitate the estimation of pile capacity based on CPT results, a computer program called CPILE was developed. CPILE has its own user-friendly graphical user interface or GUI. CPILE was developed using VB.NET programming language, which is an object-oriented programming language developed by Microsoft beginning 2002. The software is operational on Microsoft Windows operating system. It follows an easy installation procedure.

5.2 Project Information

The first window that appear when CPILE is run is the project information dialogbox. Figure 5.1 shows the project information window. In this window, information such as project name, project number, structure number, substructure number, ground elevation, and ground-water elevation are entered. The project information could be left blank initially and then updated later.

5.3 Main Window

After clicking the Ok button on the project information window, the main window shown in Figure 5.2 will be loaded. There are eight panels in this window. The first panel, which is shown in Figure 5.3 is "Input Data Column Locations". It specifies the input data column locations corresponding to the depth, cone tip resistance, local sleeve friction, pore pressure,

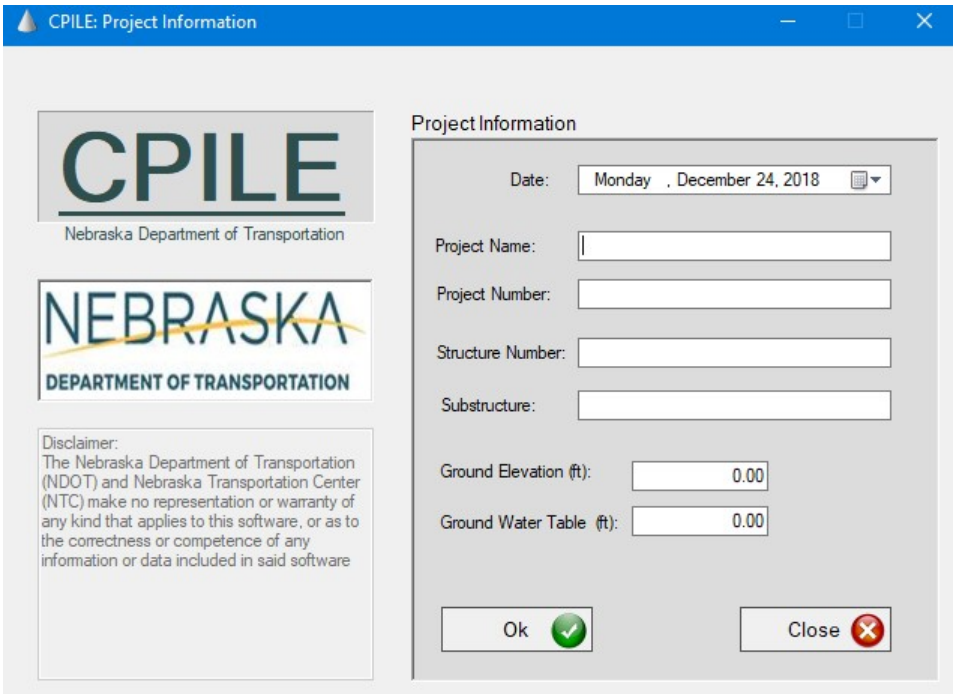

Figure 5.1: Project information window.

and SBT zones. The numbers entered in this boxes must conform with the column location in the CPT data table to be imported. For example, if 1 is entered for the depth location, then the 1st column of the CPT data to be imported should be the depth data. The next panel, which is shown in Figure 5.4 is the "Units Selection and Input Data Import". This allows user to manipulate the input and outputs data units, and import CPT data. One should make sure that the input units selected conform with the unit format of the CPT data to be imported. The output units can be changed depending on the preference of the user. Additionally, plots of CPT results could be made by clicking on plot button. The third panel, which is the "Table View", display imported data using the *output* unit selected. The fourth panel is the "Plot View" panel, which allows user to see plots of the cone tip resistance, sleeve friction, pore pressure, and SBT zones with depth. The fifth panel, which is the "Project information", depicts the project information entered at program start-up. The information could be updated any time by clicking on the "Project Information" button. The sixth panel, which is the "Magnify Plot", allows user to magnify and show the plots for the specified depth ranges entered in the "From" box and "To" box. When the button "Replot" is clicked, an updated plot will be displayed in the "Plot View" panel.

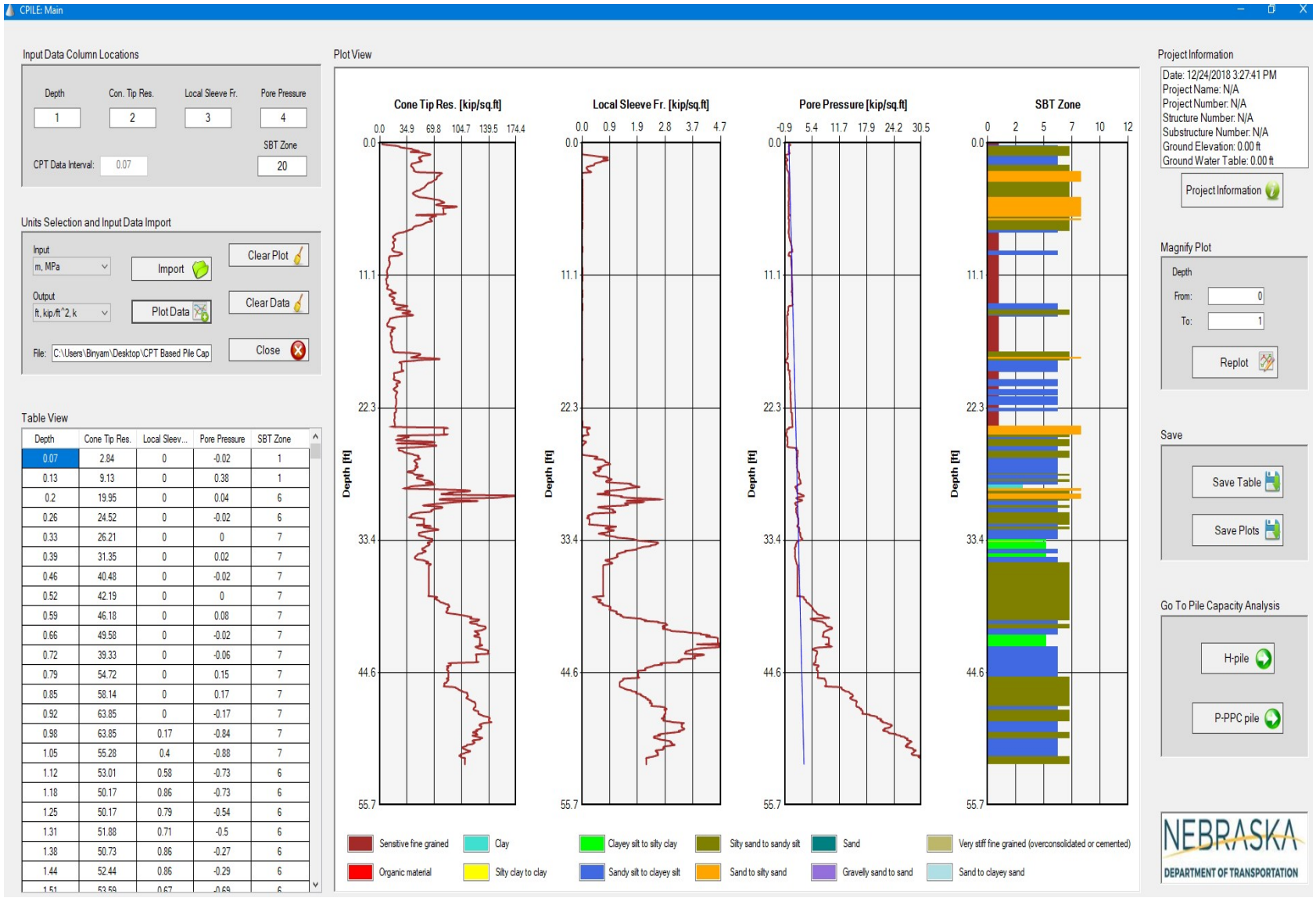

Figure 5.2: Main window.

Figure 5.3: Input data column locations panel.

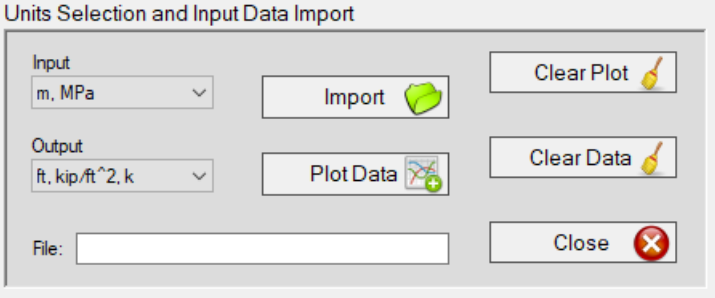

Figure 5.4: Units selection and data import panel.

The seventh panel is the "Save" panel, which can be used to save the data displayed in the "Table View" and "Plot View" panels. The table including project information is saved in *.txt file format while the plots are saved in *.png format. The last panel, which is "Go To Pile Capacity Analysis", allows user to select the specific type of CPT-based pile design desired, that is either H-pile ("H-pile") or pipe and PPC piles ("P-PPC").

5.4 *H-Pile Window*

When "H-pile" button, which is found on the "Go To Pile Capacity Analysis" panel within the main window, is clicked, the "H-pile" window shown in Figure 5.5 will be loaded. In this window, pile capacity analysis for H-piles is performed. There are six panels in this window. The first, and the second panels mainly are used to enter the required input parameters such as pile geometry information and other parameters specifically required for the modified Tumay and Fakhroo (1982) method. These parameters are summarized in Table 5.1. The third panel, which is shown in Figure 5.6 is "Pile Capacity Analysis".

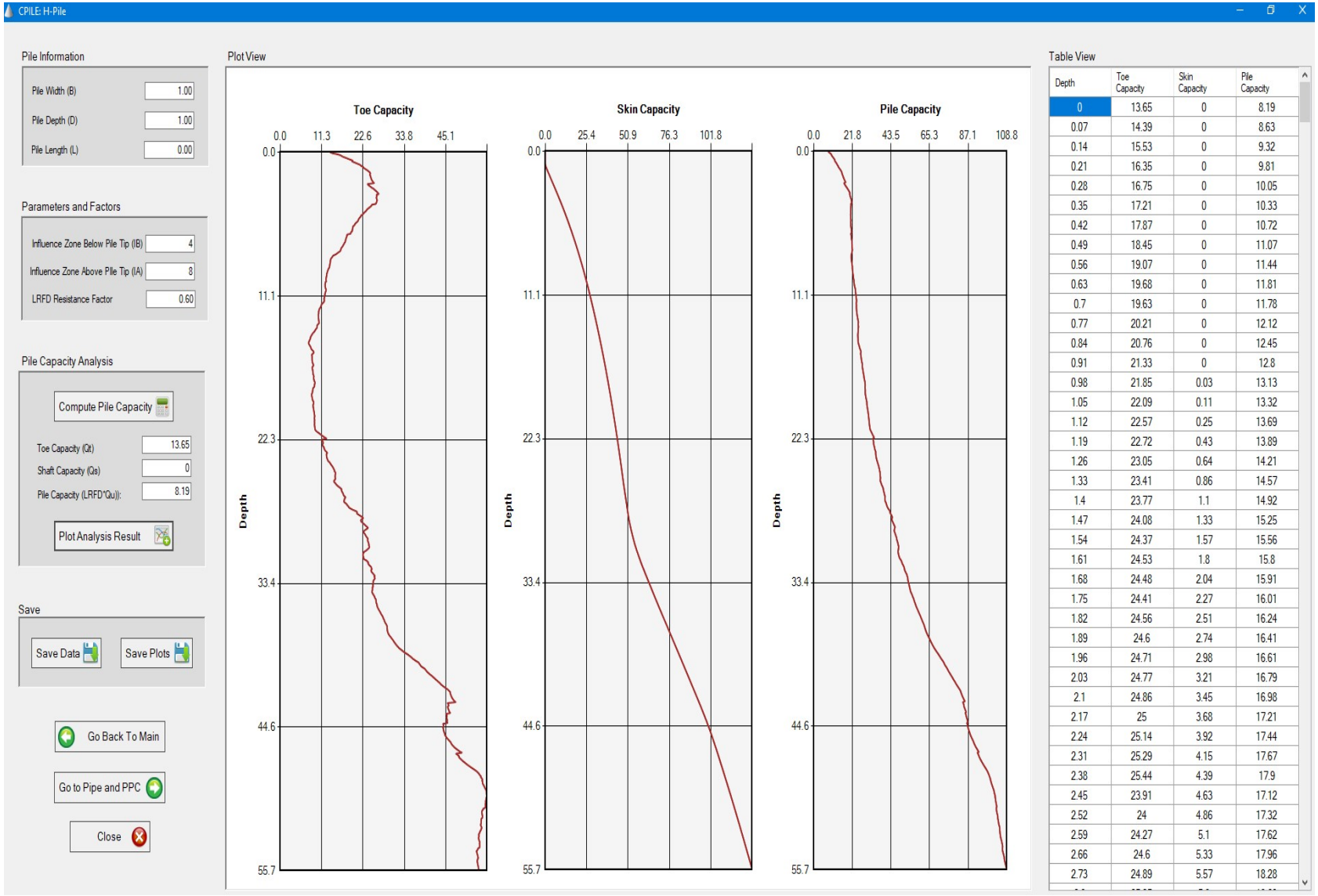

Figure 5.5: H-pile window.

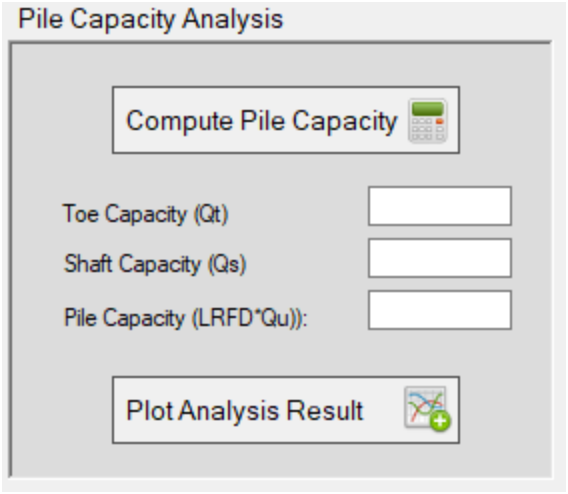

Figure 5.6: Pile capacity analysis panel for H-piles.

In this panel, by clicking the "Compute Pile Capacity" button, pile capacity computation is performed and computed pile capacity at the specified depth from the ground surface is displayed. Plots of the variation of toe-capacity, shaft-capacity and total factored pile capacity can be obtained by clicking on the "Plot Analysis Result" button. The other two panels are the "Plot View" and "Table" view panels. In these panels, output results are displayed in plot and tabular format, respectively. Finally, the outputs displayed in the "Plot View" and "Table View" can be saved by clicking the "Save Data" and "Save Plots" button found in the "Save" panel.

Table 5.1: Parameters for H-Pile analysis

Input	Description	Dimensions
Pile width(B)	Flange width	Unit of length
Pile depth(D)	Pile cross-sectional depth	Unit of length
Pile length(L)	Pile length	Unit of length
Influence zone below pile tip (IB)	Influence zone below the pile tip with respect to the pile width, i.e. IB*width(B). Default: IB = 4.	Dimensionless
Influence zone above pile tip (IA)	Influence zone above the pile tip with respect to the pile width, i.e. IA*width(B). Default: IA = 8.	Dimensionless
LRFD resistance factor	Load resistance factor applied on the nominal pile capacity estimated from CPT results.	Dimensionless

5.5 *Pipe and PPC piles Window*

Similar to the H-pile analysis, when the "P-PPC" button found on the "Go To Pile Analysis" panel in clicked, the "Pipe and PPC piles" window will be displayed, which is shown in Figure 5.7. There are six panels within this window. The first, and the second panels mainly are used to enter the required input parameters such as pile geometry information and other parameters specifically required for the modified De Ruiter and Beringen (1979) method. These parameters are summarized in Table 5.2. The third panel is the "Pile Capacity Analysis" panel, which is the same as the one shown in Figure 5.6. In this panel, by clicking the "Compute Pile Capacity" button, pile capacity computation is performed and computed pile capacity at the specified depth from the ground surface is displayed. Plots of the variation of toe-capacity, shaft-capacity and total factored pile capacity can be obtained by clicking on the "Plot Analysis Result" button. The other two panels are the "Plot View" and "Table" view panels. In these panels, output results are displayed in plot and tabular format, respectively. Finally, the outputs displayed in the "Plot View" and "Table View" can be saved by clicking the "Save Data" and "Save Plots" button found in the "Save" panel.

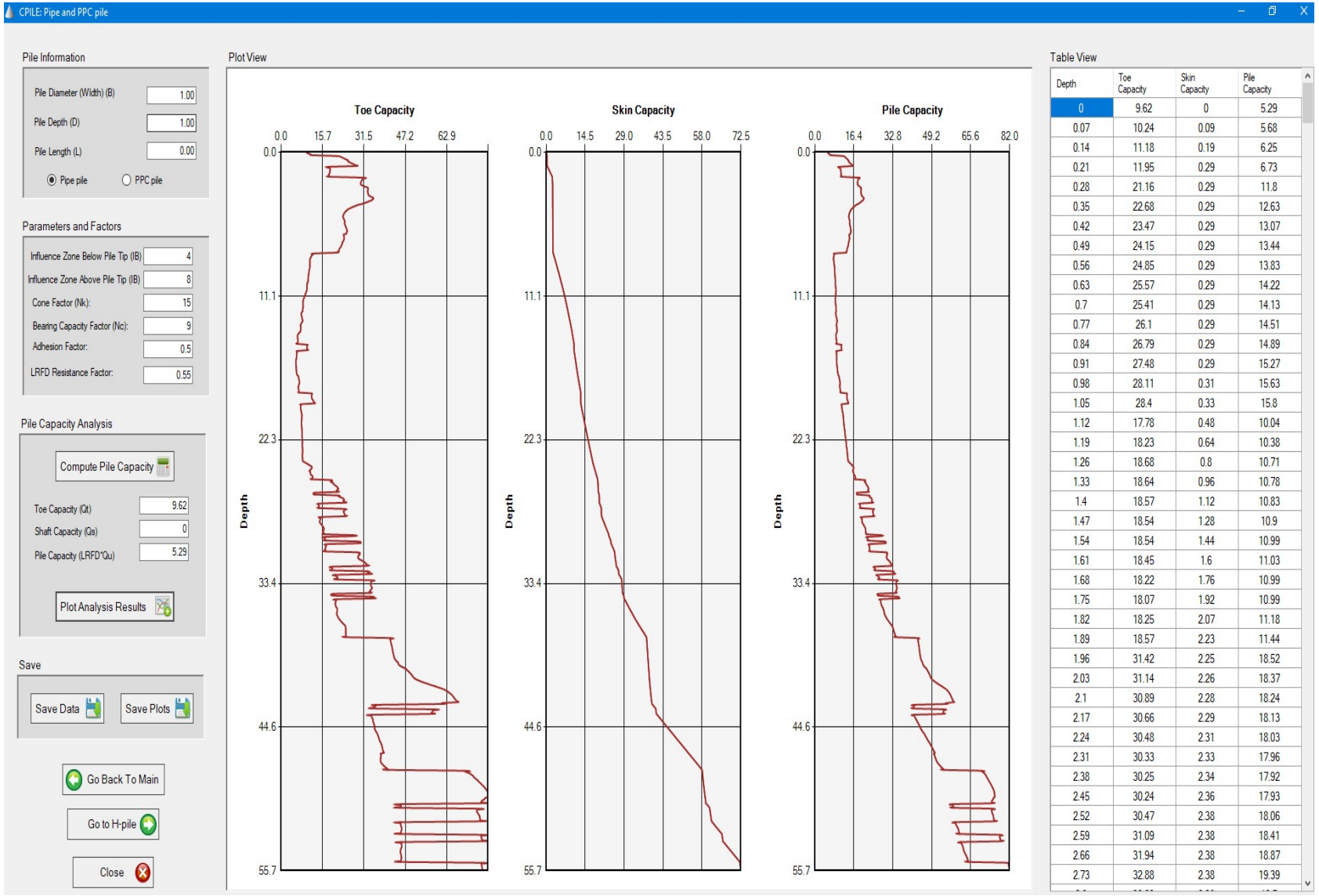

Figure 5.7: Pipe and PPC pile window.

Table 5.2: Parameters for Pipe and PPC pile analysis

Input	Description	Dimensions
Pile Diameter (width) (B)	Diameter for pipe piles and width for square PPC piles	Unit of length
Pile depth(D)	Cross-sectional depth for square PPC piles. This parameter has no influence on pipe piles	Unit of length
Pile length(L)	Pile length	Unit of length
Influence zone below pile tip (IB)	Influence zone below the pile tip with respect to the pile width, i.e. IB*width(B). Default: IB = 4.	Dimensionless
Influence zone above pile tip (IA)	Influence zone above the pile tip with respect to the pile width, i.e. IA*width(B). Default: IA = 8.	Dimensionless
Cone factor (N_k)	A factor that relates the cone tip resistance with undrained shear strength. It is set at a value of 15 by default.	Dimensionless
Bearing capacity factor (N_c)	A factor that relates the pile unit tip resistance with undrained shear strength. It is set at a value of 9 by default.	Dimensionless
Adhesion factor	A factor that relates the unit shaft resistance with local sleeve friction from CPT. It is set at a value of 0.5 by default.	Dimensionless
LRFD resistance factor	Load resistance factor applied on the nominal pile capacity estimated from CPT results.	Dimensionless

Chapter 6 CONCLUSIONS

This research report looked into the possibility of applying CPT or PCPT-based pile design methods in the analysis of pile foundations in Nebraska. To get the utmost performances of the CPT/PCPT-based methods, the calibration of the methods with respect to a more reliable and accurate pile capacity prediction method is very important. The high strain dynamic loading test (based on PDA) was sought as a viable option and subsequently used as a reference pile capacity. Proper adoption of statistical and non-statistical quantitative evaluation criteria is essential to assess the relative performances in terms of accuracy and precision of the calibrated CPT/PCPT-based design methods and pick the best performer(s).

After calibration, the modified Tumay and Fakhroo (1982) method showed the best performance for H-piles while the modified De Ruiter and Beringen (1979) method showed the best performance pipe and PPC piles. The geotechnical uncertainties related to variations of soil properties, uncertainty in design method predictions, and other construction-related measurements need to be incorporated in a suitable resistance factor (safety factor) to reach at a proper design pile capacity. In this case, the LRFD reliability based analysis was conducted to find the appropriate values of resistance factors for each CPT-based design methods proposed in this study. CPT-based pile design involves a long computational process. To facilitate the estimation of pile capacity based on CPT results, a computer program called CPILE was developed. CPILE has its own user friendly graphical user interface (GUI).

PART B

CPT-BASED SETTLEMENT PREDICTION

Chapter 1 CPT-BASED SETTLEMENT PREDICTION

1.1 Introduction

Settlement analysis often plays an important role in the design of bridges, buildings, plants, etc. For instance, excessive settlement and/or differential movement can cause distortion and crack in the superstructure of bridges. Thus, the potential settlement of foundation piles must be estimated with great care for such a high-cost structure. The prediction of pile settlements can be achieved as a sum of the pile settlement and the elastic deformation of a pile. The soil transitions from the initial stress state (i.e., overburden weight) to a new one under the additional applied load during the settlement. A major factor that greatly complicates the foundation design and the settlement prediction is that soil parameters need to be obtained from the actual construction site. In addition, current methods of the pile settlement prediction are either too simple (e.g., analytical or semi-analytical) or too complex (e.g., FEM simulation), which adds to the reliability issue of the settlement prediction.

In this research, the team focused on employing the $t-z$ method, which is widely used by FHWA and many state transportation agencies, for the prediction of pile settlement. The $t-z$ method is a commonly used static analysis for investigating pile load-settlement relations. This method considers side friction and end bearing at the pile-soil interface as well as the elastic compression of the pile.

Moreover, the $t-z$ method accounts for different mobilization of side frictions at the pile-soil interface along the length of the pile, which yields a more reliable estimate given that the soil behavior is nonlinear and soil profiles are most likely stratified. In this research, CPT testing data is combined with the t-z method to add confidence in the settlement prediction.The CPT-based settlement prediction can be categorized as either an analytical

approach or numerical approach Figure 1.1.

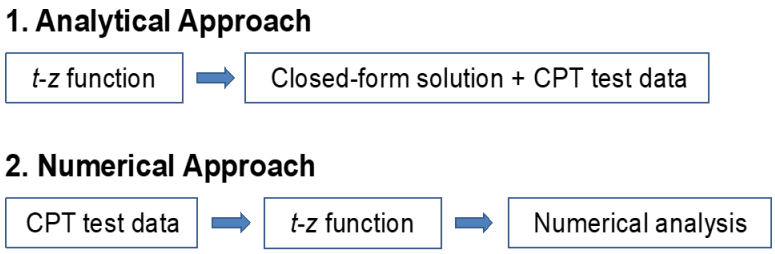

Figure 1.1: Flowcharts for CPT-based settlement prediction.

1.2 *Analytical Approach*

The $t - z$ method involves modeling the pile as a series of elements supported by discrete nonlinear springs, which represent the resistance of the soil in the skin friction (t-z springs), and a nonlinear spring at the pile tip representing the end-bearing ($q - z$) spring (Figure 1.2). The soil springs are nonlinear representations of the soil reaction, t (or q for the pile tip), versus displacement (z). Assuming the $t - z$ and $q - z$ curves are available, the axial load-settlement response can be obtained with the aid of a computer program such as TZPILE and FB-Pier. The site-specific $t - z$ (and $q - z$) curve may be derived from onsite static load tests.

In the analytical approach, a given load-transfer t-z function, which defines the relations between the shaft friction and the relative displacements as well as between the bearing stress and the pile displacement at the base, is solved to derive a closed-form solution to predict the pile settlement. During this derivation, CPT test results are used as input data. The settlement at the top of the pile, u_t, can be estimated depending on whether the pile-soil interface is in the elastic state, elastoplastic state, or plastic state (Misra and Chen, 2004; Haldar and Babu, 2008):

1. elastic state ($\xi_0 \geq 1$):

$$u_t = \frac{PL_p}{K_m} \frac{\cosh(\lambda) + \psi\lambda \sinh(\lambda)}{\lambda \sinh(\lambda) + \psi\lambda \cosh(\lambda)} \quad (1.1)$$

2. elastoplastic state ($0 \leq \xi_0 \geq 1$):

$$u_t = 0.5\left(1 - \xi_0^2 - \frac{L_p(q_0 L_p - p)}{K_m}\right)\left(1 - \xi + {}_0 u \quad {}_0\right) \tag{1.2}$$

3. plastic state ($\xi_0 \leq 0$):

$$u_t = \frac{P_u L_p}{K_m} 0.5 + \left(\frac{P}{P_u} - 1 + \left(\frac{P}{P_u} - 1\right)\frac{1}{\lambda^2 \psi}\right. \tag{1.3}$$

where P = applied load at the pile head, L_p = pile length, and q_0 = yield strength of the pile-soil interface that can be obtained as the product of the pile perimeter and the ultimate shear strength of the pile-soil interface. Axial stiffness of a pile, K_m, can be determined from:

$$K_m = EA \tag{1.4}$$

where E = Young's modulus and A = cross-sectional area of the pile. The scaling factor, λ, is obtained by:

$$\lambda = \sqrt{\frac{KL_p^2}{K_m}} \tag{1.5}$$

where K = shear modulus of the pile-soil interface.

$$K = \frac{k_1 s_{us}}{2(1 + \upsilon)} \tag{1.6}$$

where k_1 = constant, s_{us} = undrained shear near the pile shaft, and υ = Poisson's ratio of the soil. At the pile tip, soil stiffness, K_t, is calculated from:

$$K_t = \frac{0.3\pi D_p E_t}{1 - \upsilon^2} \tag{1.7}$$

where D_p = diameter of pile. Another elastic modulus of soil near the toe, E_t, is obtained from:

$$E_t = k_2 s_{ub} \tag{1.8}$$

where k_2 = constant, and s_{ub} = average undrained shear strength near the pile tip. Haldar

and Babu (2008) stated the constants k_1 and k_2 are statistical parameters that follow a log-normal distribution by analyzing 13 representative pile loading tests. The estimated means and standard deviations are 1,437 and 437 for k_1, and 317 and 144 for k_2, respectively. A non-dimensional factor, ψ, can be determined from:

$$\psi = \frac{K_t}{KL_p} \tag{1.9}$$

And the interface displacement at yield, u_0, can be obtained by:

$$u_0 = \frac{q_0}{K} \tag{1.10}$$

p_u is the ultimate shaft capacity of the pile:

$$P_u = \pi D_p L_p \tau_u \tag{1.11}$$

where τ_u = ultimate pile-soil interface shear strength, which can be calculated from:

$$\tau_s = a s_{us} \tag{1.12}$$

where a = pile-soil adhesion factor obtained from:

$$a = 0.5 \left(\frac{\sigma'_{v0}}{s_{us}} \right)^{0.45} \tag{1.13}$$

where σ'_{v0} = average vertical effective stress over the pile length. Lastly, the value of ξ_0 needs to be calculated by solving the following equations:

$$\left(\xi_0 - 1 - \frac{\tanh(\lambda \xi_0)}{\lambda} + \frac{Q_t}{Q_u} \right) - \frac{1}{\cosh(\lambda \xi_0)} \frac{\psi}{\cosh(\lambda \xi_0) + \psi \lambda \sinh(\lambda)} \tag{1.14}$$

In summary, these equations can be embedded into any mathematical software to predict a potential value of pile settlement with the given inputs. The average undrained shear strength near the pile shaft, s_{us}, and pile tip, s_{ub}, r_t above and r_b below the pile tip where: $r_t = D_p \exp(\pi \tan \varphi)$ and $r_b = D_p \exp(\varphi \tan \varphi \cos \varphi)$, the friction angle of soil φ, and the

average vertical effective stress over the pile length σ'_{v0} are obtained by analyzing CPT data.

1.3 Numerical Approaches

In the numerical approach, CPT test results are directly used to derive a proper t-z function that reflects the shear behavior at the pile-soil interface. There are three widely adopted models with which the t-z function can be derived: (1) hyperbolic load-transfer curves, (2) exponential functions, and (3) linear elastic-perfectly-plastic models.

1.3.1 Basic Algorithm

The basic algorithm is briefly described herein: a pile is discretized into N elements (element length is $L_0 = L_p/N$) and $(N+1)$ interfaces. The axial load applied on the pile top is $Q_1 = Q_t$. The position of the i^{th}-element is defined by the relative displacement of its upper interface δ_i and its lower interface δ_{i+1} (refer Figure 1.2). Axial displacement of a pile depends on the interaction of the pile with the surrounding soil and its stress state. The shaft resistance S_i is calculated from the unit side friction s_i and the dimension of the i^{th}-element. The shaft resistance and axial forces should satisfy force equilibrium.

1.3.2 Load-Displacement ($t-z$) Functions

Hyperbolic Load-Transfer Curves

Hirayama (1990) suggested the relationships between skin friction f and pile-shaft displacement z, as well as end resistance q and tip displacement z_e , based on the Kondner-type hyperbolic curves:

$$f = \frac{z}{a_f + b_f z} \tag{1.15}$$

$$q = \frac{z_e}{a_e + b_e z_e} \tag{1.16}$$

where the constants are $bf = 1/f_{ult}$, $b_e = 1/q_{ult}$, $a_f = z_{ref,f}/f_{ult}$, and $a_e = 0.25D_e/q_{ult}$ (D_e: base diameter) in which $z_{ref,f}$ is the displacement required to mobilize half of f_{ult} (generally

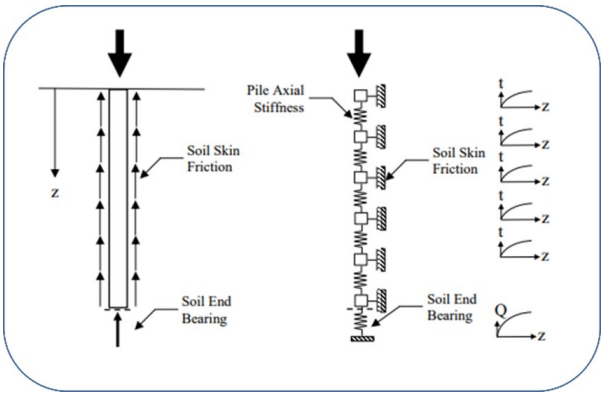

(a) Overview of pile and $t - z$ function

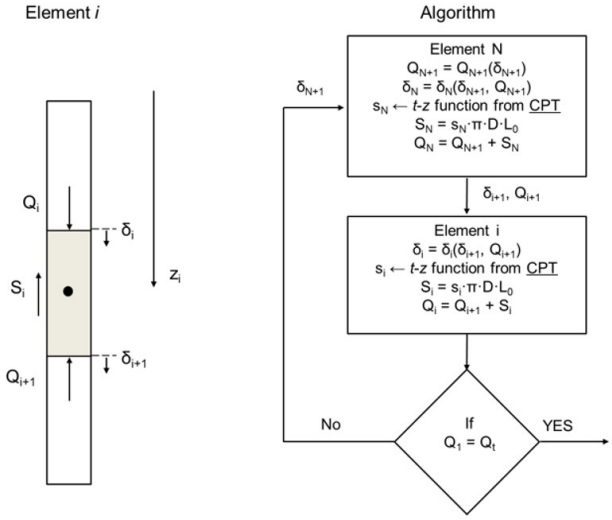

(b) Numerical simulation algorithm

Figure 1.2: Numerical approach of the CPT-based settlement prediction

$z_{ref,f} \approx 0.0025 D_s$; D_s = shaft diameter). Here, f_{ult} is the ultimate skin resistance, and q_{ult} is the ultimate tip resistance.

Exponential Functions

Gwizdala and Steczniewski (2007) suggested the $t - z$ function for the shaft of pile based on the power function:

$$t = q_{sui} \left(\frac{z}{z_v} \right)^a \quad \text{for} \quad z < z_v \tag{1.17}$$

where q_{sui} = ultimate soil resistance along the pile within the i^{th}-layer, t = shaft resistance, z = shaft displacement, and z_v = critical shaft displacement, which is defined as 3% of pile

diameter. The exponent, a, can be determined using the following formula for a pile that is installed in cohesive soils:

$$a = 0.654 - 0.809\frac{R_{su}}{R_u} \quad \text{for} \quad \frac{R_{su}}{R_u} < 5 \tag{1.18a}$$

$$a = 0.25 \quad \text{for} \quad \frac{R_{su}}{R_u} > 5 \tag{1.18b}$$

where R_{su} = ultimate soil resistance along the pile shaft and R_u is the ultimate bearing capacity. For the base of pile, the following power function is used:

$$q = q_{bu}\left(\frac{z}{z_f}\right)^{\beta} \quad \text{for} \quad z < z_f \tag{1.19}$$

where q_{bu} = ultimate base resistance, q = base resistance, z = base displacement, and z_f = critical base displacement. The displacement z_f of the pile base is assumed as corresponding to 10% of base diameter: $z_f = 0.1D_e$. The exponent, β, can be determined using the following formula:

$$\beta = 0.671 - 0.104\frac{R_u}{R_B} \quad \text{for} \quad \frac{R_u}{R_B} < 5 \tag{1.20a}$$

$$\beta = 0.15 \quad \text{for} \quad \frac{R_u}{R_B} \geq 5 \tag{1.20b}$$

where R_B = 1.0 MN.

Linear-Elastic-Perfectly-Plastic Model

Pasten and Santamarina (2014) is one of many examples that used a linear-elastic-perfectly-plastic model as the $t - z$ function to investigate the possible settlement of pile (Figure 1.3).

The side friction S_i for the i^{th}-element is defined as:

$$\begin{cases} -s_i^{ult}, & \text{if } \dfrac{\delta_i + \delta_{i+1}}{2} \leq -\delta_s^* \\ \dfrac{\delta_i + \delta_{i+1}}{2} - s, & \end{cases}$$

$$\frac{\delta + \delta}{s_i(\delta_i, \delta_{i+1}) = \square k_i} < \delta_s^*$$

$$_{i+1}, \quad \text{if} \quad \delta^* < {}^{i} \qquad _{i+1} \tag{1.21}$$

$$_{s} \quad \frac{i}{\qquad}$$

$$2 \qquad\qquad 2$$

$$2$$

$$\delta + \delta$$

$$\square s^{i}_{ult}, \qquad \text{if } \delta^* \leq$$

$$i+1$$

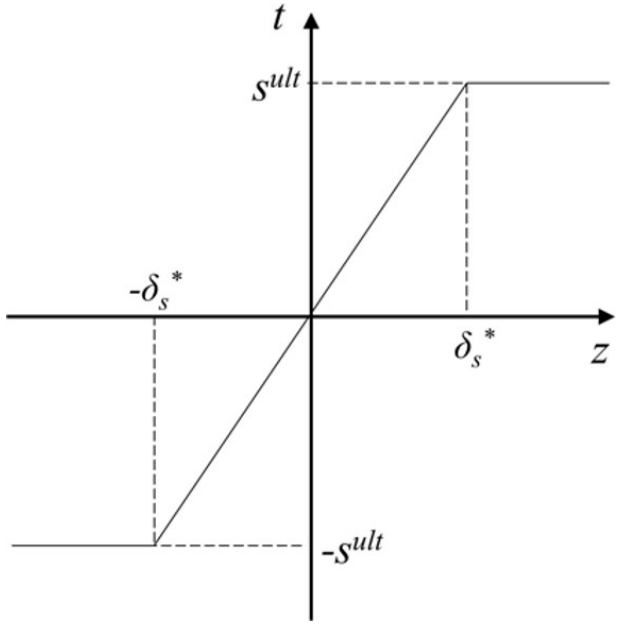

Figure 1.3: Soil constitutive model: Linear-elastic-perfectly-plastic model

where δ_i and δ_{i+1} = relative pile-soil displacement at i^{th}-element upper and lower interfaces respectively, s_i^{ult} = ultimate skin resistance, k_i = shaft stiffness $k_i = s_i^{ult}/\delta_s^*$, and δ_s^* = critical relative displacement to mobilize the ultimate skin resistance s_i^{ult}, which is assumed as 0.5% of the pile diameter. The ultimate tip resistance is defined as:

$$Q_{N+1}\delta_{N+1} = \begin{cases} \dfrac{Q_t^{ult}}{\delta_t^*}\delta_{N+1}, & \text{if } 0 < \delta_{N+1} < \delta_t^* \\ Q_t^{ult}, & \text{if } \delta_t^* \le \delta_{N+1} \end{cases} \tag{1.22}$$

where δ_{N+1} = pile tip displacement, Q_t^{ult} = ultimate tip resistance, and δ_t^* = critical relative displacement to mobilize the ultimate tip resistance Q_t^{ult}, which is assumed as 5% of the pile diameter.

1.4 *Application*

1.4.1 Evaluation Site

We selected SMC1 site for which CPT data is provided by the NDOT. In order to predict the pile settlement, either through analytical or numerical approaches, ultimate skin and tip resistances are needed. Soils within the depth of 13.00 m are divided into four layers based on the CPT data of the evaluation site, using the SBT chart (Robertson et al. (1986); Figure 3.2). The soil layer is shown in Table 1.1. Note that the CPT penetration was conducted up to the depth of 13.64 m at the evaluation site.

From PART A of this report, it was found that Tumay and Fakhroo (1982) and (De Ruiter and Beringen, 1979) (European method) are best for calculating the ultimate skin and tip resistances for the H-pile and the pipe-pile, respectively, with given Nebraska soil conditions. Details about the the above two CPT-based pile design methods is provided in PART A, chapter two of this report.

Table 1.1: Soil layers of the evaluation site

Soil layer	Depth(m)	SBT Zone	Soil behavior type
1	0 1.80	7	Silty sand to sandy silt
		3	Clay
2	1.80 8.22	4	Silty clay to clay
		5	Clayey silt to silty clay
		6	Sandy silt to clayey silt
3	8.22 8.34	7	Silty sand to sandy silt
		8	Sand to silty sand
		3	Clay
4	8.34 13.00	4	Silty clay to clay
		5	Clayey silt to silty clay
		6	Sandy silt to clayey silt

1.4.2 Pile Types

One type of H-pile and pipe-pile were chosen to evaluate the CPT-based settlement prediction. Properties and dimensions of selected piles are shown in Table 1.2.

Table 1.2: Pile type and properties

Pile Type	Young's Modulus (GPa)	Flange width (m)	Diameter (m)	Length (m)
H-pile 10x42	200	0.26	0.30 (equivalent)	11
Pipe-pile 12.75"	200	-	0.32	11

1.5 *Results*

1.5.1 H-Pile

Analytical Approach

For the evaluation site, constants k_1 and k_2 are chosen as 1,437 and 317, respectively. Other parameters are as follows: average friction angle of soil within the pile length φ=33^0 (from CPT data), pile head force P = 291 kN, Poisson's ratio υ= 0.35, cross-sectional area of pile A = 0.0645 m^2, diameter of pile D_p = 0.3 m, cross-sectional perimeter of pile S = 1.016 m, and Young's modulus of pile E = 200 GPa. The average undrained shear strength near the pile shaft is s_{us} = 108 kPa, and near the pile tip is S_{ub} = 170 kPa, respectively, based on the CPT data. The average vertical effective stress over the pile length is $\sigma'_{\upsilon 0}$=60 kPa. Through Equation 1.1 to Equation 1.14, pertinent parameters are calculated, and ξ_0 is computed as 1.46 ¿ 1. Thus, the pile-soil interface is in the elastic state, and the settlement at the top of the H-pile is estimated as: u_t= 0.53 mm in response to the applied load of 291 kN.

Numerical Approach

Hyperbolic Curve

The pile is divided into 550 elements for the numerical approach. The height of each element is 0.02 m, which is equal to the cone penetration depth. The ultimate tip resistance q_{ult} and ultimate skin resistance f_{ult} of each element are determined by using hyperbolic functions along with the Tumay and Fakhroo (1982) equation. After that, based on the pile diameter D_e, tip resistance q_{ult}, and ultimate skin resistance f_{ult}, parameters a_e, b_e, a_f, and b_f can be determined. Then, the force equilibrium is applied to each element with the load-transfer

numerical algorithm. Finally, the force on the top of the pile Q_1 is calculated. The pile head force Q^{head} was preselected as 291 kN. When the calculation error $|Q_1 - Q^{head}| \leq E$, where E is a tolerance value (selected as 5 kN herein), the forward-successive calculation stops. The distribution of axial forces, skin frictions and displacements of each sub-element along the pile length are shown in Figure 1.4. The settlement at the top of the pile is estimated as 0.50 mm in response to the applied load of 291 kN.

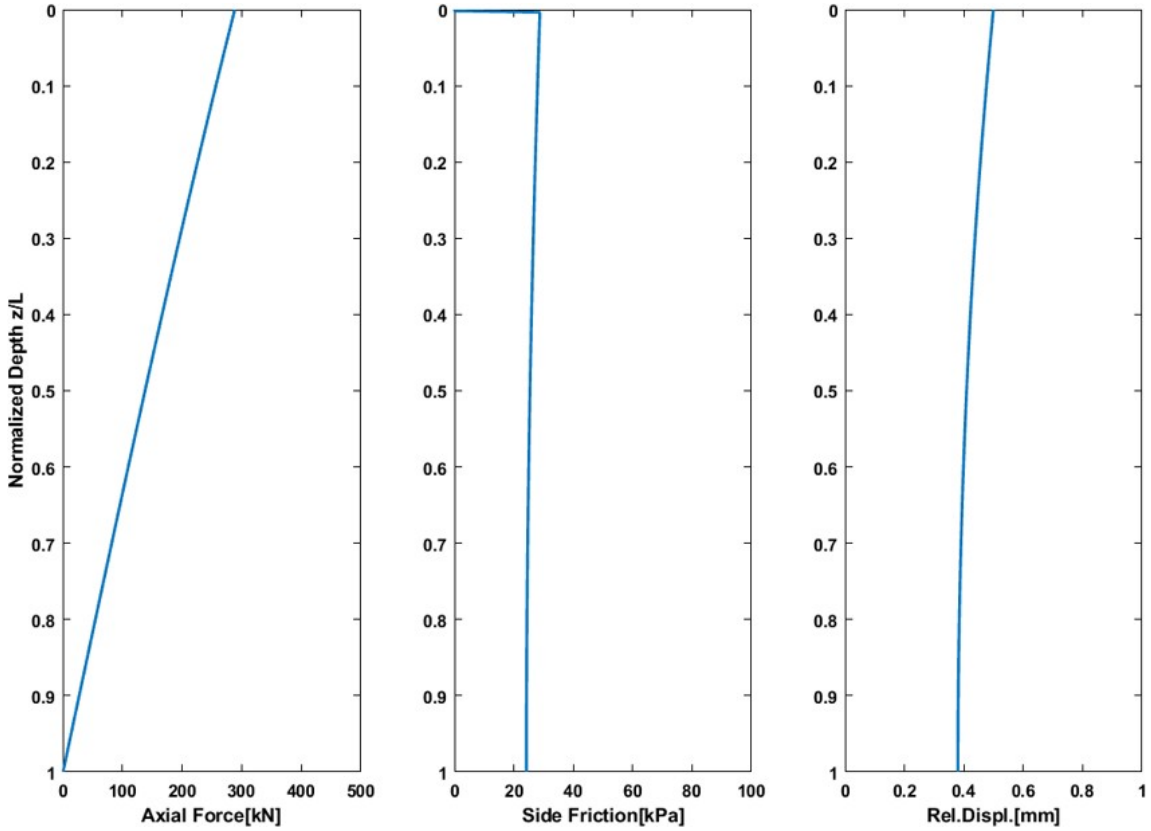

Figure 1.4: Results of numerical approach to predict the pile settlement using hyperbolic curves for the load-transfer t-z function: H-pile

Exponential Function

Similarly, the ultimate soil resistance, R_{su}, ultimate base resistance, q_{bu}, ultimate bearing capacity R_u, α and β are determined using exponential functions along with the Tumay and Fakhroo (1982) equation. Based on the equivalent pile diameter D_e, z_v and z_f are determined. The remaining procedures are the same as above, for using a hyperbolic curve

for the $t - z$ function. The settlement at the top of the pile is estimated as 0.22 mm. The detailed results are shown in Figure 1.5.

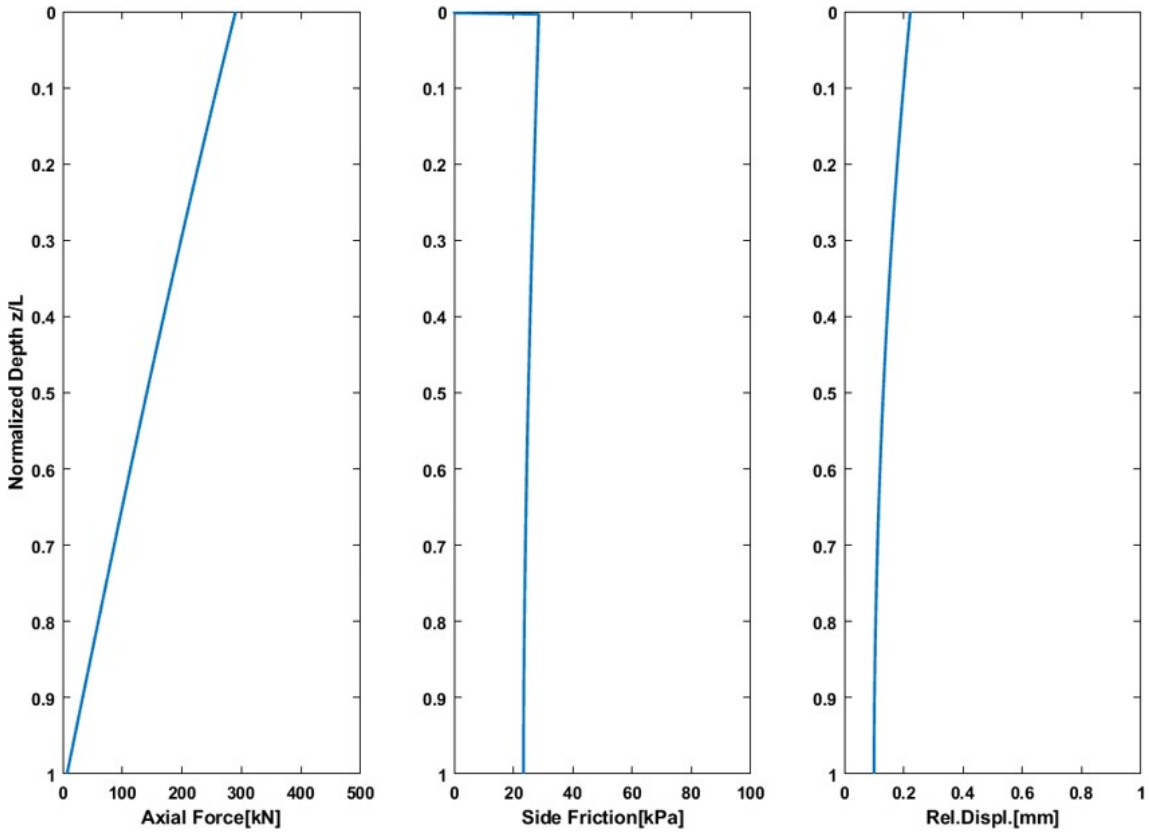

Figure 1.5: Results of numerical approach to predict pile settlement using exponential functions for the load-transfer $t - z$ function: H-pile.

Linear-Elastic-Perfectly-Plastic Model

Again, the ultimate skin resistance, s_i^{ult}, and ultimate tip resistance, Q_t^{ult}, are computed using the Tumay and Fakhroo (1982) method. Critical displacement thresholds at the pile shaft and tip, δ_s^* and δ_t^*, are then determined based on the equivalent pile diameter D_e. Remaining procedures are the same as above. The settlement at the top of the pile is estimated as 0.62 mm. The detailed results are shown in Figure 1.6.

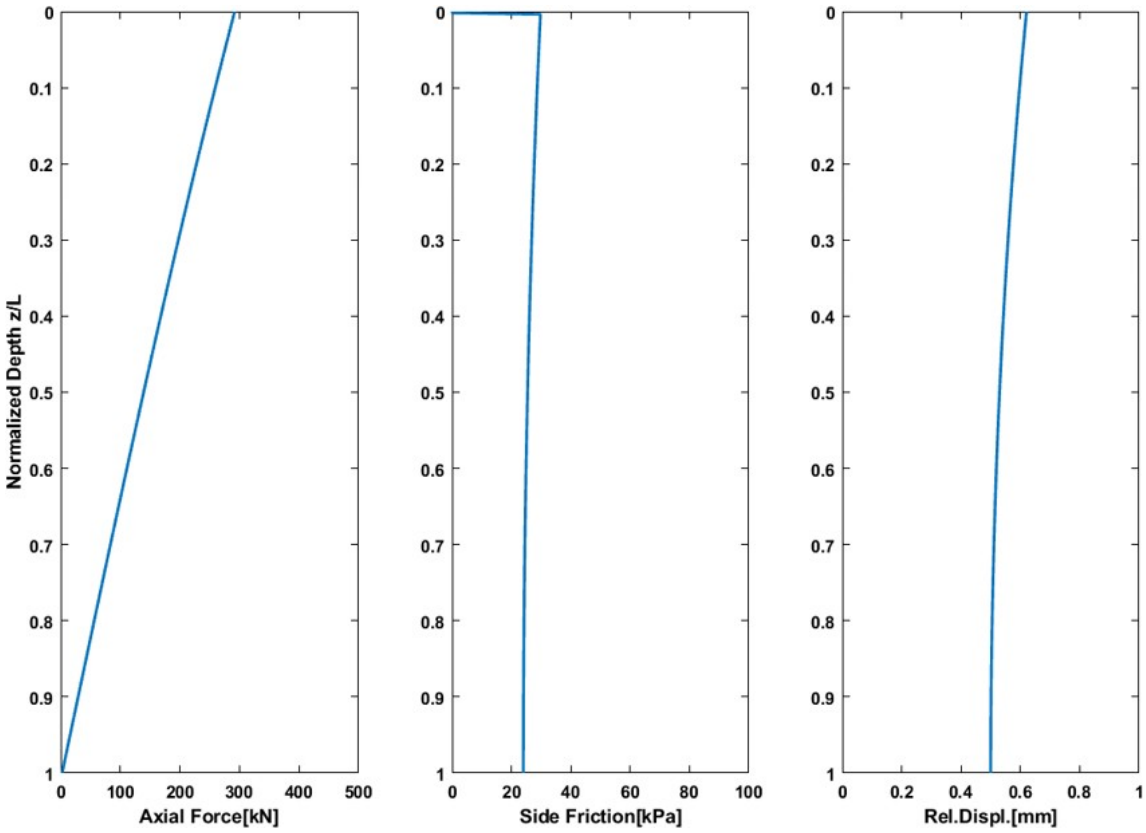

Figure 1.6: Results of numerical approach to predict pile settlement using linear-elastic-perfectly-plastic models for the load-transfer $t - z$ function: H-pile.

1.5.2 Pipe Pile

Analytical Approach

All the known parameters are the same as with those used for the calculation of H-pile, except that the applied force at the pile head is changed to $P = 214$ kN, the cross-sectional area of a pile is $A = 0.0824$ m^2, the diameter of a pile is $D_p = 0.32$ m, and the cross-sectional perimeter of a pile is $S = 1.0173$ m. Again, pertinent parameters are determined using Equation 1.1 to Equation 1.14, and the resultant ξ_0 is 1.82¿1. Similar to the case of the H-pile, the pile-soil interface is in the elastic state, and the settlement at the top of the pile is estimated as u_t =0.38 mm in response to the applied load of 214 kN.

Numerical Approach

Hyperbolic Curve

The pile-pile is again divided into 550 elements for the numerical analysis. The ultimate tip resistance q_{ult} and ultimate skin resistance f_{ult} of each element are determined using the De Ruiter and Beringen (1979) method. Other parameters b_f, b_e, a_f, and a_e are calculated based on the pile diameter D_e. After that, the force equilibrium is applied to each element with the load-transfer numerical algorithm. In the end, the force on the top of the pile Q_1 is computed. The pile head force Q^{head} is 214 kN. When the calculation error $|Q_1 - Q^{head}| \leq E$, where E is a tolerance value (selected as 5 kN), the forward-successive calculation stops. The settlement at the top of the pile is estimated as 0.61 mm in response to the applied load of 214 kN. Detailed results are shown in Figure 1.7.

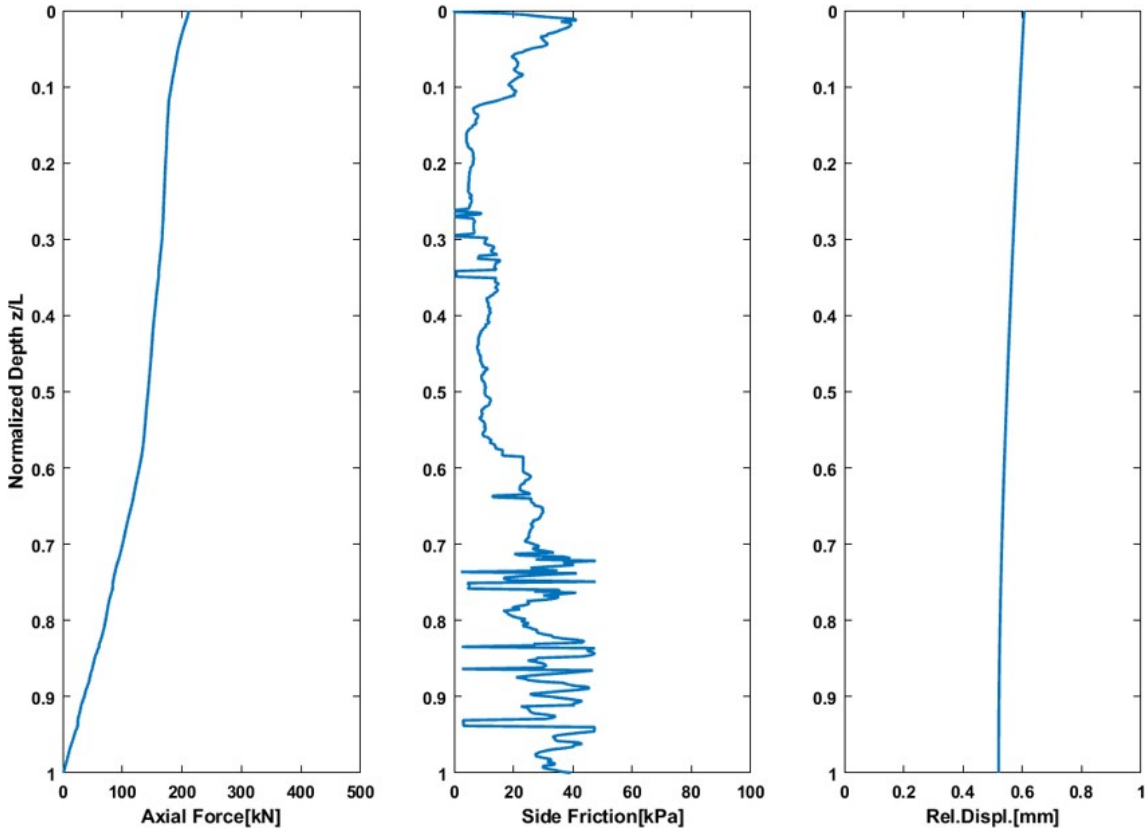

Figure 1.7: Results of numerical approach to predict pile settlement using hyperbolic curves for the load-transfer $t - z$ function: pipe-pile.

Exponential Function

Similar to the previous procedures, the ultimate soil resistance, R_{su}, ultimate base resistance, q_{bu}, ultimate bearing capacity R_u, α and β are determined using De Ruiter and Beringen (1979) (i.e., European Method). And parameters z_v and z_f are calculated based on the pile diameter. The remaining procedures are the same as above. The settlement at the top of the pile is estimated as 0.29 mm. Detailed results are shown in Figure 1.8.

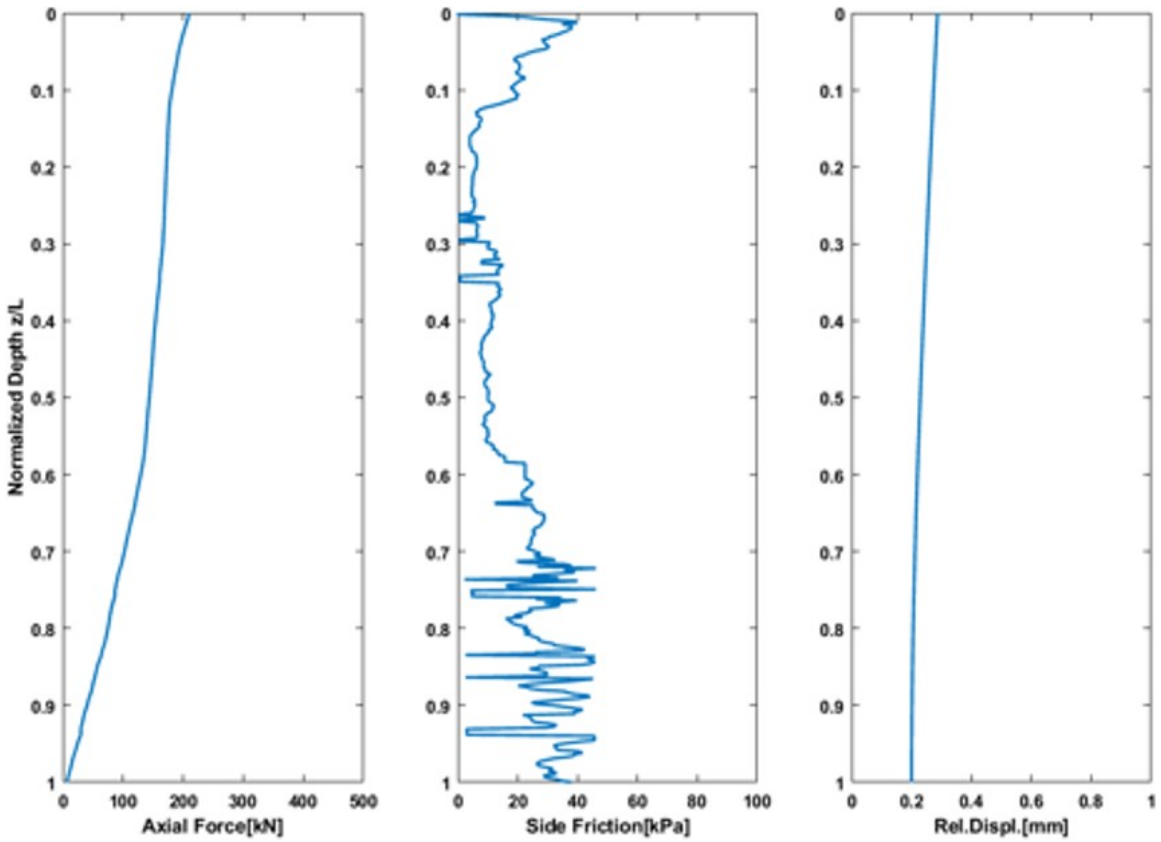

Figure 1.8: Results of numerical approach to predict pile settlement using exponential functions for the load-transfer $t - z$ function: pipe-pile.

Linear-Elastic-Perfectly-Plastic Model

Lastly, the ultimate skin resistance, s_i^{ult}, and ultimate tip resistance, Q_t^{ult}, are obtained using De Ruiter and Beringen (1979) (i.e., European Method). Critical displacement thresholds at the pile shaft and tip, δ^* and δ_t^*, are then decided based on the pile diameter. Remaining

procedures are the same. The settlement at the top of the pile is estimated as 0.70 mm. The detailed results are shown in Figure 1.9.

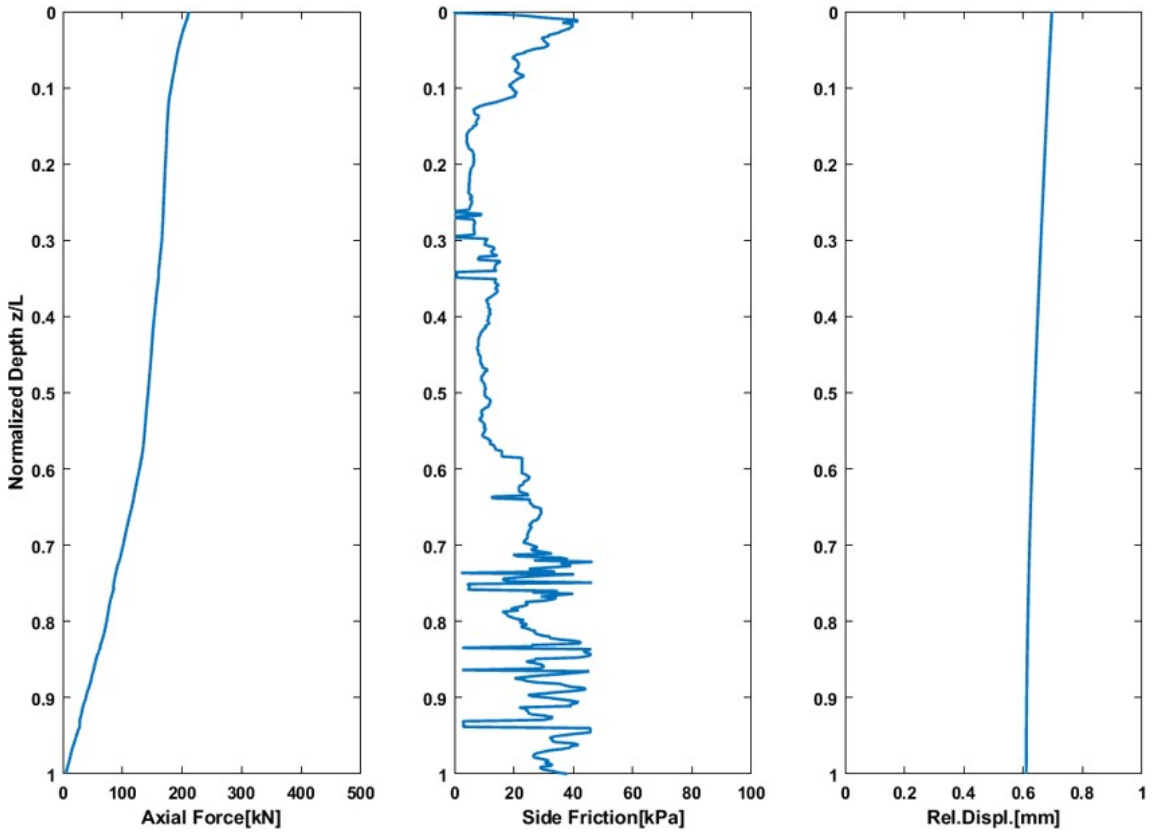

Figure 1.9: Results of numerical approach to predict pile settlement using linear-elastic-perfectly-plastic models for the load-transfer t-z function: pipe-pile.

1.5.3 Comparison of Results

We compared the predicted pile settlement values obtained via analytical and numerical approaches, which are summarized in Figure 1.10. It was observed that the numerical approach, based on the exponential function as the $t - z$ function, yielded the lowest prediction of pile settlement for both H-pile and pipe-pile. Results from the analytical approach for H-pile were similar to those from the numerical approaches that employed either the hyperbolic or the linear-elastic-perfectly-plastic method, whereas the analytical approach for pipe pile was similar to those from the numerical approach that employed the exponential function. Noticeably, results obtained from numerical approaches that employed either a hyperbolic

curve or a linear-elastic-perfectly-plastic model as the $t - z$ function were almost twice as those of the lowest predictions. Since we only applied these approaches to one investigation site, applications to more sites in Nebraska and actual field tests would help confirm the reliability of the suggested CPT-based pile settlement prediction method.

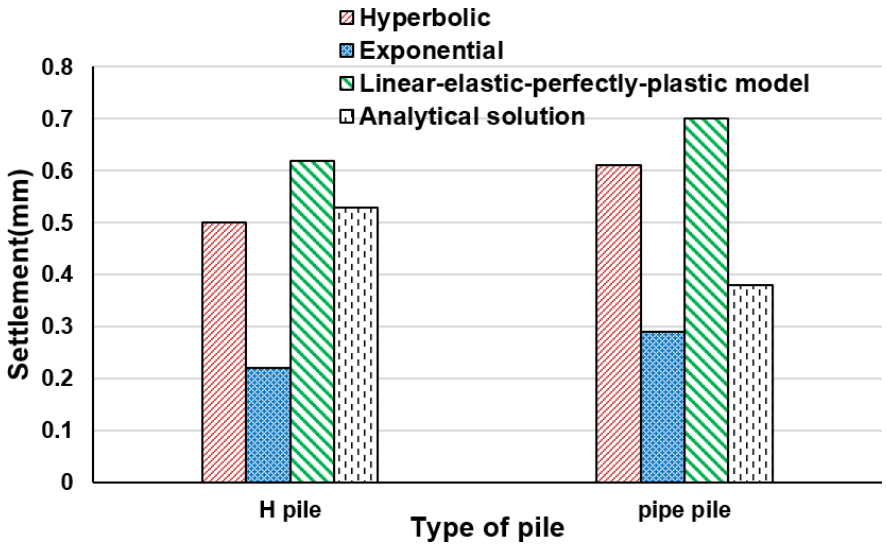

Figure 1.10: Summary of the pile settlement prediction from different approaches.

1.6 Development – Numerical Computation Code

MATLAB-based computation code and its graphical user interface (GUI) have been developed for the prediction of pile settlements that employ different t-z functions of this study. GUI is convenient for users to import CPT data, and to choose the calculation method and pile type for the settlement prediction. In order to run the code, input excel file needs to be prepared by a user. An example of the input excel file is shown in Figure 1.11. The first and second columns of the input file are the cone tip resistance, qt, and shaft friction, ft, from the CPT test. The third column of the input file is the zone of soils in the SBT chart. The fourth column of the input file is the overconsolidation ratio, OCR.

Once the excel-type-of input file is prepared and imported into the GUI ("select file" button in the GUI; Figure 1.12), settlement prediction can be quickly obtained. Screen shot of the code GUI is shown in Figure 1.12. First, the pile type needs to be selected betweenthe

H-pile and pipe-pile. Then, parameters, such as pile's diameter, length, Young's modulus, and the collection interval of the CPT data need to be filled in (left side of the GUI). Lastly, a user can select the type of t-z function between the hyperbolic, exponential, and linear-elastic-perfectly-plastic functions (right side of the GUI). Once the function is hit, the code will show the settlement prediction (green color in the GUI) as well as the profiles of axial force, side friction, and relative displacement of the pile along the penetration depth (in terms of the normalized depth, z/L; Figure 1.12).

	A	B	C	D
1	q_t [MPa]	f_t [MPa]	soil zone	OCR
2	0	0	7	9999
3	2.267	0.012	7	9999
4	3.332	0.016	7	9999
5	3.852	0.033	7	9999
6	4.617	0.037	7	9999
7	5.626	0.056	7	9999
8	5.761	0.069	7	9999
9	5.024	0.082	7	9999
10	5.434	0.082	7	9999
11	5.516	0.091	7	9999
12	5.461	0.118	6	9999
13	5.38	0.121	6	9999
14	5.216	0.107	6	9999
15	5.025	0.095	6	9999
16	4.887	0.096	7	9999
17	4.678	0.116	6	9999
18	4.395	0.108	6	9999
19	4.395	0.127	6	9999

Figure 1.11: An example of input excel file to run the code for the settlement prediction of a pile

1.7 Conclusion

CPT-based analytical and numerical computation approaches are proposed and tested for making a settlement prediction of H-piles and pipe piles in Nebraska. Through the comparison of settlement results for these pile types at the investigation site, it was observed that employing either hyperbolic or linear-elastic-perfectly-plastic models as the t-z function yields a similar settlement prediction for both pile types. Using an exponential curve as the t-z function resulted in the lowest settlement prediction among all tested approaches.

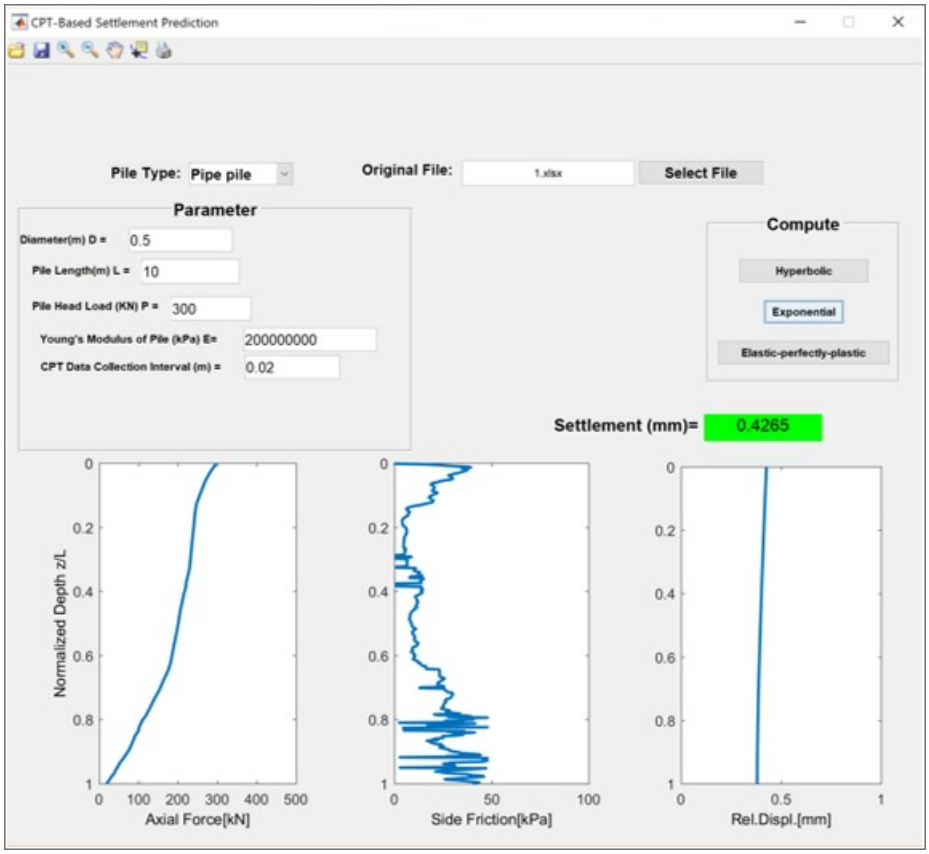

Figure 1.12: GUI of the code for the settlement prediction of a pile.

Outcomes from the analytical approach lie between those results obtained via the numerical computation approaches. Since only one investigation site was applied for these approaches, applications to more sites in Nebraska and actual field tests would help to confirm the reliability of the suggested CPT-based pile settlement prediction method. Finally, a MATLAB-based computation code that has a graphical user interface (GUI) was developed for the settlement prediction that will provide a convenient tool for users.

Appendices

Table 3: Measured and predicted pile capacities for different methods

SN	SS	Pile Type	CW [kN]	EN [kN]	M-1	M-2	M-3	M-4	M-5
C05501305P	A1	HP12x53	725	552	995.4	366.4	1481	1487.1	1179.7
S034 31644	A1	HP12x53	712	686	606.5	257.26	689.7	1073.6	906
S034 31644	A1	HP12x53	761	782	646	282.35	738.2	1104.2	970.9
S034 31644	A1	HP12x53	818	871	693.8	385	797.9	991.4	1074.3
S034 31644	A2	HP12x53	334	283	696.8	347.7	791.2	930.7	942.1
S034 31644	A2	HP12x53	440	358	798	426.5	905.5	1106.1	1106.8
S034 31644	A2	HP12x53	676	583	821.4	418.13	979.1	1401.1	1201.1
S034 31644	A2	HP12x53	663	577	880.8	516.2	1016.5	1346.8	1298.4
S034 31752	A1	HP12x53	1116	990	843	230.21	871.5	1015.7	844.9
S034 31752	A2	HP12x53	503	483	1770.5	624.6	2481	2078.7	1739.1
S034 31752	B1	HP12x53	1392	1150	1091.8	305.1	1513.4	1553.5	1069.7
S034 31752	B2	HP12x53	1036	765	1761.8	621	2457	2075.6	1735.3
S080 41341	A1	HP12x53	1712	1319	1541.3	571.1	1759.7	1948.7	1247.6
S080 41341	A1	HP12x53	1784	1787	1780.7	688.2	2115.7	2092.3	1632.5
S080 41341	A2	HP12x53	792	1002	1004.3	412.3	1727	1876	1272.9
S159 01373	N3 (P3)	HP14x89	1601	1765	1214	542.2	1915.5	2404	1964.6
S159 01373	N2 (P2)	HP14x89	2669	2340	1073.3	433.8	2110.3	2421.4	1901.4
C006602905	A2	HP10x42	467	380	995.6	239.8	1024.3	1318.5	916.8
C006602905	A2	HP10x42	512	334	1082.5	261.04	1037.7	1331.4	981.5
C006602905	A2	HP10x42	592	405	1229	315.21	1074.6	1388.6	1170.7
S080 43555	A1	HP12x53	681	394	754.8	599.6	1010.7	1714.1	1174.4
S080 43555	A1	HP12x53	792	560	791.1	639.3	1071.1	1855.7	1264
S080 43555	A1	HP12x53	916	646	891.3	714.5	1224.9	2055.1	1396.7
S080 43555	A1	HP12x53	992	715	1005.8	699.6	1346.8	2437.1	1542
S080 43555	A2	HP12x53	827	766	698.1	615.5	995.4	1592.3	1143.1
S080 43555	A2	HP12x53	912	867	913.6	748.6	1130.5	1843.8	1410.1
S080 43555	A2	HP12x53	1228	953	1137.9	776.2	1330.7	2263.3	1651.5
S080 43555	A2	HP12x53	1379	1013	1130.9	912	1520	2320.8	1758.7
S080 43555	A2	HP12x53	1726	1245	1268	1008.5	1642.5	2555.7	1997.9

SN	SS	Pile Type	CW [kN]	EN [kN]	M-1	M-2	M-3	M-4	M-5
S080 43555	P1	HP12x53	1428	1227	1040.1	802.2	1387.1	2277.7	1613.6
S080 43555	P1	HP12x53	1739	1456	1040.1	802.2	1387.1	2277.7	1613.6
S080 44207	P4	HP12x53	756	785	1427.9	756.31	1747.5	1793.5	1931.6
S080 44207	P4	HP12x53	916	968	1356.8	787.08	1633.8	1623.8	1990.9
S080 44207	P4	HP12x53	1050	1058	1490.5	852.34	1921.7	1843.7	2202.3
S080 44207	P4	HP12x53	1223	1139	1588.3	910.73	2101.7	1960.7	2372.2
S080 44207	P4	HP12x53	1397	1066	1663.9	952.59	2165.9	1975.9	2502
S080 44207	P4	HP12x53	752	727	1336.3	795.7	1655.1	1467.7	1831.4
S080 44207	P4	HP12x53	756	722	1421.1	778.23	1617.1	1633.1	1979.4
S080 44207	P4	HP12x53	956	905	1431.4	821.57	1848.9	1807.9	2106.4
S080 44207	P4	HP12x53	1477	1168	1560.5	897.05	2076.8	1948.8	2332.7
S080 41856	A1	HP12x53	761	542	574.54	502.8	852.62	1074.85	1010.57
S080 41856	A1	HP12x53	712	763	582.17	516.38	874.52	1118.95	1036.51
S080 41856	A1	HP12x53	881	933	662.1	558.58	920.8	1180.51	1120.5
S080 41856	A2	HP12x53	1228	835	1191.2	761.5	1549.9	1623.9	1773.6
S080 41856	A2	HP12x53	1343	1029	1238.8	802.1	1553.7	1665.8	1886.4
S080 41856	A2	HP12x53	1521	1191	1293.7	760.95	1649.4	1923.4	1993.6
S077 09368	A1	pipe	1993	1749	1150.3	618.1	1644.8	2234.9	1644
S077 09368	A2	pipe	1908	1530	1990.2	884.5	2097.7	2854	2241
S077 09368	A2	pipe	2002	1765	2065	930	2219	2924	2488
S077 09368	B1	pipe	2002	1751	1327.3	667.6	2044.6	2610	1937.5
S077 09368	B2	pipe	1913	1698	1873.3	789.3	2009.6	2788	2073.3
S080 08295L	A1	pipe	2010	1326	1653.8	657.6	1976.6	1679.2	1859.3
S081 08578	A1	pipe	725	769	598.3	403.03	624.2	1252.23	947.7
S081 08578	A1	pipe	378	644	475.2	327.78	582.6	1145.1	791.24
S081 08578	A1	pipe	436	727	596	356.84	613.7	1303	934.7
S081 08578	A1	pipe	756	821	606.3	369.09	671.3	1360.7	957.1
S081 08578	B2	pipe	609	404	1264.3	890.1	1645.4	1817.4	1708.6
S081 08578	B2	pipe	627	393	1454.1	980.9	1688.7	1828.8	1969.5
S081 08578	B2	pipe	516	440	1389.2	959.2	1755.5	1884.3	1924.9

SN	SS	Pile Type	CW [kN]	EN [kN]	M-1	M-2	M-3	M-4	M-5
S081 08578	B2	pipe	534	445	1317.2	931.5	1794.6	1918.9	1870.6
S080 40436	A1	pipe	854	556	792.01	530.04	962.1	1058.11	1288.31
S080 40436	A1	pipe	729	606	962.8	641.39	1127.4	1291.5	1515.4
S080 40436	A1	pipe	592	640	1078.7	696.16	1361.2	1704.2	1606
S085 0042	P1	pipe	249	316	240.75	223.45	414.5	514.75	405.9
S085 0042	P1	pipe	276	412	262.29	243.28	444.1	567.98	444.41
S085 0042	P1	pipe	316	462	279.65	257.47	474.3	606.94	470.54
S085 0042	P2	pipe	605	739	348.3	298.77	594	808.8	533.58
S085 0042	P2	pipe	614	654	405.7	371.38	714	876.3	652.2
S085 0042	P3	pipe	307	420	351	246.61	893.4	1118.7	665.1
S080 42094	A1	pipe	801	819	937.9	452.59	806.9	895	1284
S080 42094	A1	pipe	734	773	1001.6	479.09	870.4	960.3	1372.2
S080 42094	A1	pipe	676	658	1026.2	505.49	1067	1204.6	1457.9
S080 42094	A1	pipe	983	911	1402.1	773.7	1334.5	1158.3	1904.6
S080 42094	A1	pipe	885	854	1575.9	709.8	1721.6	1654.6	2028.5
S080 42094	A2	pipe	1121	1025	1460.8	630.7	1819.1	2156	1714.2
S080 42094	A2	pipe	1134	980	1575.1	664.8	1285.9	1639	1855.6
S080 42094	A2	pipe	1201	1057	1164.8	593.12	970.3	1329.4	1688.4
S080 42094	A2	pipe	1254	1138	1119.2	602.46	1124.9	1524.4	1703.1
S015 13411	A1	pipe	823	635	534.3	437.43	827.1	1088.9	801.8
S015 13411	A1	pipe	1032	736	592.3	482.9	913.1	1229.7	906.1
S015 13411	A1	pipe	1108	811	650.7	528.7	988.3	1363.4	1007
S015 13411	B1	pipe	876	1066	513.2	421.99	803.5	1048.1	765.5
S015 13411	B1	pipe	907	1325	572.1	467.69	890.7	1186.9	860.9
S015 13411	B1	pipe	992	1092	650.7	528.7	988.3	1363.4	1007
S015 13411	B2	pipe	823	897	994.8	698.5	1321.7	1618.3	1491.3
S015 13411	B2	pipe	894	944	1039.5	735.3	1388.6	1703.3	1581
S015 13411	B2	pipe	965	961	1039.5	735.3	1388.6	1703.3	1581
S080 40436	P1	Type I	738	638	984.5	666.73	1420.2	1339.33	1593.39
S080 42094	P1	Type I	778	765	1196.2	570.8	1215.3	1160.1	1623.4

SN	SS	Pile Type	CW [kN]	EN [kN]	M-1	M-2	M-3	M-4	M-5
S080 42094	P1	Type I	836	917	1081.3	640.1	1110.2	1015.3	1639.4
S080 42094	P1	Type I	863	1104	1598.8	722.2	1666.9	1472.9	2088.6
S080 42094	P1	Type I	707	851	1817.8	818.7	2272.8	1946.8	2314.6
S080 42094	P1	Type I	890	1077	1880.2	884.4	2812	2314	2502.7

Table 4: Measured and predicted pile capacities for different methods

SN	SS	Pile Type	CW [kN]	EN [kN]	M-6	M-7	M-8	M-9	M-10	M-11
C05501305P	A1	HP12x53	725	552	1430.9	929.8	960.4	1141.4	1380.3	908.4
S034 31644	A1	HP12x53	712	686	933.3	467.4	596.6	933.9	1380.3	661
S034 31644	A1	HP12x53	761	782	944.7	526.2	663.3	1019.4	1466.9	872.34
S034 31644	A1	HP12x53	818	871	973.5	581.4	677.3	1109.1	1567.1	1825.5
S034 31644	A2	HP12x53	334	283	880	631.1	656	1012.1	1234.7	2045
S034 31644	A2	HP12x53	440	358	956.2	731.9	729.5	1149.4	1397.3	3860.7
S034 31644	A2	HP12x53	676	583	1007.5	821	700.1	1267	1478.3	5962.87
S034 31644	A2	HP12x53	663	577	1081.2	868.8	745.5	1345.7	1601.8	7286.9
S034 31752	A1	HP12x53	1116	990	1361	487	748.3	733.8	1094.7	257.2
S034 31752	A2	HP12x53	503	483	1777.1	1212.2	1478.3	1499	3056	1397.7
S034 31752	B1	HP12x53	1392	1150	1654.5	788.6	1030.6	1049.5	1540.6	452.4
S034 31752	B2	HP12x53	1036	765	1773.8	1206.4	1473.5	1493.4	3043	1373.7
S080 41341	A1	HP12x53	1712	1319	1858.4	1744.6	1524.4	1756.5	1364.1	1070.2
S080 41341	A1	HP12x53	1784	1787	1912.9	1334.4	1780.1	1317.5	2349	1275.2
S080 41341	A2	HP12x53	792	1002	1911.9	1329.7	1079.8	1413	1151.5	827.1
S159 01373	N3 (P3)	HP14x89	1601	1765	2586	1081.3	1323.4	1980.9	2542.1	859.8
S159 01373	N2 (P2)	HP14x89	2669	2340	2806	1523.7	1241.3	2086	2289.4	965.7
C006602905	A2	HP10x42	467	380	1073.3	624.31	1020.8	1037	1480.5	339.5
C006602905	A2	HP10x42	512	334	1080.1	659.2	1091.3	1081.9	1549.3	363.6
C006602905	A2	HP10x42	592	405	1104.8	740.2	1248.8	1208.4	1950.3	424.2
S080 43555	A1	HP12x53	681	394	990.8	876	721.4	1099.4	1918	1450.6
S080 43555	A1	HP12x53	792	560	1079.2	931.1	705.8	1156.3	2093.2	1447.7

SN	SS	Pile Type	CW [kN]	EN [kN]	M-6	M-7	M-8	M-9	M-10	M-11
S080 43555	A1	HP12x53	916	646	1210.6	1076.7	814.6	1318.3	2291.9	1714.1
S080 43555	A1	HP12x53	992	715	1306.7	1250.6	903.3	1507.9	2476	1347.57
S080 43555	A2	HP12x53	827	766	1060.2	927.8	590.8	998.1	1747.4	2003.8
S080 43555	A2	HP12x53	912	867	1293.2	1094.5	675.7	1182.3	2106.3	2370.8
S080 43555	A2	HP12x53	1228	953	1363.8	1304.7	812.8	1403.4	2471	2777.67
S080 43555	A2	HP12x53	1379	1013	1518.8	1526.6	913.1	1664.3	2807.1	3603.5
S080 43555	A2	HP12x53	1726	1245	1699	1729.1	980.4	1890.1	3095.9	3929.4
S080 43555	P1	HP12x53	1428	1227	1338.9	1255.7	921.7	1515.2	2558.2	1963.9
S080 43555	P1	HP12x53	1739	1456	1338.9	1255.7	921.7	1515.2	2558.2	1963.9
S080 44207	P4	HP12x53	756	785	1467.8	1459.9	1189.1	1946	2590.1	3850.81
S080 44207	P4	HP12x53	916	968	1408	1392.6	1022.4	1955.5	2519.1	4719.47
S080 44207	P4	HP12x53	1050	1058	1603	1574.8	1173	2278.8	2734	6211.56
S080 44207	P4	HP12x53	1223	1139	1791.5	1646.6	1236.3	2490.9	2969.9	7940.07
S080 44207	P4	HP12x53	1397	1066	1818.3	1741.7	1309.8	2662.3	3126.3	9242.96
S080 44207	P4	HP12x53	752	727	1468.3	1292.4	1049.7	1763.5	2465.4	4227.7
S080 44207	P4	HP12x53	756	722	1296.4	1474.1	1111.7	1971.3	2508.2	4379.45
S080 44207	P4	HP12x53	956	905	1534	1533.8	1143.1	2188.7	2654.8	5325.47
S080 44207	P4	HP12x53	1477	1168	1761.8	1644.2	1221.8	2461.5	2918.7	7583.95
S080 41856	A1	HP12x53	761	542	830.29	715.19	524.12	1108.73	1698.8	1141.4
S080 41856	A1	HP12x53	712	763	871.8	711.5	525.68	1133.42	1758.5	1106.76
S080 41856	A1	HP12x53	881	933	1011.4	733.13	595.28	1194.71	1866.6	1149
S080 41856	A2	HP12x53	1228	835	1372.9	1328.6	948.8	1733.2	2669.1	3728.2
S080 41856	A2	HP12x53	1343	1029	1346.4	1422.5	948.1	1843.7	2752.8	5994
S080 41856	A2	HP12x53	1521	1191	1416.7	1518.3	975.7	1965.6	2898.8	7872.68
S077 09368	A1	pipe	1993	1749	1805.2	1123	1146.2	1635.5	2182	1123.1
S077 09368	A2	pipe	1908	1530	2018	2080.2	2043.6	2672	2630.8	4659.7
S077 09368	A2	pipe	2002	1765	2040.4	1910.8	2065.5	2489	3240	4706
S077 09368	B1	pipe	2002	1751	1950.5	1769.9	1401.5	2326	2234.3	1352.2
S077 09368	B2	pipe	1913	1698	1997.2	1671.2	1782.3	2237.6	2260.3	4477.4
S080 08295L	A1	pipe	2010	1326	1436.9	1579.3	2224.4	1912.5	3438	929.4

SN	SS	Pile Type	CW [kN]	EN [kN]	M-6	M-7	M-8	M-9	M-10	M-11
S081 08578	A1	pipe	725	769	924.3	544.1	561	937.8	1446.4	906.7
S081 08578	A1	pipe	378	644	887.2	427.23	467.5	795.23	1293.5	684.6
S081 08578	A1	pipe	436	727	922.8	663	552.3	1060.7	1433.1	618.4
S081 08578	A1	pipe	756	821	993.3	580.6	580	980.3	1501.6	614.49
S081 08578	B2	pipe	609	404	1450.8	1284.6	1041.9	1418.9	2459.3	2046.9
S081 08578	B2	pipe	627	393	1385.7	1474.8	1090.1	1618.1	2607.2	2426.5
S081 08578	B2	pipe	516	440	1422.8	1449.6	998.2	1589.8	2652.9	2403.4
S081 08578	B2	pipe	534	445	1448	1510.1	966.6	1648.9	2684	2610.8
S080 40436	A1	pipe	854	556	997.6	849.61	675.2	1312.85	1525.6	1268.3
S080 40436	A1	pipe	729	606	1170.9	940.55	834.3	1544.26	1833	1477.3
S080 40436	A1	pipe	592	640	1426.2	1102.2	961	1810.4	2147.7	1434.22
S085 0042	P1	pipe	249	316	559.9	264.67	288.31	365.21	774.63	477.35
S085 0042	P1	pipe	276	412	600.4	279.39	302.15	397.01	836.18	477.35
S085 0042	P1	pipe	316	462	634.6	292.95	312.31	421.54	869.92	592.01
S085 0042	P2	pipe	605	739	683.4	496.2	387.3	640	1082.7	552.65
S085 0042	P2	pipe	614	654	777.9	447.29	391.4	580	1195.8	806.3
S085 0042	P3	pipe	307	420	1094.7	578.3	392.5	715.1	929.2	568.98
S080 42094	A1	pipe	801	819	1141.9	799.4	788.1	1298.7	1503.5	840.54
S080 42094	A1	pipe	734	773	937.1	998.3	1067.7	1576.8	1454.8	926.3
S080 42094	A1	pipe	676	658	1307.9	708.6	854.2	1344.89	1654.4	882.5
S080 42094	A1	pipe	983	911	1424.4	865.7	1110.9	1507.96	1904.2	1372.9
S080 42094	A1	pipe	885	854	1558.7	1276	1368.5	1957.8	2471	1395.8
S080 42094	A2	pipe	1121	1025	1988.4	1201.2	1252.5	1603.8	2102	1164.1
S080 42094	A2	pipe	1134	980	1414	1295.4	1438.5	1777.8	2593	1225.3
S080 42094	A2	pipe	1201	1057	1094.6	1023.2	991.2	1610.2	1746.4	1199.62
S080 42094	A2	pipe	1254	1138	1265.9	984.7	1001.1	1649.1	1933.9	1222.54
S015 13411	A1	pipe	823	635	972.9	569.5	513.3	809.3	1397.5	1019.3
S015 13411	A1	pipe	1032	736	1061.5	658.5	550.6	906.5	1600.3	1164.4
S015 13411	A1	pipe	1108	811	1115.4	749.3	606.5	1010.7	1747.4	1315.7
S015 13411	B1	pipe	876	1066	950.5	546.2	504.4	786.8	1342.3	989.4

SN	SS	Pile Type	CW [kN]	EN [kN]	M-6	M-7	M-8	M-9	M-10	M-11
S015 13411	B1	pipe	907	1325	1036.4	629.4	554.7	873	1532.6	1116.3
S015 13411	B1	pipe	992	1092	1115.4	749.3	606.5	1010.7	1747.4	1315.7
S015 13411	B2	pipe	823	897	1283.4	1148.4	852.1	1497.3	2431.1	1893.5
S015 13411	B2	pipe	894	944	1329.3	1234.2	888	1609	2592.8	2014.5
S015 13411	B2	pipe	965	961	1329.3	1234.2	888	1609	2592.8	2014.5
S080 40436	P1	Type I	738	638	1248.4	1021.4	990.96	1640.17	1909.4	1600.3
S080 42094	P1	Type I	778	765	1133.7	1093.4	1453.6	1760.8	1733.4	1073.3
S080 42094	P1	Type I	836	917	1319	773.34	1120.7	1512.26	1674.5	1185.8
S080 42094	P1	Type I	863	1104	1360	1289.3	1726.1	2075.7	2095.1	1365.1
S080 42094	P1	Type I	707	851	1785.3	1802.9	2049.1	2626.5	2809	1693.7
S080 42094	P1	Type I	890	1077	2146	1918.8	2024.2	2829.1	2995	1885.6

Abbreviations
SN : Structure Number
SS: Substructure
CW: CAPWAP
EN: LRFD Driving Equation
M-1: Aoki and de Alencar (1975)
M-2: Clisby et al. (1978)
M-3: Schmertmann (1978)
M-4: De Ruiter and Beringen (1979)
M-5: Philipponnat (1980)
M-6: Tumay and Fakhroo (1982)
M-7: Prince and Wardle (1982)
M-8: Bustamante and Gianeselli (1982)
M-9: Almeida et al. (1996)
M-10: Eslami and Fellenius (1997)
M-11: Takesue et al. (1998)

References

AbdelSalam, S. S., Sritharan, S., and Suleiman, M. T. (2010). "Current design and construction practices of bridge pile foundations with emphasis on implementation of load resistance factor design." *Journal of Bridge Engineering*, 15(6), 749–758.

Abu-Farsakh, M. Y., Chen, Q., Haque, N., et al. (2013). "Calibration of resistance factors for drilled shafts for the new fhwa design method.." *Report no.*, Louisiana Transportation Research Center.

Abu-Farsakh, M. Y. and Titi, H. H. (2004). "Assessment of direct cone penetration test methods for predicting the ultimate capacity of friction driven piles." *Journal of Geotechnical and Geoenvironmental Engineering*, 130(9), 935–944.

Abu-Hejleh, N., DiMaggio, J., and Kramer, W. (2011). "Implementation of lrfd geotechnical design for bridge foundations." *Report No. FHWA NHI-10-039*, FHWA Resource Center.

Almeida, M. S., Danziger, F. A., and Lunne, T. (1996). "Use of the piezocone test to predict the axial capacity of driven and jacked piles in clay." *Canadian Geotechnical Journal*, 33(1), 23–41.

Alvarez, C., Zuckerman, B., and Lemke, J. (2006). "Dynamic pile analysis using capwap and multiple sensors." *GeoCongress 2006: Geotechnical Engineering in the Information Technology Age*, 1–5.

Aoki, N. and de Alencar, D. (1975). "An approximate method to estimate the bearing capacity of piles." *Proc., 5th Pan-American Conf. of Soil Mechanics and Foundation Engineering*, Vol. 1, International Society of Soil Mechanics and Geotechnical Engineering Buenos Aires, 367–376.

ASTM-D4945 (2008). "Standard test method for high-strain dynamic testing of deep foundations." *D4945*.

Axelsson, G. (2002). "A conceptual model of pile set-up for driven piles in non-cohesive soil." *Deep Foundations 2002: An International Perspective on Theory, Design, Construction, and Performance*, 64–79.

Bandini, P. and Salgado, R. (1998). "Methods of pile design based on cpt and spt results." *Proceedings of the 1st International Conference on Site Characterization*, 967–976.

Barker, R. M., Duncan, J., Rojiani, K., Ooi, P., Tan, C., and Kim, S. (1991). *Manuals for the design of bridge foundations: Shallow foundations, driven piles, retaining walls and abutments, drilled shafts, estimating tolerable movements, and load factor design specifications and commentary*. Number 343.

Basu, D., Salgado, R., and Prezzi, M. (2008). "Analysis of laterally loaded piles in multilayered soil deposits.

Bloomquist, D., McVay, M. C., and Hu, Z. (2007). "Updating florida department of transportation's (fdot) pile/shaft design procedures based on cpt & dpt data." *Report no.*, Florida Department of Transportation.

Briaud, J.-L. and Tucker, L. M. (1988). "Measured and predicted axial response of 98 piles." *Journal of Geotechnical Engineering*, 114(9), 984–1001.

Buckley, R., Kontoe, S., Jardine, R., Maron, M., Schroeder, F., and Barbosa, P. (2017). "Common pitfalls of pile driving resistance analysis–a case study of the wikinger offshore windfarm." *Offshore Site Investigation Geotechnics 8th International Conference Proceeding*, Vol. 1246, Society for Underwater Technology, 1246–1253.

Bustamante, M. and Gianeselli, L. (1982). "Pile bearing capacity prediction by means of static penetrometer cpt." *Proceedings of the 2-nd European symposium on penetration testing*, 493–500.

Cai, G., Liu, S., Tong, L., and Du, G. (2009). "Assessment of direct cpt and cptu methods for predicting the ultimate bearing capacity of single piles." *Engineering Geology*, 104(3-4), 211–222.

Clisby, M., Scholtes, R., Corey, M., Cole, H., Teng, P., and Webb, J. (1978). "An evaluation of pile bearing capacities." *Volume I, Final Report, Mississippi State Highway Department*.

Danziger, B., Lopes, F., Costa, A., and Pacheco, M. (1996). "A discussion on the uniqueness of capwap-type analysis." *Proceedings of the Fifth International Conference on the Application of Stress-Wave Theory to Piles*, 394–408.

de Jong, G. D. J. (1956). "Wat gebeurt er in de grond tijdens het heien." *De Ingenieur*, 68(25), 77–88.

De Ruiter, J. and Beringen, F. (1979). "Pile foundations for large north sea structures." *Marine Georesources & Geotechnology*, 3(3), 267–314.

Douglas, B. and Olson, R. (1981). "Soil classification using electronic cone penetrometer." *Symposium on Cone Penetration Testing and Experience, ASCE, New York*, 209–227.

Eslami, A., Aflaki, E., and Hosseini, B. (2011). "Evaluating cpt and cptu based pile bearing capacity estimation methods using urmiyeh lake causeway piling records." *Scientia Iranica*, 18(5), 1009–1019.

Eslami, A. and Fellenius, B. H. (1997). "Pile capacity by direct cpt and cptu methods applied to 102 case histories." *Canadian Geotechnical Journal*, 34(6), 886–904.

Eslami, A. A. and Gholami, A. M. (2006). "Analytical model for the ultimate bearing capacity of foundations from cone resistance.

Fellenius, B. H., Brusey, W. G., and Pepe, F. (2000). "Soil set-up, variable concrete modulus, and residual load for tapered instrumented piles in sand." *Performance Confirmation of Constructed Geotechnical Facilities*, 98–114.

GRL engineers, I. (2018). "Capwap signal matching software. Accessed: 2018-22-10.

Gwizdala, K. and Steczniewski, M. (2007). "Determination of the bearing capacity of pile foundations based on cpt test results." *Studia Geotechnica et Mechanica*, 29(1-2), 55–67.

Haldar, S. and Babu, G. S. (2008). "Reliability measures for pile foundations based on cone penetration test data." *Canadian Geotechnical Journal*, 45(12), 1699–1714.

Hannigan, P. J., Goble, G. G., Thendean, G., Likins, G. E., and Rausche, F. (1997). "Design and construction of driven pile foundations-volume i." *Report no.*

Hirayama, H. (1990). "Load-settlement analysis for bored piles using hyperbolic transfer functions." *Soils and Foundations*, 30(1), 55–64.

Jardine, R. and Bond, A. (1989). "Behaviour of displacement piles in a heavily overconsolidated clay." *12th Int. Conf. Soil Mechanics and Foundation Engineering*, 1147–1151.

Komurka, V. E., Wagner, A. B., and Edil, T. B. (2003). "A review of pile set-up." *Proc., 51st Annual Geotechnical Engineering Conference*.

Likins, G. and Rausche, F. (2008). "What constitutes a good pda test?." *Proceedings of the Eighth International Conference on the Application of Stress Wave Theory to Piles*, 403–407.

Likins, G. E. and Rausche, F. (2004). "Correlation of capwap with static load tests." *Proceedings of the Seventh International Conference on the Application of Stresswave Theory to Piles*, Citeseer, 153–165.

Long, J. H. and Wysockey, M. H. (1999). "Accuracy of methods for predicting axial capacity of deep foundations." *Analysis, Design, Construction, and Testing of Deep Foundations*, ASCE, 180–195.

Massarsch, K. (2005). "Ground vibrations caused by impact pile driving." *Proc., Environmental Vibrations: Prediction, Monitoring, Mitigation and Evaluation (ISEV 2005), Taylor & Francis, London*, 369–379.

Misra, A. and Chen, C.-H. (2004). "Analytical solution for micropile design under tension and compression." *Geotechnical & Geological Engineering*, 22(2), 199–225.

Ng, K. W., Roling, M., AbdelSalam, S. S., Suleiman, M. T., and Sritharan, S. (2012). "Pile setup in cohesive soil. i: experimental investigation." *Journal of Geotechnical and Geoenvironmental Engineering*, 139(2), 199–209.

Nguyen, T. D., Lee, J.-H., Kim, S.-R., et al. (2016). "Applicability of cpt-based methods in predicting toe bearing capacities of driven piles in sand." *Acta Geotechnica*, 11(2), 359–372.

Nowak, A. S. (1999). "Calibration of lrfd bridge design code." *Report no.*

Paikowsky, S. G. (2004). *Load and Resistance Factor Design (LRFD) for Deep Foundations*, Vol. 507. Transportation Research Board.

Pasten, C. and Santamarina, J. C. (2014). "Thermally induced long-term displacement of thermoactive piles." *Journal of Geotechnical and Geoenvironmental Engineering*, 140(5), 06014003.

Philipponnat, G. (1980). "Méthode pratique de calcul d'un pieu isolé, à l'aide du pénétromètre statique." *Revue Francaise de Geotechnique*, (10), 55–64.

Price, G. and Wardle, I. (1982). "A comparison between cone penetration test results and the performance of small diameter instrumented piles in stiff clay." *Proceedings of the 2nd European Symposium on Penetration Testing, Amsterdam, the Netherlands*, Vol. 2, 775–780.

Rausche, F., Alvarez, C., and Likins, G. (2017). "Dynamic loading tests: a state of the art of prevention and detection of deep foundation failures." *3rd Bolivian International Conference on Deep Foundations*, 177–197.

Rausche, F., Goble, G. G., and Likins Jr, G. E. (1985). "Dynamic determination of pile capacity." *Journal of Geotechnical Engineering*, 111(3), 367–383.

Rausche, F., Likins, G., Liang, L., and Hussein, M. (2010). "Static and dynamic models for capwap signal matching." *Art of foundation engineering practice*, 534–553.

Robertson, P. (1990). "Soil classification using the cone penetration test." *Canadian Geotechnical Journal*, 27(1), 151–158.

Robertson, P. K. and Cabal, K. (2010). "Guide to cone penetration testing for geotechnical engineering." *Gregg Drilling & Testing*.

Robertson, P. K., Campanella, R., Gillespie, D., and Greig, J. (1986). "Use of piezometer cone data." *Use of in situ tests in geotechnical engineering*, ASCE, 1263–1280.

Schmertmann, J. H. (1978). "Guidelines for cone penetration test: performance and design." *Report no.*, United States. Federal Highway Administration.

Skov, R. and Denver, H. (1988). "Time-dependence of bearing capacity of piles." *Proc. Third International Conference on the Application of Stress-Wave Theory to Piles. Ottawa*, 25–27.

Smith, E. A. (1962). "Pile-driving analysis by the wave equation." *American Society of Civil Engineers Transactions*.

Takesue, K., Sasao, H., and Matsumoto, T. (1998). "Correlation between ultimate pile skin friction and cpt data." *Geotechnical Site Characterization*, 2, 1177–1182.

Tumay, M. and Fakhroo, M. (1982). “Friction pile capacity prediction in cohesive soils using electric quasi-static penetration tests.” *Interim Research Rep*, 1.

Wardhana, K. and Hadipriono, F. C. (2003). “Analysis of recent bridge failures in the united states.” *Journal of performance of constructed facilities*, 17(3), 144–150.